POLITECNICO DI MILANO

School of Industrial and Information Engineering Department of Chemistry, Materials and Chemical Engineering "G. Natta"

Master of Science in Materials Engineering and Nanotechnology

Bipolar plasma electrolytic oxidation to enhance the localized and uniform corrosion resistance of titanium

Supervisor: Professor Marco ORMELLESE

Co-supervisor: Luca CASANOVA

Master Thesis by:

Marcello LA PADULA – ID 877284

Academic Year 2018/2019

Ringraziamenti

Desidero ringraziare il professor Marco Ormellese, che ha reso possibile la partecipazione a questo progetto di tesi, e al gruppo PolilaPP che mi ha accolto con amicizia.

Un ringraziamento particolare al dottorando Luca Casanova, che mi ha guidato nelle attività di laboratorio, nel quale ho trovato non solo un punto di riferimento fondamentale per affrontare questa sfida, ma anche un amico.

Un ringraziamento speciale alla mia famiglia, che mi ha motivato e supportato, ai quali dedico questo elaborato e l'intenso lavoro alle sue spalle.
Infine, ringrazio Caterina, la mia splendida ragazza, che ha sempre creduto in me.

Abstract

Titanium is a metal with unique characteristics, thanks to the combination of high mechanical properties together with incredible resistance to corrosion. For these reasons, researchers are attracted to its use in different types of industry, especially those that have aggressive environments, such as the petrochemical sector, or where applications require a high strength-to-weight ratio, for example in the Aerospace field.

The first chapter of this thesis begins with an overview on titanium, from its discovery to its pure refining, to continue on its physical characteristics and properties. The latter in particular are linked to commercial classification. The first section ends with an in-depth study of the titanium market in relation to its applications.

Despite the anticorrosive properties are of an exceptional nature, by virtue of its natural oxide film, titanium suffered in particular environments. A second paragraph, therefore, deals in detail with the forms of corrosion (uniform, localized and environment-induced cracking) and the chemical agents that attack titanium.

Finally, the chapter concludes with the treatments that are applied to improve corrosion resistance: chemical and thermal oxidation, ion implantation and grain refinement, along with the various elements with which titanium can be alloyed to improve its mechanical characteristics. Finally, a review of the anodizing process, which allows the development of the titanium dioxide film to be controlled, is reported. The treatment can be traditional or by spark deposition (ASD), also called plasma electrolyte oxidation (PEO). The advantage of these techniques lies in the low cost and ease of implementation. Using a programmable power supply it is possible to control process parameters such as duty cycle, frequency and voltage. In this way it is possible to perform PEO with a monopolar pulsed regime, allowing to obtain the desired morphological and structural changes of the oxide layer and an interesting level of energy saving with respect to the DC approach. The key point of this work is the introduction of two new parameters which are the phase of cathodic polarization, replacing the rest time in the monopolar, and the intensity of this phase, expressed in cathode peak. The PEO bipolar process is thus defined.

In Chapter 2, the experimental methodology used is treated in detail: the preparation and anodization of the samples, the latter performed at a controlled temperature in a solution of 0.5 M sulfuric acid with duty cycles 90%A - 10%C and 60%A - 40%C at frequencies 20 Hz and 1000 Hz and cathodic peaks 2%, 5%, 7% and 10%; the execution of corrosive tests, according to the ASTM directives (G1 and G31 for immersion tests in reducing acids and G5 for potentiodynamic tests of anodic type, in NaBr, and cathodic, in H_2SO_4); surface characterization in terms of morphology, structure and roughness, through the techniques of SEM, XRD, GDOES and profilometry.

All the results of the aforementioned experimental investigations are discussed in chapter 3. The conditions of anodization have greatly influenced the morphology, the thickness, the quantity of crystalline phases and the corrosion behavior. The obtained data, for this reason, have been crossed to identify the parameters of interest for possible industrial applications.

Table of content

List of figures

List of tables

CHAPTER 1 – Introduction

1.1 – Titanium & its alloys

1.1.1 – Brief history

The discovery of titanium has recently been compared to other prehistoric metals, such as iron, copper and bronze, and its first identification occurred almost simultaneously in England and Germany in the XVIII century.

In 1791 an amateur geologist, Reverend William Gregor, took a sample of black, magnetic sand in a stream in the parish Mannaccan in Cornwall (England); he analyzed and found that the sand was mainly composed of magnetite (Fe_3O_4) mixed with rather impure red oxide of a new metal, which he named "maccanite" in honor of the parish. The mineral is nowadays called "ilmenite" ($FeTiO_3$), a mixture composed mainly of iron and titanium oxides.[1][2]

Figure 1.1.1 - Ilmenite ($FeTiO_3$) powder.

Four years later, Martin Heinrich Klaporth, a German chemist, rediscovered the "new metal" in form of its rutile oxide (TiO_2), in Hungarian mines. He named it "titanium", from Greek mythology, for its outstanding mechanical characteristics; the Titans were the sons of Jupiter and Hera, they were not Gods, but they had enough strength to rebel against them.

A few years later, Klaporth proved that his red oxide was the same of Reverend Gregor; he was rewarded for the discovery of the new metal, but the scientists preferred the name "titanium" in spite of "maccanite".

The isolation of pure titanium has required more than 100 years of research.

In 1910, the metallurgist Matthew A. Hunter, at Rensselaer Polytechnic Institute (Troy, New York, US), in cooperation with the General Electric Company, hypothesized that titanium had a boiling point of 6000°C and could be a candidate for the incandescent-lamps filaments, but the metal was produced with a melting point of 1800°C and the project was abandoned; in spite of that, the Hunter process showed that the pure titanium (99,9%) had a specific ductility. This process involves reducing titanium tetrachloride (TiCl4) with sodium (Na) in a steel batch reactor under high pressure and 700-800°C; the product is titanium powders called sponge fines.[3]

$$TiCl_4(g) + 4Na(l) \rightarrow Ti(s) + 4NaCl(l)$$
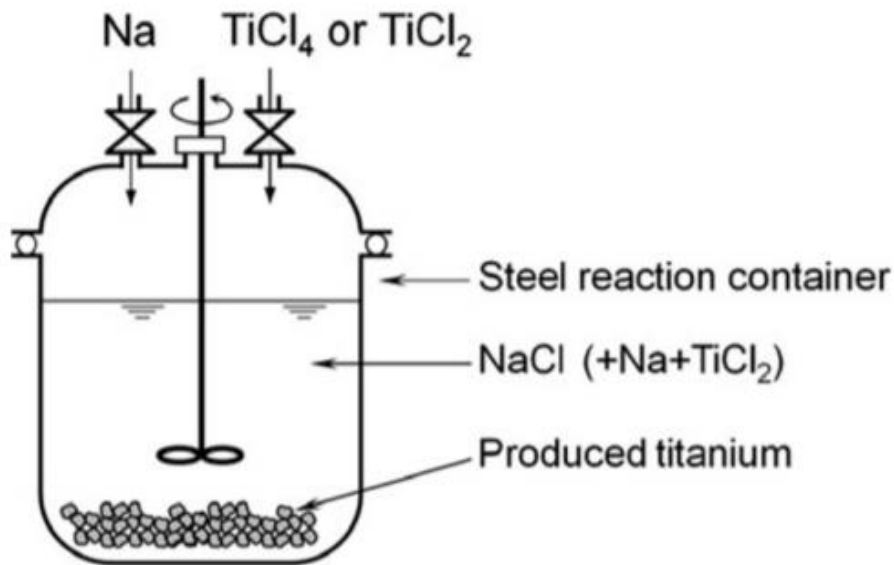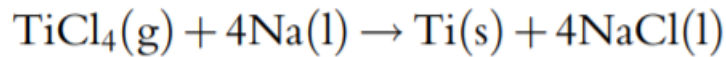
Figure 1.1.2 - Hunter process: reactor and chemical formula.[64]

In 1925, Anton Eduard van Arkel and Jan Hendrik de Boer succeeded in producing highly pure titanium by the disproportionation reaction (pyrolysis) of crude titanium iodides (TiI$_x$). This method is called "iodine process" and despite its low productivity, it had been used for the production of highly pure titanium in the semiconductor industry.

In 1932, to overcome the limitation of the Hunter process, that is the development of high heat and difficulty to separate pure titanium from NaCl, William Justin Kroll, a Luxemburg

metallurgist, substituted sodium with calcium; he took eight years to refine the process that is nowadays known as the Kroll process, where $TiCl_4$ is reduced with magnesium.

$$TiCl_4(l, g) + 2Mg(l) \rightarrow Ti(s) + 2MgCl_2(l)$$
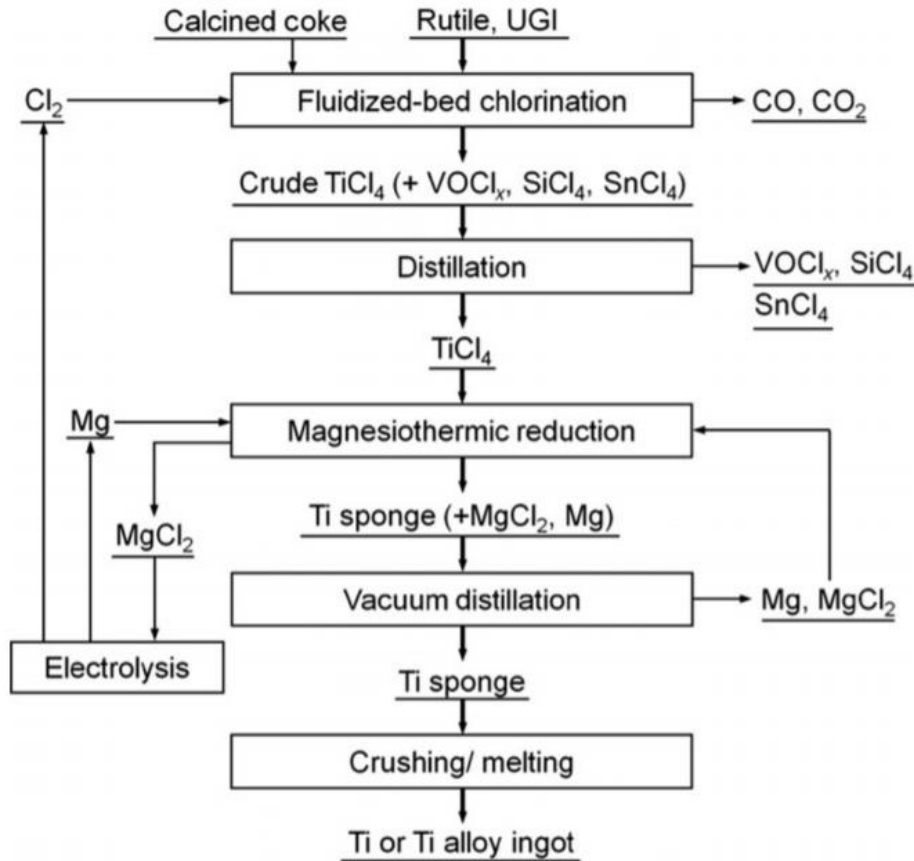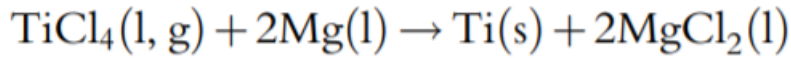
Figure 1.1.3 - Flow diagram Kroll process.[37]

The Kroll process consists of four steps : I) TiO_2 is chlorinated with carbon to produce $TiCl_4$; II) $TiCl_4$ is reduced by magnesium metal, forming "pure sponge titanium" in the inner wall of the reactor and separated the product from unreacted magnesium in the pores by heating and vacuum; III) the Ti sponge is crushed and melted to ingot in a vacuum arc furnace or an electron beam furnace; IV) $MgCl_2$ is electrolyzed into chlorine gas and magnesium.[4]

In the 1950s and 1960s, during the Cold War, the titanium was recognized as a resource of strategic importance in military applications, both in U.S. and Russian. In particular, the interest was turned towards the aerospace industry to produce high-performance jets, thanks to the excellent strength to weight ratio of titanium compared to steel and aluminum. In 1948,

a first large-scale production was started by the DuPont company; however, the U.S. encouraged many other companies from different sectors to increase the market. Similarly, other countries, such as Japan, China, Russia, and the United Kingdom, started the industrial development of titanium and contributed to its market (Figure 1.1.4).[3]

	1950	1980	1995	2005	2010	2013
sponge production	5000	80000	120000	200000	250000	300000
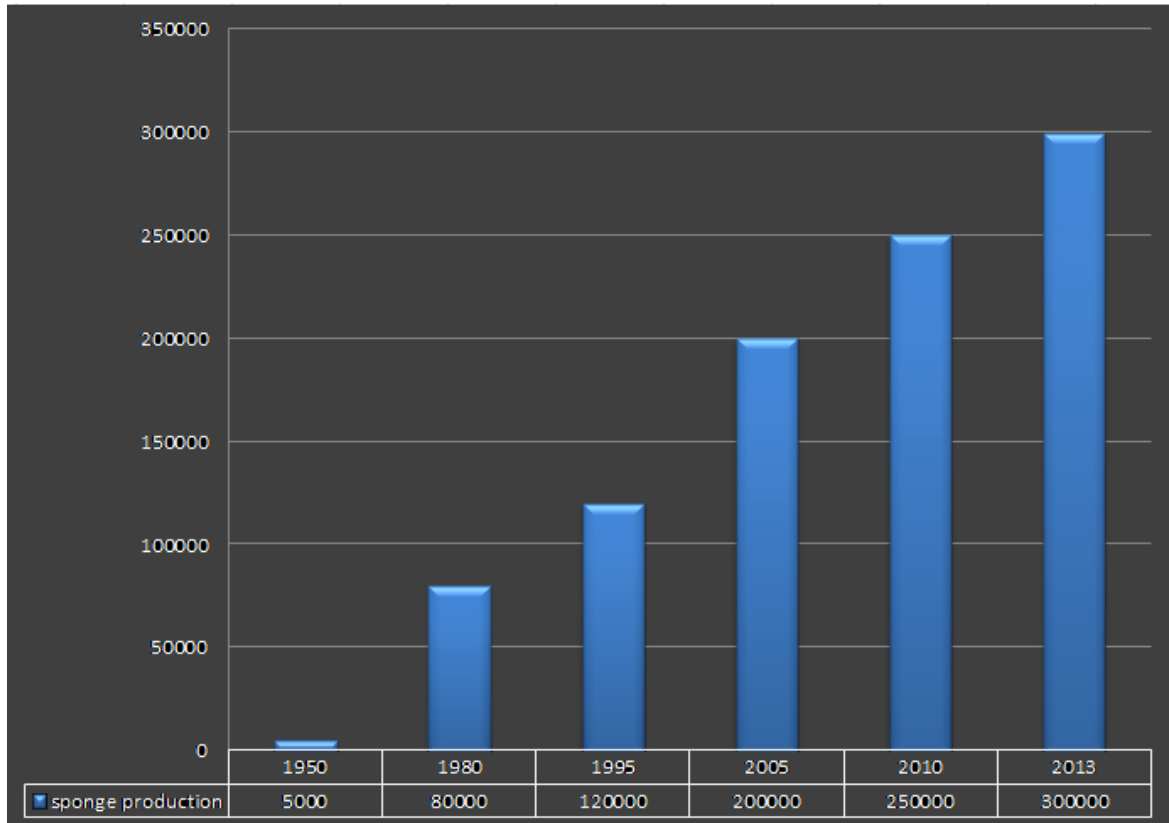
Figure 1.1.4 - World trend of titanium sponge production, in metric tons.[5]

Even today, the aerospace sector is the leading consumer of titanium (about 80%), despite cycles of high and low demand; but also other markets, such as architecture, chemical processing, medicine, power generation, marine and offshore, sports and leisure, and transportation are gaining ground.[6]

1.1.2 – Main aspects

The Universe is characterized by the presence of titanium, as matter of fact it has been found in interstellar dust, in stars and in meteorites, beyond our Earth's crust [7]. In this latter, its percentage is around 0.6%, thus occupying the position of the ninth most abundant element and fourth if compared to structural metals, after aluminum, magnesium and iron.

Titanium (Ti) is located in the periodic table at number 22, in the IV group, and it is a transition metal (Figure 1.1.5); in standard conditions, it is solid and has a silvery gray color.
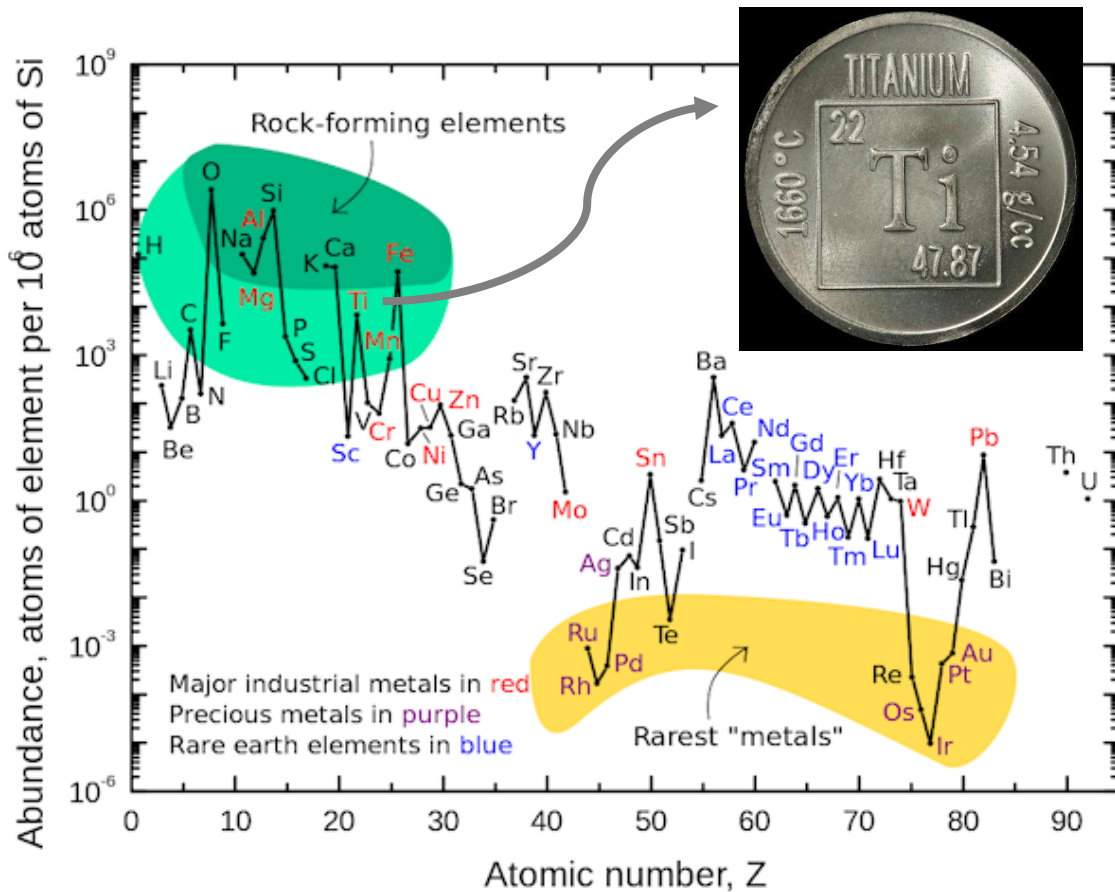
Figure 1.1.5 - The abundance of elements on the Earth's crust respect to their atomic number.

Its properties can be concentrated in two concepts: **high strength-to-weight ratio and excellent resistance to corrosion**.

Titanium with its **density** of 4.51 g/cm^3 is the heaviest of light metals. Although twice as heavy as aluminum, the classic light metal has only half the specific weight of iron or nickel (Figure. 1.1.6).
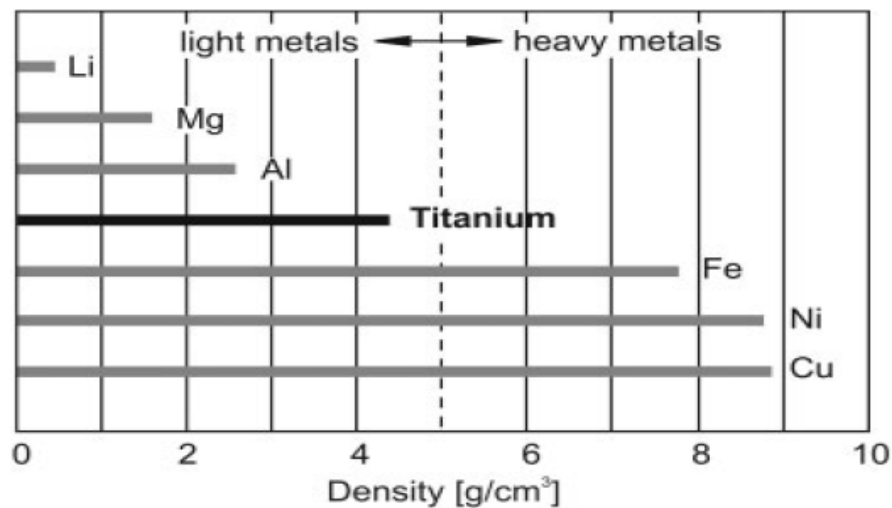
Figure 1.1.6 - Comparison of specific weight values of some metals.

The **mechanical resistance** is high in the various forms of titanium, commercially (CP) pure or in alloy; for example, CP-Ti shows an ultimate tensile stress comparable to some low-grade steel and twice as much as some 6061 aluminum alloys. Furthermore, the low modulus of elasticity absorbs a lot of elastic energy and therefore undergoes considerable deformations. Table (1.1.1) shows the comparison between Ti-6Al-4V, a carbon, low alloy and stainless steel and Al 7075-T6, materials that can be used for structural purpose.

Table 1.1.1 - Mechanical properties of some structural materials.[8][9][10][11][12]

	Density (g/cm3)	Tensile Stress (N/mm2)	Yield Stress (N/mm2)	Elongation to break (%)	Young Modulus (GPa)
Ti 6Al 4V	4,4	950	880	14	114
AISI 1015	7,8	425	325	37	200
AISI 1340	7,8	703	434	25,5	200
AISI 314	7,8	689	345	40	200
Al 7075 T6	2,7	600	530	8	70

The **corrosion resistance** of titanium is due to the natural passivation of the surface when it is in contact with oxygen, in air or in aqueous solution. The oxide which forms is generally reported with the formula TiO_2, also called titania, but the structure is more complex: in direct contact with the metal, there is the formation of TiO, subsequently an intermediate TiO_x level and finally the TiO_2 configuration in contact with the environment.[13]

The spontaneous oxide can be 10 nm thick and prevents from the further oxidation of the metal, moreover it allows a certain immunity from a vast range of acids and oxidizing or reducing environments.

It is possible to improve the corrosion resistance through the surface composition, such as the addition of small quantities of palladium (Pd), or increasing the thickness of the oxide, through anodization, chemical or thermal oxidation.

Other qualities of titanium are:

- complete **non-magneticity** allows it to be used in fields where the formation of magnetic interference is to be avoided;

- the total **biocompatibility** and **non-toxicity** of the material allows its full and advantageous use in the health, biomedical, dental and surgical sectors as well as in the food processing and storage field. Various tests have been carried out to quantify the possible loss of metal due to electrochemical effect in physiological solutions, but in no case tissue destruction was observed in areas containing titanium;[14][15]

- has a particularly **low radioactive half-life**, which makes it suitable for use in the nuclear field.

- the **low coefficients of thermal conduction and thermal expansion** guarantee excellent performance in a whole series of applications characterized by high operating temperature. In this sense, even the quite **high melting temperature** is an advantage.

Table 1.1.2 - Thermodynamic and transport properties of titanium.

Melting Point	1668°C
Thermal Expansion Coeff.	~8,6 µm/(m*K)
Thermal Conductivity	16-22 W/(m*K)
Electrical Conductivity	1,798*10^6 (S/m)

However, it does not present itself in a pure state and it is difficult to find it in high concentration in nature; it occurs in the form of complex oxides in igneous rocks, the major sources being rutile [16] (with 95% of TiO_2), leucoxene [17] (about 90% of TiO_2)(Figure 1.1.7) and ilmenite (between 50/60% of TiO_2).

Figure 1.1.7 - On the left, rutile mineral from U.S.A. On the right, leucoxene mineral from Germany.

Titanium, in its pure metallic form, crystallizes in two forms: the hexagonal close-packed structure (HCP), also called alpha titanium, and the body-centered cubic structure (BCC) or beta titanium; each is stable in a defined temperature range. The beta transition temperature, or allotropic temperature, is 882°C for the pure state (Figure 1.1.8).

A first classification of titanium alloys can be based on the type of structure, and they are four: alpha, beta, alpha-beta alloys and intermetallic (like Ti_xAl, where x = 1 or 3). The choice of alloy elements influences the type of alloy by modifying the allotropic temperature and thus its physical, mechanical and technological properties, that are determined by the arrangement, volume fraction and individual properties of the two phases α and β (Table 1.1.3).
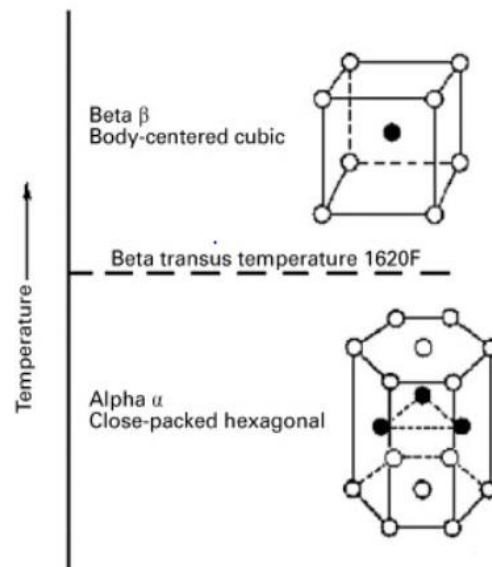
Figure 1.1.8 - The crystal structure of pure titanium: alfa e beta.[37]

The α-alloys are the unalloyed commercially pure (CP) titanium family and the alloys with small trace of aluminum tin or interstitial elements, like oxygen, nitrogen or carbon; while the β-alloys show these elements: Mo, V, Ta, Fe, Mn, Cr, Co, Ni, Cu, Si, and H.[6][18]

Table 1.1.3 - Properties of α, α+β and β Ti alloys.[6]

	α	α+β	β
Density	+	+	-
Strength	-	+	++
Ductility	-/+	+	+/-
Fracture toughness	+	-/+	+/-
Creep strength	+	+/-	-
Corrosion behavior	++	+	+/-
Oxidation behavior	++	+/-	-
Wendability	+	+/-	-
Cold formability	--	-	-/+

In aerospace, for example, alloys with a mix of α and β phases are used, the former to maintain a high resistance to corrosion and high temperatures, the latter for mechanical strength properties. For non-aerospace applications, α-alloys are generally used for their best anticorrosive properties (Table 1.1.3), these include commercially pure titanium and alloys with added platinum group metals (PGM)[19].

Titanium aluminide (Ti_xAl) shows potential for applications up to 900°C, as for gas turbine engines requiring low-density alloys with enhanced mechanical properties at high temperatures (Figure 1.1.9). The major disadvantage of this alloy group is the low ambient temperature ductility.[18]
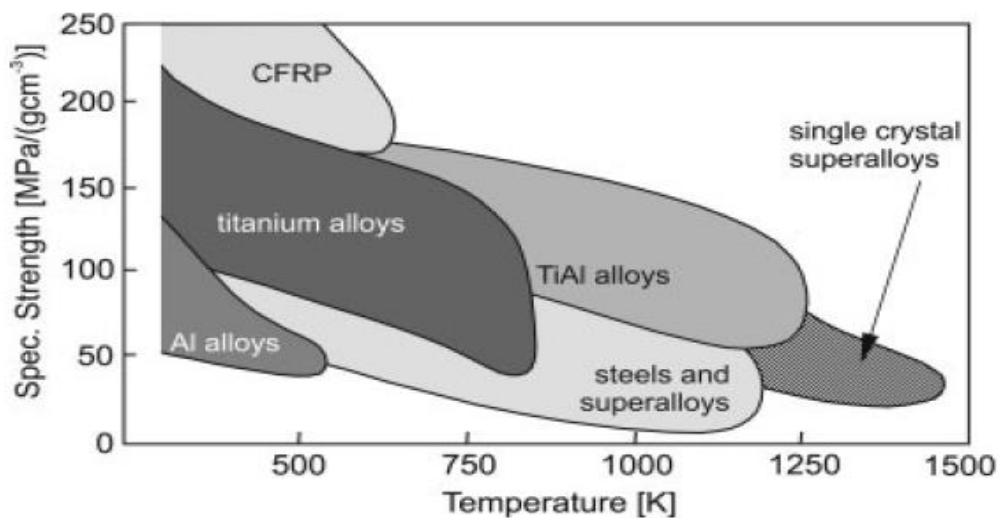
Figure 1.1.9 - Structural materials graphic with specific strength vs temperature.[6]

9

1.1.3 – Commercial classification of Titanium by ASTM

The known number of titanium alloys are nowadays more than 100; only thirty of these are used commercially. The Ti-6Al-4V, developed for the first time in 1950, covers more than 50% of usage. Unalloyed titanium covers 20-30% of total consumption; more properly defined as commercially pure (CP-Ti) with different Grade, from 1 to 4, based on the concentration of impurities.[6]

The Table 1.1.4 shows the values of alloy elements and impurities in the different Ti Grade alloy, from 1 to 7, according to American Society for Testing and Materials International (ASTM International).

Table 1.1.4 - Ti Grade from 1 to 5 and 7 composition by ASTM International.[20]

Element	Commercially Pure					Ti-6Al-4V
	Grade 1	Grade 2	Grade 3	Grade 4	Grade 7	Grade 5
Nitrogen	0.03	0.03	0.05	0.05	0.03	0.05
Carbon	0.08	0.08	0.08	0.08	0.08	0.08
Hydrogen	0.015	0.015	0.015	0.015	0.015	0.015
Iron	0.20	0.30	0.30	0.50	0.30	0.40
Oxigen	0.18	0.25	0.30	0.40	0.25	0.20
Aluminum	-	-	-	-	-	5.5-6.75
Vanadium	-	-	-	-	-	3.5-4.5
Palladium	-	-	-	-	0.12-0.25	-
Titanium	Balance	Balance	Balance	Balance	Balance	Balance

The Table 1.1.5 shows the properties of commercially pure titanium, from Grade 1 to 4 and 7, and the Ti-6Al-4V alloy.

Table 1.1.5 - Properties comparison between CP-Ti Grade 1-2-3-4-7 and Ti-6Al-4V.[21]

	Commercialy Pure				Ti-6Al-4V
	Grade 1	Grade 2	Grade 4	Grade 7	Grade 5
Rm (MPa)	240	345	550	375	900
Rp 0.2 (MPa)	170	275	485	345	830
Elongation (%)	24	20	15	20	10
Hardness	120 HB/30	160HB/30	250 HB/30	160HB/30	36 HRC
Modulus of elasticity (GPa)	103	103	107	107	110
Weldability	Excellent				Good
β Transition (°C)	882	900	940	900	1000

1.1.4 – Market and applications

Titanium, despite its massive presence on earth, is considered a precious metal, as its extraction and processing (Figure 1.1.10) are very expensive. Along with other metals, such as aluminum and steel, its industries are limited in number, and this leads to an oligopolistic market, where the price appears to be higher than in competitive market products. Last but not least, the value is influenced by the variability of consumption demand in current applications and the development of new fields of application [22]. The titanium market is divided into two segments: in the form of TiO_2 pigments which collects 95% of the market and in the form of a titanium sponge which takes the remaining 5%.

Production Stage	Steel	Aluminum	Titanium
Metal refining	0.4	1.0	5.0
Ingot forming	0.6	1.0	10.7
Sheet forming	0.4	1.0	18.0

SOURCE: Hurless and Froes, 2002.
NOTE: Process costs were estimated in dollars per cubic inch of the relevant material and then normalized to the cost of aluminum.

Figure 1.1.10 - Cost comparison of the stages of metal production.[22]

Titanium dioxide pigment has been in use as a pigment and opacifier for more than 50 years. It is used to enhance color and quality, by its excellent whitening, high refractive index and light scattering capabilities. The fields of application are in paints, paper, plastics, ink and rubber. The paint and coatings sector is the largest consuming market for TiO_2 pigment, with a contribution of 58% to global usage, followed by plastics (22%), such as food packaging, paper (9%) etc. Other uses of TiO_2 pigment include catalysts, ceramics, coated fabrics and textiles, floor covering, printing ink, also in tattoo, roofing granules and cosmetic, for example in nanosized for sunscreens to protect from UV radiations.[23]

Titanium metal products, originating from its sponge, were initially, during the Cold War, centered in the military sector; particularly in the production of jets, to reduce their weight thanks to the low density of titanium, but to maintain the mechanical properties at high temperatures, replacing steel and aluminum. In a completely natural way, its use has also involved commercial aviation, especially thanks to long-term contracts with large

companies, such as Airbus and Boing [24]. In the Table 1.1.6, examples of titanium alloys used for structural parts and for engines in aircraft can be found [25]. The demand for metal required in the aerospace field increases by about 20% per year, despite the different fluctuations in the past.[26]

Table 1.1.6 - Selected aerospace system and parts vs titanium alloys.[25]

Systems and parts	Materials
Airframe structures	
Hydraulic tubing	Ti-3Al-2.5V
Floors	CP-Ti
Landing gear	Ti-10V-2Fe-3Al; Ti-6-6-2
Windows frames	Ti-6Al-4V
Springs	Ti-15V-3Cr-3Sn-3Al
Gas turbine engines	
Fan discs and blades	Ti-6Al-4V; Ti-6-2-4-2S
Compressor disc	Ti-6Al-4V; Ti-6-2-4-2S
Compressor blades	Ti-6Al-4V; Ti-6-2-4-2S
Compressor stators	Ti-35V-15Cr
Nozzle assembly	TIMETAL 21S

Titanium provides an economically efficient material in many corrosive environments. The corrosion resistance prolongs the life cycle of equipment and reduces the maintenance costs. The second sector for consumption of Ti (about 20-30%) is the industrial field, mainly in chemical and petrochemical plants and for the heat transfer. Heat exchangers, exhaust coatings and piping systems are widely used in different industrial sectors. Due to its superior resistance to seawater, titanium is also used in offshore rigs, ships' propellers and rigging, desalination plants, in submarine ball valves, fire pumps; during the processing of aggressive compounds like nitric acid, organic acids, chlorine dioxide, inhibited reducing acids and hydrogen sulfide, titanium is an excellent material choice also for vessel, tanks and agitators; in the hydrometallurgical extraction of metals from ores, in form of electrodes, even in the food and pharmaceutical industries and in power plants [27]. The industrial sector shows a growth demand for titanium having values around 4% per year. [25][27][26]

The remaining market is divided: in the automotive sector, but given the high cost it is concentrated in the racing sector or high-end vehicles and in the nuclear storing waste [28]; in biomedical applications, as a substitute for stainless steel or cobalt alloys; examples include artificial hip joints, artificial knee joints, bone plates, screws for fractures, cardiac valve prostheses, peace-makers, and artificial hearts [29]. For similar reasons titanium is used in the aircraft industry and in the sporting goods market, such as tennis rackets, lacrosse sticks, golf clubs, bikes, camping gear and more; eyeglass frames, jewelry and watches are just some of the many fashion industries [30]; ; more recently, titanium has also made its way into information industry products (IT): mobile phones, notebooks and mobile accessories, for example with Apple products [31]; Ti is widely used in various building types like museums, temples and shrines as well as in housing, in marine and polluted environment [32].

Table 1.1.7 - Titanium-made consumer products with relative reason for application.[31]

	Scale (t/y)	Material	Corrosion resistance	Light weight	Strength	Flexibility	Thermal conductivity	Non-toxicity	Color development	Surface appearance
Eyeglass frames	450	Wire, plate		O	O	O		O	O	O
Wrist watches	300	Bar, plate	O	O				O		O
Golf clubs	350	Bar, plate	(Alloys)	O	O					O
Cameras	30	Sheet		O	O				O	O
Cooking utensils	40	Sheet	O	O	O		Δ	O		
Outdoor goods	30	Sheet	O	O	O		Δ	O	O	O
Fishing gears	10	Wire	O	O	O					O
Mountain climbing goods	10	Plate		O	O					O
Bicycles	20	Tube		O	O	O			O	O
Wheelchairs	10	Tube		O	O	O		O		
Water purifiers	10	Sheet	O					O		
Ornaments	10	Sheet	O	Δ				O	O	O
Others	30	Various		O	O				O	O
Total	1,300									

Despite the high cost of titanium, its market is constantly spreading in various sectors; this has led to a greater focus on new mining and refining technologies to meet the demand and to reduce costs.

1.2 – Corrosion phenomena

"Corrosion is an irreversible interfacial reaction of a material (metal, ceramic, polymer) with its environment which results in consumption of the material or in dissolution into the material of a component of the environment. Often, but not necessarily, corrosion results in effects detrimental to the usage of the material considered. Exclusively physical or mechanical processes such as melting or evaporation, abrasion or mechanical fracture are not included in the term corrosion." Definition from International Union of Pure and Applied Chemistry (IUPAC) [33]. The term "corrosion" is usually associated with metals, while for polymers and ceramics the term "degradation" is used.

Corrosion phenomena can be divided into three main categories: **general corrosion, localized corrosion and environment-induced cracking** (Figure 1.2.1). Localized corrosion can also be pitting, galvanic, crevice, selective, intergranular, erosion, cavitation and fretting corrosion; in the third category due to the environment, there is stress cracking corrosion (SCC), hydrogen embrittlement and fatigue corrosion.
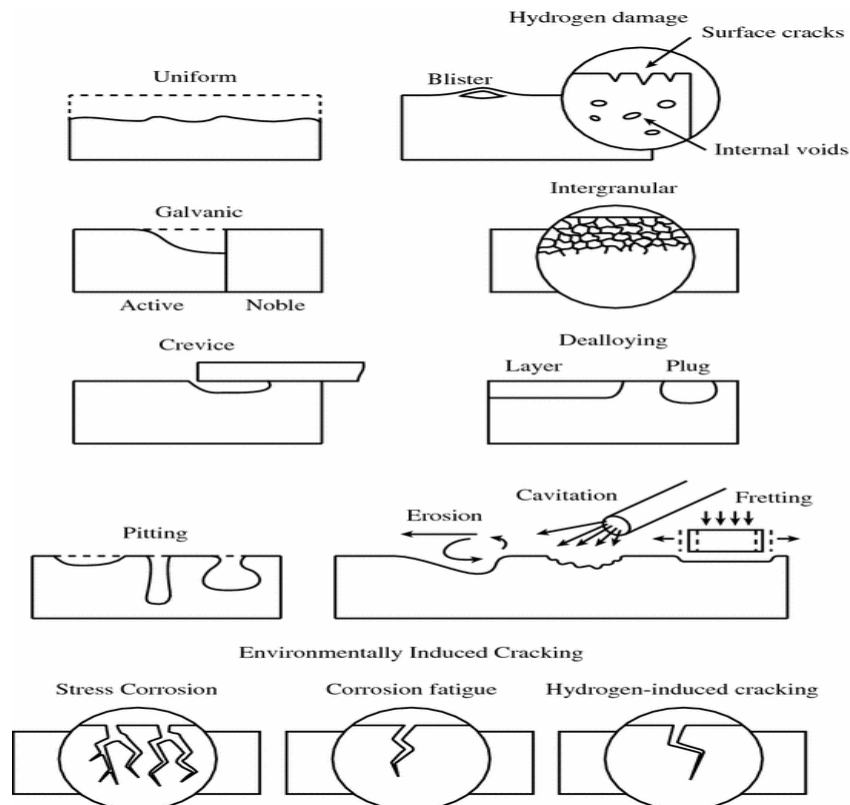
Figure 1.2.1 - Representation of different types of corrosion.[34]

Regardless of the triggering mechanism, in order to have corrosion it is necessary that the **electrochemical processes** take place, to which the metallic material (acting as an anode) and the corrosion environment (which acts as an electrolyte) take part. Corrosion is caused by the development of an oxidation reaction, which takes place at the anode, while a reduction reaction occurs at the cathode. The chemical element involved in the oxidation reaction is mainly metal, while the chemical element involved in the reduction reaction depends on the reaction environment.[35]

Titanium is a very reactive metal against oxygen and naturally develops its oxide (TiO_2), which reaches around 10 nm. Moreover, other metals show a similar behavior and are for example zirconium (Zr), aluminum (Al), tantalum (Ta) and hafnium (Hf) [36]. This oxide is dense, compact and well adherent to the metal surface, it allows to block a further oxidation of the metal and gives a remarkable protection in different aggressive environments; this aspect explains why the valve metals are widely used in the construction of the chemical apparatus.

Despite this, titanium and its alloys can suffer from uniform and localized corrosion, in **strongly reducing acid media**, **pitting** and crack attack **in halogen-containing solutions**, stress cracking in some high-strength alloys, hydrogen embrittlement, fretting corrosion and erosion. Surface treatments practically and economically overcome the limitations of natural oxide to a large extent, by adding a very small quantity (<0.25% by weight) of platinum group metals (**PGM**), or by increasing the oxide film through oxidation techniques such as **anodizing** or chemical/thermal treatments.[37]

1.2.1 – Types of corrosion

1.2.1.1 – Uniform Corrosion

General corrosion, also called "uniform corrosion", is the most common corrosion that can occur both in aqueous and aerated environment. This type of attack proceeds uniformly over the entire exposed surface of the metal. The mechanism involves the dissolution of the metal, the reduction of the cathodic reactant and the uniform formation of corrosion products, as a matter of fact, purely homogeneous corrosive attack is unlikely to occur. There are always areas, especially in complex metal parts, that are corroded faster than the others, determining a surface more or less rough with an irregular covering of corrosion products. The decrease

in thickness of any component, which the loss of its structural characteristics, can be adequately estimated based on previous experiments evaluating the corrosion rate (in mm/y). Through these average values it is possible to calculate the life expectancy of a component and therefore improve it by increasing its thickness in the original design.

Generalized corrosion in some cases may be helpful, as listed below:

- to obtain optimal **surface roughness** conditions (for example in the case of orthopedic implants to promote osseointegration [38]);

- to create at the same time **perfectly glossy finishes**;

- to create **special patterns** on the metal surface (appropriately shielded) (i.e. on molds);

- to produce dies for **artistic used** by the engraving of suitably shielded metal plates (of copper, steel, zinc, titanium) [39];

- to remove oxides and various products to metal surfaces by the **pickling**, which indeed also removes the first layers of metal [38];

- to highlight the structure of metallic materials, from crystalline grains to structural constituents, by the **metallographic attack** [40].[41]

The natural TiO_2 on the surface is thermodynamically stable in a vast range of potentials and pH, as it can be seen in the Pourbaix diagram (Figure 1.2.2); under passive stability conditions, the corrosion rate does not exceed 0.02 mm/y, well below the 0.13 mm/y limit it is considered acceptable in design.[42]
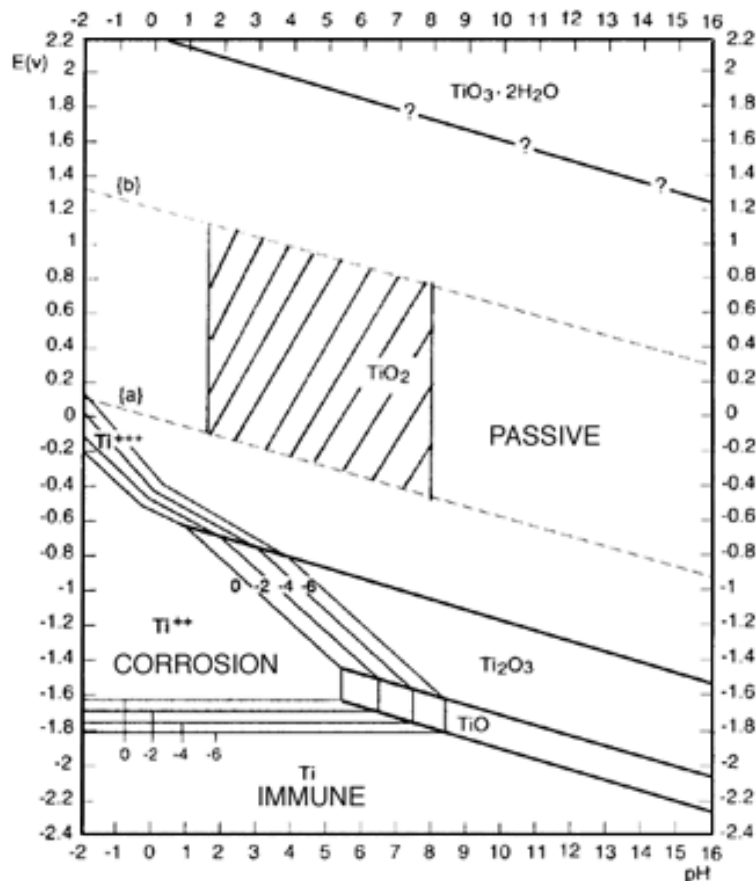
Figure 1.2.2 - Pourbaix diagram of Ti in water, E(V) vs pH.[43]

However, the titanium oxide becomes vulnerable in conditions of strong oxidation, in this case the oxide is dissolved, and in conditions of strong reduction, there is the formation of hydrates.

Uniform corrosion occurs particularly in strongly reducing acids, dissolving the oxide and oxidizing the pure metal into soluble trivalent ions: $Ti \rightarrow Ti^{3+} + 3e^-$. In presence of oxygen in solution, these Ti^{3+} ions pass into the Ti^{4+} state and immediately hydrolyzed to form TiO_2, reducing corrosion propagation; on the other hand, in the absence of oxygen, hydrates are formed on the titanium surface, giving it a silvery gray color.[44]

The nature of the environment in contact with titanium dioxide is thus fundamental, which protects the metal substrate from dissolution, in order to determine its resistance to corrosion.

The **marine environment** usually turns out to be a very corrosive environment due to the presence of different pollutants in the water; despite this, titanium, thanks to its passive layer,

turns out to be immune in almost all conditions. The presence of micro-organisms, which can induce corrosion (MIC), or dry and wet cycles have no effect on it; there is no uniform corrosion up to 260°C [45]. Titanium immunity in sea water offers appreciable advantages in applications in contact with the latter, for example in desalination plants both in low and high temperature regions, or in power plant condensers on the coast; as matter of fact, the heat exchangers reach temperatures of around 130°C, far below the limit for general corrosion [46]. In addition to heat exchangers, titanium is suitable for other applications, including sea water, such as submarine hulls, ships, oil and gas platforms, evaporators for desalination and salt production and water jet propulsion systems. Titanium Metal Corporation (TIMET) is an important American manufacturer of titanium-based metal products, mainly focused on aerospace. It tested titanium in many cases for a very long time, for about tens of years. The surface of the metal in contact with sea water appeared to be discolored even after 30 years with no evidence of corrosion; in addition, no evidence of pitting or crevice corrosion with the presence of marine deposits was found. Exposure of titanium to marine atmospheres or splash or tide zone does not cause corrosion (Figure 1.2.3). It has also been reported that Ti does not suffer erosion and cavitation up to 36 m/s of the fluid flowing.[45]

Alloy	Ocean Depth ft (m)	Corrosion Rate mpy (mm/y)
Unalloyed titanium	Shallow	3.15×10^{-5} (0.8×10^{-6})
	2,362-6,790 (720-2070)	<0.010 (<0.00025)
	4,264-4,494 (1300-1370)	<0.010 (<0.00025)
	5-6,790 (1.5-2070)	(0.0)
	5,642 (1720)	0.002 (0.00004)
TIMETAL 6-4	5-6,790 (1.5-2070)	<0.010 (<0.00025)
	5,642 (1720)	3.15×10^{-5} (8×10^{-6})
	5,642 (1720)	≤0.039 (≤0.001)

Figure 1.2.3 - Corrosion of titanium in seawater environment.[45]

The medical implants sector has an eye of interest towards titanium, as it is a low density material (4.5g/cm^2) and comparable to human bones (average 3.88 g/cm^2 for men and 2.9 g/cm^2 for women) and at the same time it is biocompatible and non-toxic. These factors are closely linked to the anticorrosive properties that limit the amount of ions released into the environment in which they are placed, reducing a possible rejection [47]. Combining the

previous properties of titanium with high mechanical strength, it is an excellent choice for orthodontic, prosthetic and cardiovascular implants. The inspection and maintenance of these devices are usually not possible and as they must withstand their entire life in the human body, in constant contact with different types of fluids potentially changing, priority is corrosion resistance. This aspect, already naturally optimal for titanium, can be improved through an anodizing process, increasing the thickness of the oxide; furthermore, if properly tuned, it leads to the growth of hydroxyapatite ($Ca_5(PO_4)_3(OH)$), the main constituent of bone tissue which, however, requires a high surface roughness, improving osseointegration, but at the same time affecting corrosion resistance [48]. The presence of Ca and P ions, another important requirement of bone-like Ti apatite, induced by ion implantation counterbalances the effects of roughness, being a well-known technique to improve anti-corrosion characteristics [49]. The Simulated Body Fluid (SBF) test is the most widely used investigation technique to evaluate the corrosive and bioactive behavior of titanium. This procedure, which is fast and inexpensive, reproduces the inorganic part of human plasma through a supersaturated solution of calcium phosphate with pH 7.4 [50]; although, changes in pH and composition in the human body may occur due to external agents, such as toothpaste containing fluoride [51], or phenomena internal to the body including inflammation or the presence of particular bacteria (such as *Streptococcus mutans* in oral cavity [52]).

Environments with different chemicals show different feedbacks from titanium dioxide in terms of corrosion.

Fluoride ions are the most dangerous halogens for titanium, as they have the ability to destroy its passivity, even in presence of oxygen, thus being able to observe a reduction in the open circuit potential (OCP) and an increase in the corrosion rate. Nagakawa et al.[53] identifies how the pH threshold for corrosion with the F^- concentration varies, showing a linear behavior with the concentration in logarithmic scale (Figure 1.2.4). These results were obtained by anodic polarization and immersion tests (OCP monitoring), who were in agreement. A further investigation by the same author concerns the behavior from an aerated solution to a deaerated solution; the shift of the critical pH value from 3.8 to 5.1 with 0.05% in weight of NaF and from 5.5 to 6.0 with 1.0% NaF.
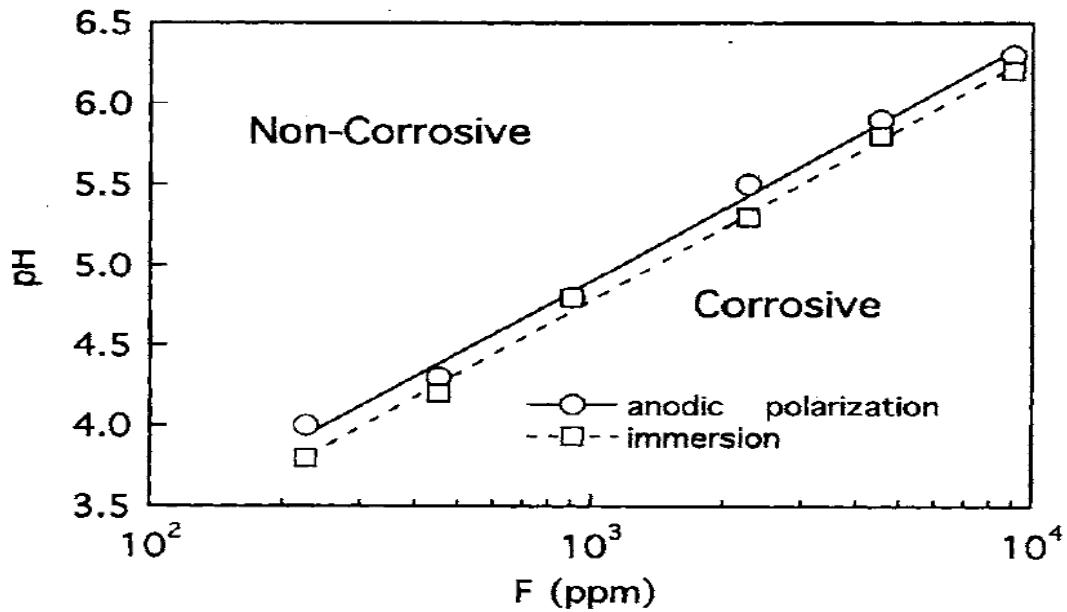
Figure 1.2.4 - Limit values of F⁻ concentration and pH obtained by anodic polarization (circles) and immersion (squares) tests, at which corrosion behavior of titanium changes.[53]

The behavior of titanium can be of three types in solutions containing fluorine: passive, non-passive and active. The definition of these conditions originates itself from the complex impedance plan of the EIS (Electrochemical Impedance Spectroscopy) analysis and suggests the formation of a porous film with a large storage capacity at low pH. The value of the final OCP achieved after a long exposure to different electrolytes with fluorine content is: -0.1 V vs Ag/AgCl in passive conditions, 0.5 V vs Ag/AgCl in non-passive conditions, -1 V vs Ag/AgCl in active conditions [54]. Wang et al. [55] deepens into the interaction between titanium oxide and fluorine ions, in various concentrations, in a sulfuric acid solution at 0.05 M. Potentiodynamic polarization tests show the existence of multiple potentials of corrosion, up to three for 0.001 M and 0.002 M of F⁻; the system shows instability close to the critical value of fluorides. In the Figure 1.2.5, an ideal representation of the potentiodynamic curves is represented: the case of the L3 curve (0.002 M fluoride concentration), in which the intersections of the cathodic and anodic curves are in the active, active-passive and passive region. The limit value for Ti to show spontaneous passive behavior is identified with the point where the maximum anodic current I_m is equal to the cathodic current $(|I_c|)_{Em}$. Above this value, the titanium is in the active state, while below it is in the passive state, showing in this way a good resistance to corrosion.
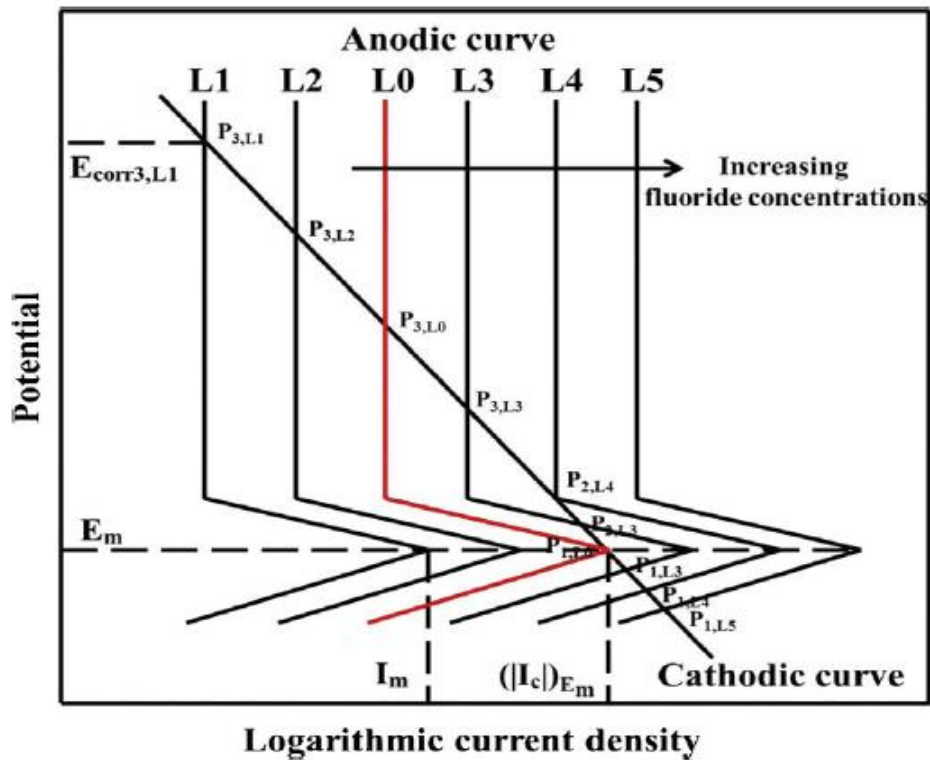
Figure 1.2.5 - An ideal schematic mechanism of the corrosion process of titanium in 0.05 M H_2SO_4 solutions with various fluoride concentrations.[55]

The Figure 1.2.6 shows an ideal representation of what happens to the titanium barrier layer: in absence of fluorides it is compact and adherent; a small concentration of F^- only superficially affects the oxide layer, inducing porosity; once exceeded the critical value of fluorine ions, the barrier layer is totally porous and protects the substrate.
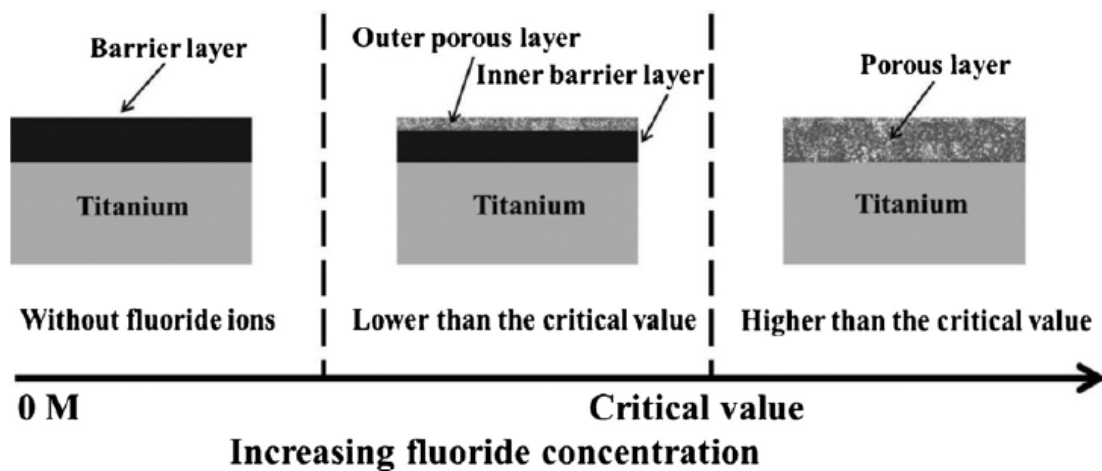
Figure 1.2.6 - Schematic diagram of the influence of the fluoride ion on the structure of the film formed on titanium at OCP in sulfuric acid solution.[55]

If halogens are considered, solutions containing **chlorides** are taken into account. Hydrochloric acid is its pure representation of these solutions; it is a non-oxidizing acid, therefore the resistance of titanium oxide can be compromised. The Table 1.2.1, for aerated, and Table 1.2.2, for deaerated, show that the values of the corrosion rate increase as the concentration and temperature increase. The corrosion resistance is maintained with concentrations up to 5% at room temperature, but at 100°C the HCl concentration must be reduced by 10 times.[44]

Table 1.2.1 - Corrosion of titanium in aerated HCl solutions.[44], [56], [57][56][57]

Concentration [%]	Temperature [°C]	Corrosion rate [mm/year]
0.05	Boiling	0.02
0.1	Boiling	0.10
0.2	Boiling	0.23
0.4	Boiling	0.53
0.5	35	0.001
	100	0.009
	Boiling	0.84
1	35	0.003
	50	0.006
	60	0.004
	100	0.46-2.48
	Boiling	1.83
2	50	0.028
	60	0.016
	66	0.61
	100	7.00
6	25	0.07
	50	2.10
	100	44.45
10	35	1.07
	60	6.80
15	35	2.40
20	35	4.40
37	35	15.00

Table 1.2.2 - Corrosion of titanium in deaerated HCl solutions. (B.P. for border passivity).[44][58]

Concentration [%]	Temperature [°C]	Corrosion rate [mm/year]
1	35	0.003
	Boiling	0.0025-2.0 (B.P.)
3	35	0.13
	Boiling	6.10
5	35	0.28
7.5	35	0.48
10	35	0.76
15	35	1.65
20	35	3.18

In neutral chloride solutions, the corrosion resistance of titanium remains excellent up to extremely high concentrations and temperatures.[44], [58]

In **hydrobromic acid** solutions they act differently on titanium depending on their concentration. As matter of fact, if on one hand there it can increase in passivation of titanium for low concentrations of HBr, on the other hand it tends to dissolve the surface film for high concentrations. In the graphs (Figure 1.2.7), for Ti and Ti-6Al-4V, it is shown how the open circuit potential varies according to the quantity of the acid. Below 1 M of HBr, the oxygen shows a greater affinity with the Ti than with the bromide ions, therefore the oxygen is absorbed on the surface increasing the thickness of the oxide; as a consequence, there is an increase in the OCP, from -0.3 to 0.4 V vs AgCl. As far as concentrations greater than 1 M of Br^- are concerned, there is a removal of oxygen and consequent destruction of the passivity and of the oxide. Another important aspect concerns concentrations between 0.5 M and 1 M: in this case, oxide resists, but it does not grow.[59]
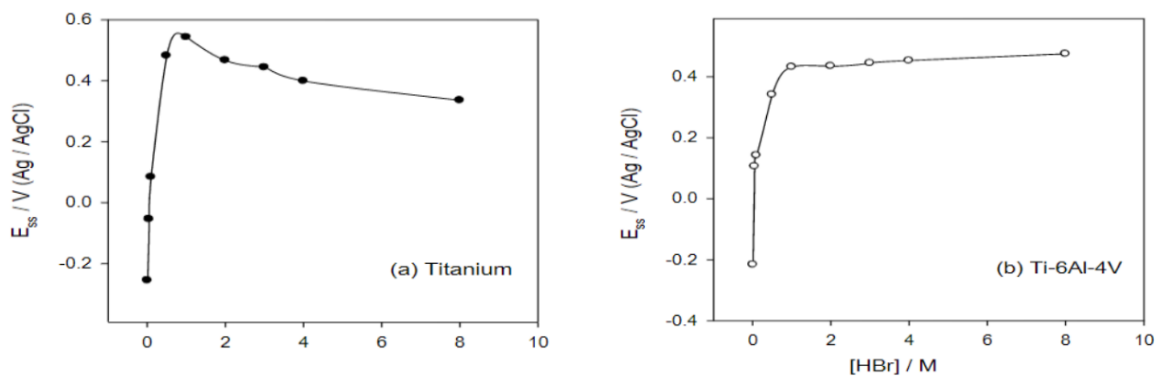
Figure 1.2.7 - Open Circuit Potential as a function of HBr concentration for Ti and Ti-6Al-4V at 298K.[97]

Sulfuric acid is a chemical reagent widely used from chemical manufacture up to the decalcification of heat exchangers in desalination plants, due to the optimal dissolution of carbonates in this acid [60]. The choice of titanium is advantageous, as it can withstand concentrations of 10 wt% at room temperature; however, like other acids, as temperature increases, the resistance to corrosion decreases: for example bringing the acid to 100°C with concentrations of 1 wt.% there is a corrosion rate of 9 mm year [61]. If the variation of the concentration up to 10 wt.% is observed, there is a fairly linear increase in the corrosive attack, then, up to 40 wt.%, the attack on the titanium increases less quickly; from 40 wt.% of H_2SO_4, the corrosion rate decreases to a minimum reached at 60 wt.%, it starts to grow again up to a maximum of 80 wt.%. Corrosion increases dramatically when high temperatures are combined with deaerated solutions; a small addition of oxidizing agents can overcome this problem, thus increasing the corrosion resistance. An example is shown in the Figure 1.2.8.[45]

% H_2SO_4	Addition	Temperature °F (°C)	Corrosion Rate mpy (mm/y)
20	None	210 (99)	>2400 (>61.8)
20	2.5 Grams Per Liter Copper Sulfate	210 (99)	<2 (<0.051)
20	16 Grams Per Liter Ferric Ion	Boiling	5 (0.127)

Figure 1.2.8 - Effects of inhibitors on the corrosion rate of unalloyed titanium in 20% of H_2SO_4.[45]

Table 1.2.3 - Titanium C.R. in mm/year in sulfuric acid with different concentrations and temperature. B.P.is border passivity[44]

Concentration [%]	At 25°C	At 60°C	Boiling T
1	0.0025	0.008	9
2		0.008	
3	0.005	0.013	
4		1.70	
5	0.0025-0.2 (B.P.)		4.8
10	0.25		
40	1.80		
60	0.60		
80	15.00		

Phosphoric acid is another widely used chemical, particularly in the fertilizers production. The attack of this acid on titanium is less weak than HCl, for this reason titanium can be used both in aerated and deaerated conditions up to a concentration of 30 wt.% at 35°C. In addition, in this case, the corrosive attack of H_3PO_4 grows with increasing concentrations and temperature. Titanium shows moderate corrosion in 1% of acid at a temperature of 250°C, showing the formation of a thin layer of titanium oxide phosphate hydrates (Figure 1.2.9); these corrosion products reach a thickness of 25 µm in 24 h with a concentration of 10% of H_3PO_4, but do not show a complete corrosion inhibition [62][63].
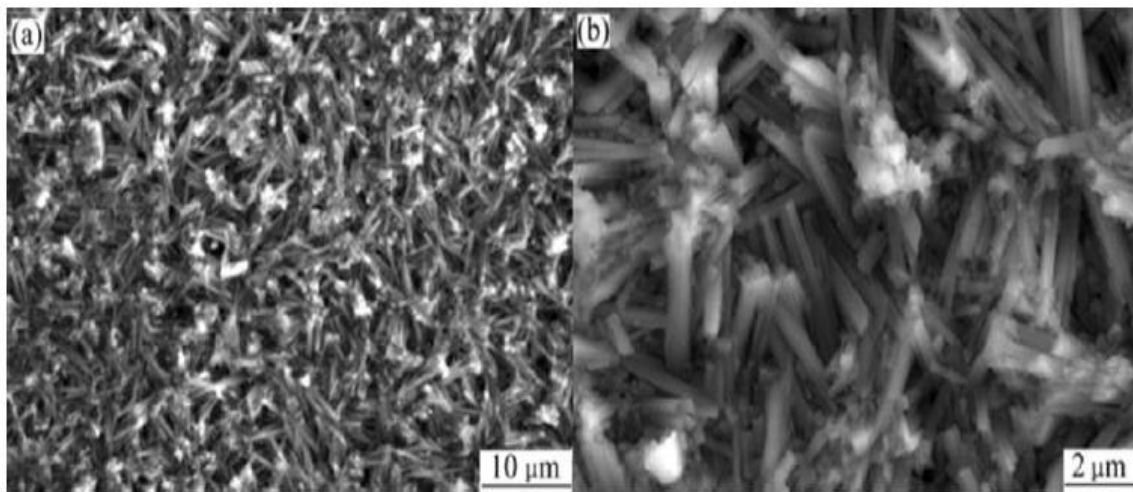
Figure 1.2.9 - Morphology of corrosion products on Ti surface after 24h immersed in 0,1 M of H_3PO_4.[62]

Table 1.2.4 - Corrosion rate of Ti in H_3PO_4 with different concentrations and temperature.[44]

Concentration [%]	At 35°C	At 60°C	At 100°C	Boiling T
1			0.003	0.25
2			Nil	0.86
3			0.99	
5	0.0033	0.06	2.36	3.5
10	0.005	0.09	5.00	
20	0.015	0.33	17.4	
30	0.018	1.5	26.4	
40	0.33			
50	0.46			
60	0.56			
70	0.66			
80	0.74			
85	0.76			

Oxidizing acids do not corrode titanium for a wide range of temperatures and concentrations, as they ensure stability of the oxide. However, in conditions of high oxidation, at high temperatures, there is a low rate of corrosion due to the continuous oxidation of the metal. Moreover, **nitric acid**, which is part of this family of acids, can attack the metal in particular conditions, including its purity. At room temperature, Ti can be considered immune from corrosion up to a concentration of HNO_3 of 65%; in any case, at high temperatures, with concentrated pure acid and in an environment with condensed steam, there is an increase in dissolution. In the Table 1.2.5, values of corrosion rates such as changing temperature and HNO_3 concentrations are reported.[44][45]

Table 1.2.5 - Corrosion rate of Ti at different temperature and concentrations of HNO_3.[44]

Concentration [%]	At 35°C	At 60°C	At 100°C	At 190°C	At 200°C	At 290°C
5	0.002		0.015			
10	0.004	0.012	0.023			
20	0.0045	0.017	0.0038			0.36
30	0.0069	0.022	0.10	1.5	3.5	
40	0.0058	0.0175	0.05	2.8	5.0	
50	0.0058	0.010	0.18	2.8		
60	0.0071	0.008	0.05	1.5		
69.5	0.011	0.0079	0.019			
70				0.38		1.1
98	0.002					

In the Figure 1.2.10 the trend of corrosion with respect to the concentration of nitric acid at different temperatures is shown; it can be highlighted that in the range between 40% and 50% of HNO_3 the corrosion is maximum [64]. High temperature corrosion can be inhibited by adding very small amounts of various metal species such as Si, Cr, Fe, Ti or various precious metal ions (i.e. Pt, Ru).[45]
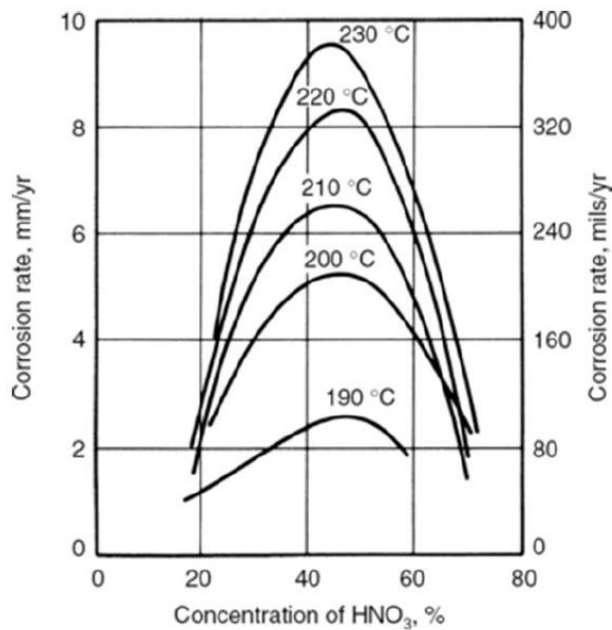
Figure 1.2.10 - CP Titanium's corrosion trend respect concentration of HNO₃ for different high temperatures.[97]
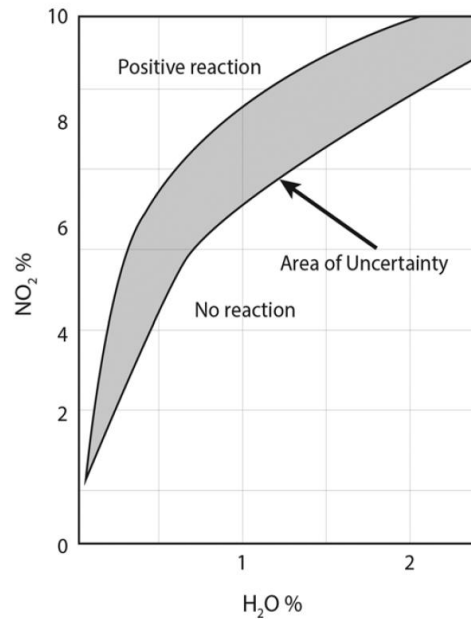
Figure 1.2.11 - HNO₃ composition to avoid pyrophoric reaction of Ti.[44]

While titanium has good anti-corrosion properties in white fuming nitric acid, red fuming nitric acid can be dangerous at high temperatures and concentrations. A pyrophoric reaction is possible, which is always preceded by a rapid corrosive attack, producing consequently fine intergranular particles on pure titanium. These particles detonate in presence of a strongly oxidizing acid, such as fuming nitric acid. A small amount of water inhibits this effect, which is no longer observed after the addition of 2% H_2O, as it can be seen in Figure 1.2.11.[45]

Generally **organic acids** do not affect titanium, either pure or in alloy, except oxalic. Weak acids, such as adipic, hydroacetate, acetates, tannic, benzoic, tartaric and others, have a null corrosion up to 100°C; while, in strong and deareated organic acids, corrosion becomes relevant in condition of increasing temperature and concentrations. Some of these organic acids are formic, lactic, oxalic and trichloroacetic acids. Aeration improves the resistance of titanium in most of these nonoxidizing acid solutions. The importance of the study of titanium in organic acids is not only important in the medical sector, in the form of medical implants of different nature, but also as a standard construction material in chemical plants, for example in the production of acetaldehyde by oxidation of ethylene in an aqueous solution of metal chlorides. The Table 1.2.6 collects values of corrosion rate of different acids at different temperature and concentration parameters.[44][45]

Table 1.2.6 - Collection of Ti corrosion rates in different organic acids at different T[°C] and concentration [%].[45]

Organic acid	Concentration [%]	Temperature [°C]	Corrosion rate [mm/year]
Formic (aerated)	20	200	0.06
	25	Boiling	2.4
	25	100	0.001
	50	100	0.001
	80	200	20.25
	90	100	0.0013
Formic (deaerated)	10	Boiling	Nil
	25	Boiling	2.40
	45	Boiling	11.00
	50	Boiling	7.60
Lactic	10	100	0.048
	25	Boiling	0.028
	50	100	0.008
	85-100	Boiling	0.01
	90-92	180	0.09
	100	Boiling	0.008
Oxalic	0.5	60	2.40
	1	35	0.15
	1	60	0.45
	1	100	21.0
	5	35	0.13
	10	60	11.4
Trichloroacetic	100	Boiling	14.55

1.2.1.2 – Pitting Corrosion

"Corrosion is non-uniform if the time average of the corrosion current through a unit area depends on its position on the surface. Non-uniform corrosion can be due to inhomogeneities of structure or of composition of the corroding material, or to inhomogeneities of the environment. […]" Definition from IUPAC.[33]

Pitting corrosion is a non-uniform corrosion that leads to the creation of small holes or "pits" in the metal. This form of attack is mainly found on passive metals, such as aluminum,

titanium and stainless steel, where the resistance to corrosion is due to the thin layer of oxide on the surface. The corrosive phenomenon involves the localized breakdown of the oxide and then an accelerated dissolution of the metal substrate. The "pit" site is due to the heterogeneity of the surface, as in the case of commercially pure titanium, that are inclusions, second phases, dislocations or mechanical damage; by pitting is meant an attack occurring on an open surface, otherwise, in the case of an occluded area, it is called crevice corrosion. These closely related forms of localized corrosion can lead to accelerated failure of structural components by perforation or by acting as an initiation site for cracking. Pitting corrosion only occurs in presence of aggressive anionic species, such as halide ions. The severity of pitting tends to vary according to the logarithm of bulk anion concentration.

Pitting corrosion is an autocatalytic process: once the pit is formed, it begins to grow and at the same time conditions arise for the growth of the pit. The metal oxidizes in its ions in the pit, causing an increase in acidity that is maintained by the spatial separation of the cathodic and anodic half-reactions. This separation causes a potential gradient and electromigration of aggressive anions into the pit. The cathodic reagent, is depleted inside the pit and this moves the cathodic reaction onto the exposed surface that surrounds it, as this is more abundant; inside the pit there is an enrichment of the metal cations and of the anionic species, which balance the charge of the cations by electro-migrating inside.[65]
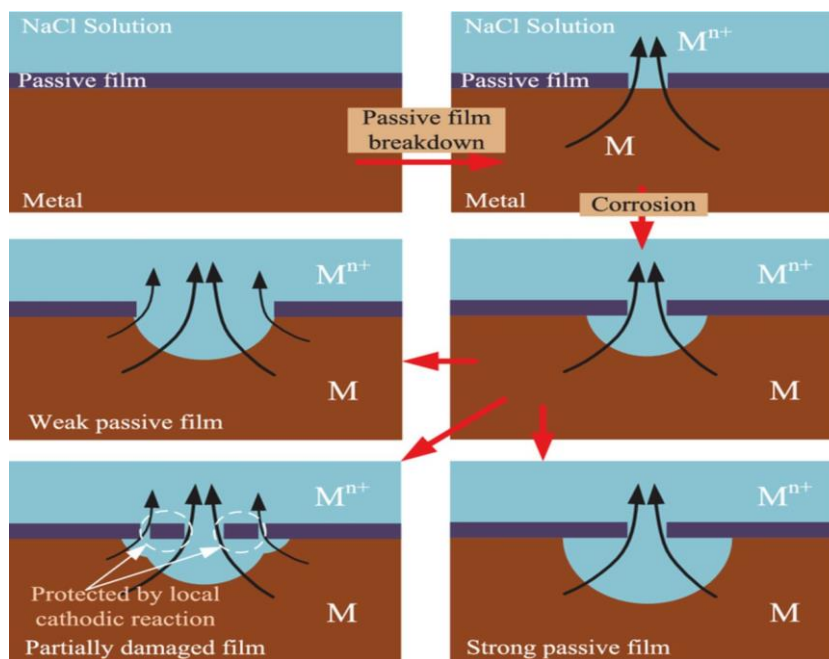
Figure 1.2.12 - Schematic representation of pit involving.[66]

An aggressive acid environment is developed and this development helps the propagation of the pit, from the reaction [65]:

$$Me^{2+} + 2H_2O \rightarrow Me(OH)_2{}^+ + 2H^+$$
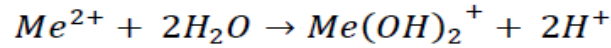
In order to study this type of corrosion, the fundamental parameter is the **pitting potential (E_{pitt})**; as matter of fact, it has been observed that the electrochemical depassivation, or pitting, appears only above a certain potential, starting almost immediately as a function of the scanning speed of the experiment; on the contrary, below this value, the material is safe regardless of the duration of the exposure. The E_{pitt} depends on the environment in which the material is immersed, on the temperature, on the pH and on the type of material itself. The second fundamental parameter to consider is **the potential for re-passivation or protection (E_{rp})**. In the case of a potential between E_{pitt} and E_{rp}, defined area of imperfect passivity, there is no formation of new pits but those already existing continue to grow; the pits stop only when the potential becomes inferior to E_{rp}, zone of perfect passivity, whose value is linked to the occlusion of the pit.[66] (Figure 1.2.13)
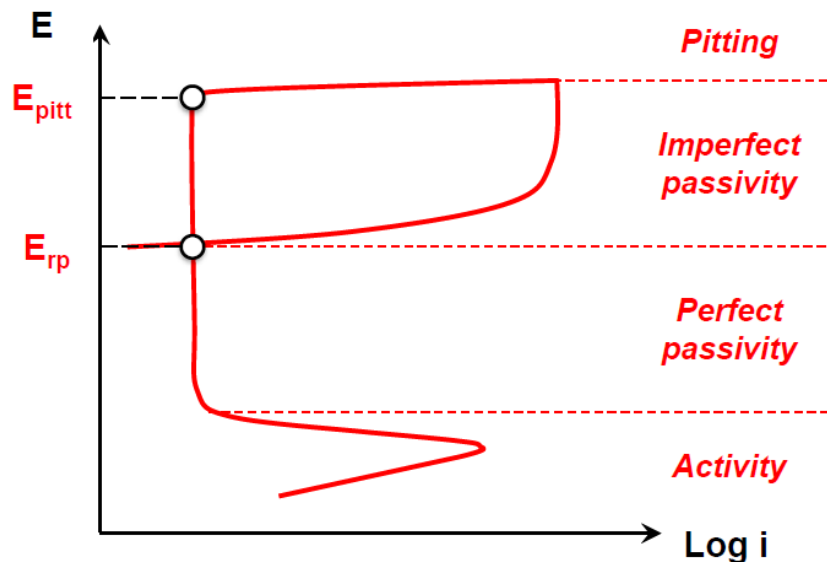
Figure 1.2.13 - General Evans diagram for a material with passive behavior.

The surface oxide of titanium, mechanically strong and chemically inert, has excellent resistance to pitting corrosion in many environments; however, it can suffer anodic dissolution in severe working conditions. The pitting attack is strongly influenced by the temperature and concentration of the halogens, which follow this order of severity $Cl^- < I^- <$

Br⁻ for titanium, with the exclusion of F^- because it usually attacks in the form of uniform corrosion.[67]

In **chloride ion** solutions, the attack requires much higher potential values than the spontaneous corrosion potential and the accumulation of oxychloride at the metal/film interface causes the oxide film to break as a nucleation event. The presence of oxidizing metal ions can cause serious pitting, since the E_p value follows the sequence: no addition > $FeCl_2$ > $FeCl_3$ > $CuCl_2$. In contrast, the addition of oxygen-containing anions, in particular SO_4^{2-}, SeO_4^{2-}, CrO_4^{2-} and HPO_4^{2-} delays the corrosion of Ti in solutions containing chloride.[44]

In titanium, the strongest pitting corrosion occurs in solutions containing **bromide ions**. Experimental data show a much lower E_{pitt} bromide solutions than those in Cl⁻ ion solutions; this suggests a strong chemical interaction between titanium dioxide and bromides ions. In the oxide sites, with relatively high conduction in relation to the film that surrounds it, there is a break with a chemical type mechanism. The failure of the film does not occur with thermal and electrical mechanisms. In the Figure 1.2.14, an explanation of how the mechanic happens: A) the oxide is stable below 1.2 V vs Ag/AgCl; B) there is the oxidation of Br⁻ in Br_2 and the thickening of TiO_2 reducing its local conductivity; C-D) chemical absorption of bromide ions leading to the dissolution of the oxide and the development of the pit.[44][68]
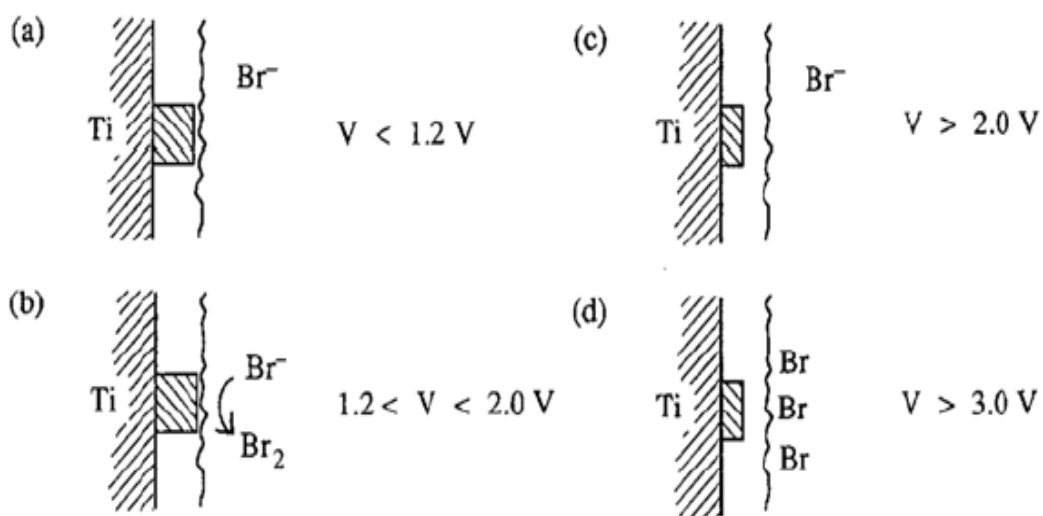
Figure 1.2.14 - Schematic drawing of the proposed sequence of events occurring during voltammetric scan of Ti electrode in 1M KBr, 0.05M H₂SO₄.[68]

Table 1.2.7 - Pitting potential of Ti in two different bromides solution (room T).[44]

Solution	Concentration	E_{corr} [V vs SSC]	E_{pitt} [V vs SSC]
NH₄Br	1 M	-0.33	0.98
	4 M	-0.40	0.90
	Saturated	-0.50	
NaBr	0.01 M	-0.55	1.60
	0.1 M	-0.56	1.24
	1 M	-0.56	0.90
	Saturated	-0.51	

1.2.1.3 – Crevice Corrosion

Crevice corrosion is usually associated with stagnant solutions between two surfaces in contact (metal/metal or metal/non-metal); for example: gaskets, washers, insulating material, fixing heads, surface deposits, unbound coating, threads, splice joints and clamps. Titanium is affected by this corrosion only in hot chloride solutions strongly depending on temperature, generally higher than 70°C and regardless of the pH; while if the latter is higher than 10, the crack starts regardless of temperature, although a 50 μm gap is required to initiate the cracking phenomena.

The corrosion phenomenon is divided into three phases: initiation, propagation and repassivation. When the passivity is locally broken and, due to the occluded geometry, the oxygen cannot permeate to favor the re-passivation, the dissolution occurs inside the fissure, therefore acidifying the internal environment. In the crevice, the halides or sulfide spread inside, in order to balance the charge. The deposition of corrosion products occurs when conditions of neutrality are arise encountered. During the propagation phase, oxygen is reduced to the periphery of the crevice; the reduction of oxygen decreases and the evolution of hydrogen increases over time, causing the penetration of corrosion into the crack; for longer times, the penetration of corrosion is controlled by the ohmic fall between the anodic and cathodic regions, the cathodic reaction causes an increase of the local pH which leads to a possible re-passivation. After 30 days, the penetration is maximum and develops only laterally.[69][44]

The presence of iron, as an impurity, inside the commercial titanium affects this corrosion; for high iron concentrations, the Ti_xFe formula is obtained, which acts as catalytic sites for the evolution of hydrogen, increasing the pH, reducing the corrosion rate and eventually promoting re-passivation. Oxidizing species, such as oxygen, chlorine, ferric ions and cupric ions, inhibit general corrosion, but accelerate the kinetics of cathodic reduction in crevice corrosion, thus increasing the corrosion rate; these species do not penetrate into the crevice and therefore do not inhibit the attack. On the other hand, certain anionic oxidizing species, such as NO_3^-, ClO_3^-, OCl^-, CrO_3^-, ClO_4^-, and MnO_4^- can migrate into the crevice and inhibit crevice attack in halide solutions.[44]

1.2.1.4 – Environment Induce Cracking

The simultaneous action of particular environments, which by nature are only slightly corrosive or even completely harmless, along with the action of tensile stresses characterized by forces lower than those required to cause purely mechanical breakages, can give rise to the formation of cracks, causing them to break.

Stress corrosion cracking (SCC) depends simultaneously on three parameters: a susceptible material, a sufficiently aggressive environment and sufficient tensile stress; if one of these criteria is missing, the corrosion can be eliminated or reduced considerably: for instance the material can be modified or the environment can be changed. Tensile stresses can be external, applied directly, or residues, due to manufacturing or strengthening processes. The SCC mechanism can be divided into two categories: in anodic dissolution of the metal at the tip of the crack and hydrogen embrittlement. The first process begins at the localized site of corrosion, such as the pit or the crevice, and propagates in a non-severe manner; the second phenomenon is based on the absorption of hydrogen atoms, produced by its evolution, within the crack tip and its diffusion into the metal, giving rise to embrittlement. Commercially pure titanium is generally resistant to SCC except in few specific environments, such as aqueous halides, anhydrous methanol, nitrogen tetroxide (N_2O_4), red fuming nitric acid, liquid or solid cadmium, liquid mercury.[44][70]

Hydrogen-induced cracking, abbreviated **HIC**, requires more hydrogen than absorbed from the previous case. When hydrogen is absorbed into the metal, it causes embrittlement depending on the nature of the metal. There are three forms of hydrogen embrittlement:

internal (resulting from hydrogen trapped during processing), external (diffusion of hydrogen in the metal matrix without the formation of new phases) and reaction. The latter is the form found in titanium and consists of the chemical reaction of the hydrogen mixed with the metal, forming new phases, hydrides and methane gas bubbles created by the presence of carbon in the grain boundaries, that generate voids possibly leading to failure. Crevice corrosion can be a source of hydrogen atoms by the reaction: $Ti + 4H^+ \rightarrow Ti^{4+} + 2H_2$; but non-crevice source or inert crevice could also be sustained corrosion by reaction with water under neutral conditions, following the slow-rate reaction: $Ti + 2H_2O \rightarrow TiO_2 + 2H_2$. During the first step, the hydrogen generated must pass through the TiO_2 film before absorption into the underlying titanium alloy. Absorption occurs through the redox transformation ($Ti^{4+} \rightarrow Ti^{3+}$) in the oxide film [71]; this requires a significant cathodic polarization of the metal, obtainable in the field only by galvanic coupling with other active materials (i.e. carbon steel) or the application of a cathodic protection potential. When titanium with low hydrogen concentrations is stressed at low speeds, a plastic collapse is observed without any rapid unstable fractures. Ductile collapse prevents the fragile fracture in these circumstances, because the plastic deformation prevents from reaching a sufficiently high stress. Above a critical hydrogen value, a rapid fracture occurs with a relatively low stress intensity factor and plastic collapse is no longer observed.[72]
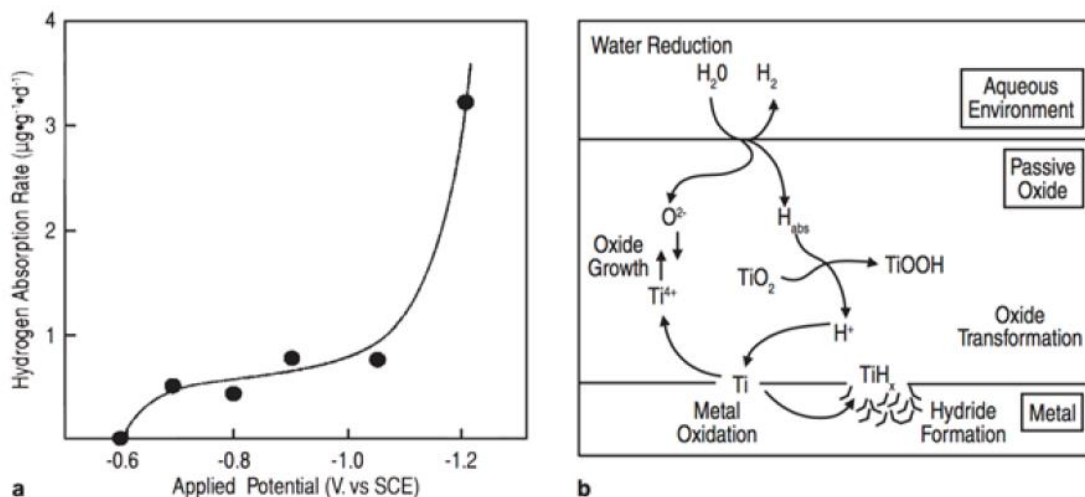
Figure 1.2.15 - a) Hydrogen absorption rate as a function of applied potential on Ti in artificial seawater at 30°C, b) a schematic representation of the cathodic transformations occurring in TiO₂ films, after hydrogen absorption.[71]

1.3 – Surface Treatments

Titanium has an excellent resistance to corrosion thanks to its passive layer that forms spontaneously; despite this, it reaches a value of about 10 nm, which suffers from corrosion in particularly aggressive environments. To overcome this problem, the surface treatment of the metal is fundamental. These treatments can change the chemical composition of the surface, the problem with these techniques is that they are expensive. Otherwise, to improve the corrosion resistance of titanium, it is possible to work on TiO_2 thickness through chemical or thermal oxidation or with anodizing processes.

1.3.1 – Alloying with ennobling elements

The addition of ennobling elements in titanium significantly improves corrosion resistance in strongly reducing environments. These are divided into two groups: the first group gives more stability to the Ti-oxide and includes molybdenum, zirconium and chromium, thermodynamically more stable and resistant to acids [37]; the second group is called platinum group metals (PGMs), which includes palladium, platinum and ruthenium. The PGM, along with nickel, accelerate hydrogen evolution reactions (HERs), facilitating cathodic depolarization in reducing acids; very small addition of them bring to a drastic reduction in the corrosion rate (Figure 1.3.2).
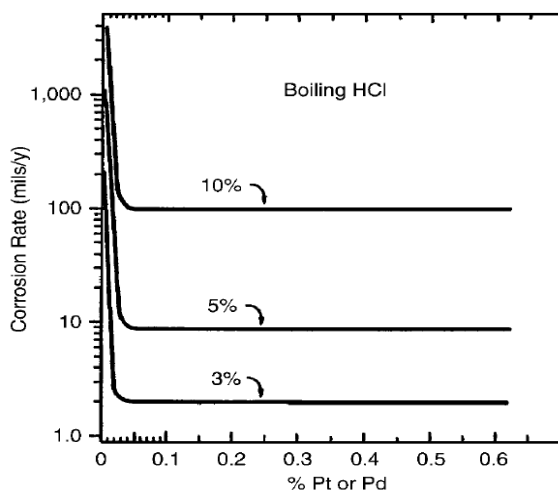
Figure 1.3.2 - Effect of minor PGM alloying additions to titanium on corrosion rate in dilute reducing acid.[96]
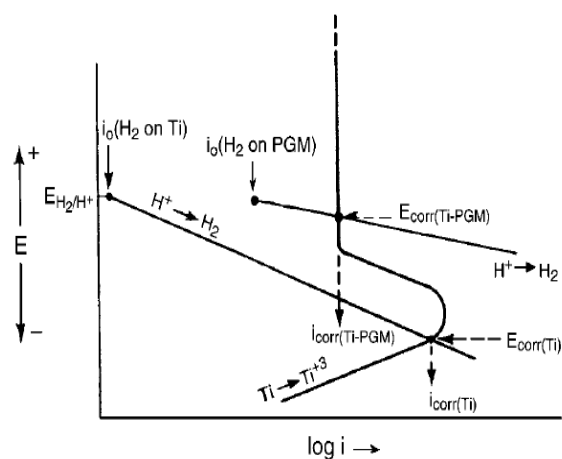
Figure 1.3.1 - Evans Diagram showing how alloying titanium with PGMs achieves passivation in reducing acids via cathodic depolarization.[97]

Among Ti alloys, Grade 7 has the best corrosion resistance. The addition of palladium, with a percentage between 0.12-0.25 improves the resistance to the reduction of acids, such as sulfuric, hydrochloric and phosphoric, but also increases the critical temperature at which the corrosion of cracks in sea water could occur. The Pd alters the cathodic process and causes a lower overvoltage for HER, shifting the working condition in the passive region of the alloy, avoiding the critical anodic ring (Figure 1.3.1)[37]. They also found that Pd absorbs hydrogen to form a protective titanium hydride layer [44][73]. Brossia and Cragnolino [74] propose Ti-Pd in the use of high-level nuclear waste counter, bringing a comparison between Ti grade 2 and 7 from the point of view of corrosion resistance, in a 1 M solution of Cl at 95°C. The pitting potential increases from 1.08 V vs. SCE to 7.69 V vs. SCE going from Ti grade 2 to Ti grade 7. However, palladium is an expensive material that greatly influences the final cost of titanium alloys, so other studies focus on the use of ruthenium (Ru), another element belonging to the PGM family but costing about five times less, because it offers similar properties, improvements [75][76].

1.3.2 – Grain refining

Grain boundaries are regions of high-energy discontinuity in the material, moving from coarse grains (CG) to ultra-fine grains (UFG) usually leading to an improvement in mechanical properties but also in corrosive ones [77]. The equal channel angular pressing (ECAP) was used on titanium to obtain UFGs with an average size of 300 nm from Balyanov et al. [78]; in the Table 1.3.1, the difference of the free corrosion potential and the corrosion rate between titanium with coarse grains and ultra-fine grains in solutions of HCl and H_2SO_4 with different concentrations is reported. The values show a greater resistance to corrosion for UFGs titanium, due to a more rapid re-passivation than its CG counterpart.

Table 1.3.1 - Free corrosion potential (OCP, V SCE) and mass loss rate (g/m^2h) for coarse grain (CG) and ultrafine grain (UFG) titanium, measured in HCl and H_2SO_4 acids.[78]

	Solution					
	1M HCl	3M HCl	5M HCl	1M H_2SO_4	3M H_2SO_4	5M H_2SO_4
CG Ti OCP [V]	0.193	-0.252	-0.362	0.237	-0.235	-0.352
UFG Ti OCP [V]	0.210	-0.242	-0.358	0.256	-0.223	-0.345
OCP [Δ%]	8.8	4.7	1.1	8.0	5.1	2.0
CG Ti C.R. [g/m²h]	0.62	1.37	1.98	0.76	1.46	1.87

UFG Ti C.R. [g/m²h]	0.42	0.90	1.38	0.58	0.78	1.09
C.R. [Δ%]	32	34	30	24	47	43

1.3.3 – Thermal Oxidation

Heat treatments are fundamental metallurgical processes that allow improvement in different mechanical properties, such as fracture toughness and fatigue strength; in the case of titanium, this also allows an improvement of the anticorrosive properties in presence of oxygen. Thermal oxidation greatly increases the thickness of titanium dioxide, going from a few nanometers to hundreds of nanometers; moreover the structure changes from amorphous to crystalline; the latter depending on the temperature can be anatase or rutile [79]. For temperatures up to 500°C there is anatase; by increasing it, there is a progressive transformation into rutile around 800°C [80]. The thickness, in the same way, increases from tens of nm to hundreds of nm, improving the resistance to corrosion, but going above 800°C there is the phenomenon of spallation that reverses the trend. The chemical resistance of the oxide produced through a heat treatment is high and a sand-blasting or caustic descaling bath process is required to remove it. In contrast, the oxide exhibits brittle behavior and is disrupted at low strain stresses [79][81][82]. An aspect not to be undervalued is that the oxide is not always uniform in this type of treatment, moreover it can present a mix of the phases of anatase and rutile, which leads to a preferential dissolution in some crystallographic directions. [83]

1.3.4 – Chemical Oxidation

Thermal oxidation has the disadvantage of reaching high temperatures (around 500°C) and the need to purify the surface from surface contamination of titanium (for example iron) through an acid pickling and low reproducibility, in particular for large pieces size. These problems can be overcome through chemical oxidation. In this technique the solutions of H_2O_2 or NaOH reach a maximum temperatures of 90°C; to these solutions it is possible to add HCl or H_2SO_4 to remove surface contaminants. The thickness of the oxide grows linearly with the duration of the process and is comparable with those formed by other oxidation, anodizing or thermal techniques. The presence of HCl leads to the formation of a thicker

TiO$_2$ with a pure rutile phase, while H$_2$SO$_4$ promotes the formation of pure anatase [84]. The oxide can be further improved through annealing. A first example is reported by Wang et al. [85], in which a thermal process was performed at four different temperatures on the samples (350°C, 400°C, 500°C and 600°C)after a chemical oxidation in H$_2$O$_2$; the samples showed a different wettability that influenced the corrosion behavior, as shown in the Figure 1.3.3. Krupa et al. [86] reports a different result for the oxidized titanium in NaOH and subsequently heated to temperatures of 500°C, 600°C and 700°C; as matter of fact, the corrosion resistance follows the following order 700°C > 500°C > 600°C > untreated. The explanation refers to the formation of sodium titanate hydrogel in the oxide during the oxidation process. The hydrogel is dehydrated above 700°C in crystalline format 500°C in amorphous form and at 600°C in a mix of crystalline and amorphous form, whose morphology has a negative effect on corrosion resistance.
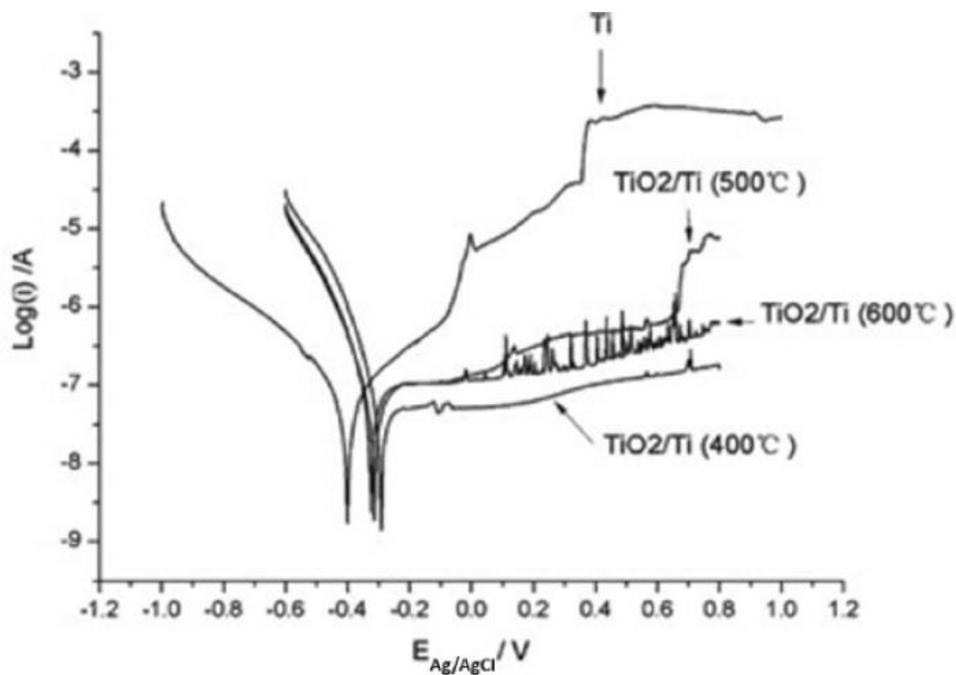
Figure 1.3.3 - Potentiodynamic test results in sea-water solution for annealed and chemically oxidized Ti samples.[85]

1.3.5 – Ion Implantation

Ionic implantation is a process at low temperatures in which the ions of an element are introduced into the surface of the solid target by bombardment. The biggest advantage lies

in being able to introduce any element into a material, in spite of limiting thermodynamic factors. In the conventional technique there is the disadvantage of a line-to-sigh implantation, being able to exploit it only on substrates with a simple geometry: the overcoming of this problem occurs using plasma immersion ion implantation (PIII), in which the piece to be treated is uniformly coated with a plasma and then a strongly negative pulsed potential is applied. The ions to be implanted are in this way found in the plasma that covers the entire surface, even with non-simple geometries and when the pulsed-bias is applied, they are accelerated perpendicularly to the surface.[87]

Most of the studies of this technique on titanium and its alloys is linked to medical applications to increase their biocompatibility [88]. The introduction of specific species on the surface of the metal makes possible to increase its resistance to corrosion, thus increasing biocompatibility, but also changing its mechanical properties, such as hardness, or even its morphology, in order to enhance its osseointegration. For instance, calcium implanted with a dose of 10^{17} Ca^+/cm^2 through an amount of energy of 25 keV on the surface reduces the uniform corrosion rate in the SBF solution; in contrast, it reduces the localized corrosion resistance with the formation of pits [89]. Phosphorus similarly introduced into the metal at concentrations above 10^{16} P^+/cm^2 creates a new phase, TiP, which increases with increasing dose. The layer thus formed shows a corrosion resistance improved by 2.5 times compared to the untreated material; this is due both to the corrosion resistance of the TiP phase and to the amorphization of the layer, which avoids the presence of defects such as grain boundaries found in the crystalline phases [90].

If both Ca and P ions are implanted at the same time, the anticorrosion behavior of the surface is further improved, avoiding the formation of pits as in the case of Ca alone [91][92]. Other elements have also been studied: oxygen implantation [93], which has detrimental effect on corrosion resistance in strong reducing acids; carbon implantation, which forms a continuous and nanocrystalline layer of TiC improving the corrosion behavior, as can be seen from the Table 1.3.2 [94]; finally, the nitrogen implantation forming particles of TiN nanocrystalline coherent with the lattice of the titanium surface and uniformly distributed and having an effect similar to carbon (Table 1.3.3)[88].

Table 1.3.2 - Free corrosion potential and polarization resistance on titanium samples implanted with different amounts of C.[88]

C implanted dose	E$_{corr}$ [mV]	Rp [MΩcm^2]
Not implanted	-95	2.5
5x10^{15} ions/cm^2	34	6
1x10^{16} ions/cm^2	65	12
1x10^{17} ions/cm^2	220	50
2x10^{17} ions/cm^2	330	54

Table 1.3.3 - Free corrosion potential and polarization resistance on titanium samples implanted with different amounts of N.[88]

N implanted dose	E$_{corr}$ [mV]	Rp [MΩcm^2]
Not implanted	-95	2.5
1x10^{16} ions/cm^2	85	6.6
1x10^{17} ions/cm^2	233	62.9
6x10^{17} ions/cm^2	230	40.3
1x10^{18} ions/cm^2	160	4.8

1.3.6 – Anodization

The valve metals belong to the groups IV and IVB and allow the formation of ionically conductive oxides [95]. They have a great affinity with oxygen and thanks to this, they spontaneously form a protective oxide layer in particular environmental conditions. This oxide, which is usually very thin, makes them incredibly corrosion resistant. Anodic oxidation is a process applied to all these materials and their alloys, used to increase their thickness and to optimize some surface-related properties such as resistance to corrosion, porosity, conductance (of semiconductive or insulating type), surface area for unit of volume, etc. Anodizing allows the development of the oxide with the required characteristics through process parameters. Titanium and aluminum are among the most investigated metals in this surface modification process.[96]

The instrument for the anodization process is the electrochemical cell that is a closed electrical circuit as shown below (Figure 1.3.5): two electrodes are immersed in an electrolyte solution that allows ion conduction but not electronic conduction [97]. The anode electrode is the valve metal upon which the oxide growth process will take place,

electrolytically connected to a counter electrode; both are electrically connected to an external circuit, from which the process parameters (potential and current) can be controlled thanks to the use of specific power supply. With regard to titanium, a polarization will be applied to this, by imposing a current flow between the two electrodes. The Ti atoms will be oxidized into Ti^{4+} ions, which will react with the oxygen atoms of the electrolyte to form the protective layer. The growth mechanism is based on inward and outward migration, in which the O_2 charge carriers reach the metal surface where the Ti^{2+} cations are produced and then oxidized into Ti^{4+} ions diffusing in opposite way through the oxide layer (Figure 1.3.4).
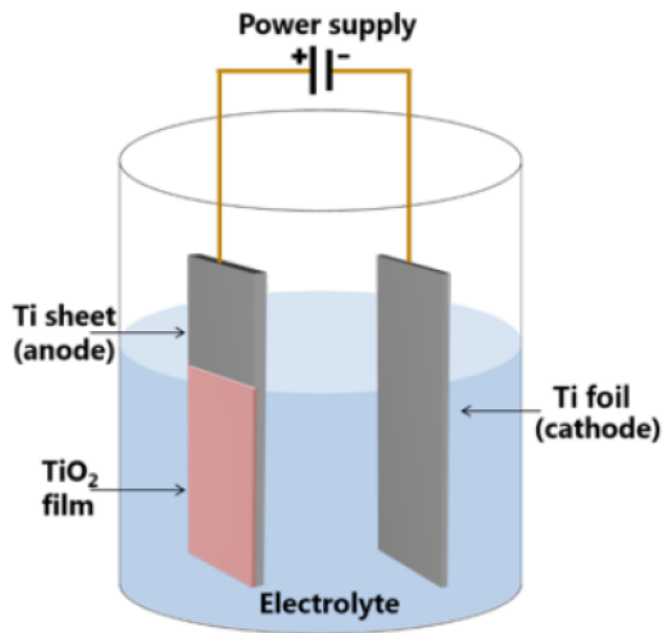
Figure 1.3.4 - Schematic representation of electrochemical cell for anodizing process.[96]
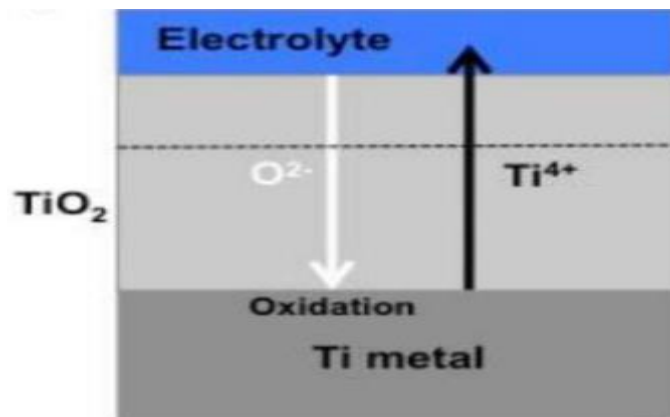
Figure 1.3.5 - Schematic representation of Ti and O ions movement for oxide formation.

The electrolyte can be an acid, such as H_2SO_4 or H_3PO_4, or a salt, such as $(NH_4)_2SO_4$, Na_2SO_4, NH_4BF_4. An important consideration is the aggressiveness of the electrolyte, as it can compromise the growth of the oxide if it has a high dissolution rate [98]. Furthermore, it has been shown that the addition of halogen acids, for example hydrochloric acid or hydrobromic acid, to the electrolytic solution roughens the surface [99][100]. The anodization acts not only on the thickness and configuration of the superficial pores, but also on the crystalline structure and on the composition of the oxide, since an anionic incorporation can occur [101]. All these factors make anodized titanium particularly relevant to scientific and technological applications, such as memristors and sensor devices, for instance lambda probes and VOC detectors; its mechanical strength and lightness makes the metal particularly suitable for applications in bioengineering, where most of the devices and prostheses for osteosynthesis are made of anodized titanium in suitable conditions in order to improve its biocompatibility and to reduce the possible wear and therefore to release metal ions. Moreover, the semiconductive nature of crystalline titanium oxides makes it suitable for photoactive applications, as an anode in dye-sensitive solar cells, as a photocatalyst in environmental cleaning technologies and as a sensor in environmental applications.[102]

The fundamental parameters in an anodizing process to guide the characteristics of the developing oxide are:

- the **current density** and the **supply voltage** are the parameters used to optimize and control the thickness of the layer and its crystalline phase. Tensions up to 100V allow to obtain a thin amorphous, smooth and porous free layer that can reach 300 nm; the surface appears coloured due to light diffraction phenomena relied by Bragg's law and related to the oxide thickness. In particular different final voltages determine different thicknesses and so different colours, ranging from yellow for a 10V anodization to green for a 100V anodization. The corrosion resistance increases with the thickness of the oxide, as shown in the Table 1.3.4. The process in this range of parameters is called traditional or colored anodization. On the other hand, voltages greater than 120V are typical of the anodic spark deposition (ASD) process, or PEO anodizing which leads to a partially crystalline oxide with a thickness ranging from a few micrometers to hundreds of micrometers, assuming an opaque gray color. This surface has pores due to the formation of arcs in the weak points of the oxide and these arcs then move over the entire surface. The high energy density in these points

causes the local fusion of the oxide in which, on one hand, modifies the crystallinity of the oxide and on the other hand, allows the electrolyte ions to enter the solid matrix modifying the oxide composition. The PEO does not show a linear growth of the oxide, but it is possible to calculate the thickness of the oxide layer through Faraday's Law [103]. This law is associated with the theory of high field-assisted ionic transport that can explain the relationship between the anode current and the intensity of the electric field through the anodic film: $i=Aexp(BE)$, where i is the ionic current, A and B are electronic constants and E is the intensity of the electric field which can be replaced by V/d, with V as forming voltage and d as the thickness of the oxide layer. From this equation, in galvanostatic anodization characterized by constant current density, the applied potential must be increased to maintain the field strength.[104]

As a result, initially the oxide grows almost linearly with the applied voltage, whose speed depends on the electrolyte and its concentration: once values around 120V have been reached, the quasi-linearity is lost, even if there is no univocal defined value due to other phenomena including the presence of pores with gas evolution and oxyde crystallization possibly occurring from 70V [46][101]. It has to be stressed that the oxide is an insulating material: by increasing its thickness, it is necessary to increase the voltage beyond a potential limit called dielectric breakdown potential, thus breaking the oxide in particular weak points and allowing the passage of current and ions from the electrolyte;

Table 1.3.4 - Anodic films grown on titanium anodized in sulfuric acid: refractive index, thickness, free corrosion potential and corrosion rate. SCE=saturated calomel electrode.

Anodizing voltage [V]	λ_{max} [nm]	Anodic film refractive index	Anodic film thickness [nm]	Corrosion potential [mV vs. SCE]	Corrosion Rate [μm/year]
5	259	1.458	44	-399.7	391
10	319	1.454	84	-365.1	2.3
15	348	1.451	59	-339.9	0.96
20	366	1.449	63	-336.9	2.35
25	398	1.446	68	-355.2	1.01
30	452	1.440	78	-293.1	4.38
35	541	1.427	94	-287	5.41
40	519	1.430	90	-338.5	3.51

45	545	1.427	95	-260.3	2.87
50	569	1.423	99	-251.4	7.78
55	643	1.410	114	-236.9	3.16
60	780	1.379	141	-247.2	7.3
65	802	1.374	145	-264.9	12.21
70	8026	1.376	150	-261.9	8.67
75	912	1.342	169	-256.2	4.95
80	1000	1.311	190	-295.6	11.48

- the nature and concentration of the **electrolyte** are important parameters in the evaluation of oxide growth. During anodization, a dynamic balance is established between the tendency of the electrolyte to dissolve the oxide film and its formation [104]. Very weak acids usually identified with organic acids produce very adherent but limited thickness translucent films. Strongly basic electrolytes cause titanium oxide precipitates or react so quickly with the titanium surface that the entire substrate is rapidly converted to oxide; these electrolytes make it difficult to control the process. Most neutral or near-neutral salt-type electrolytes produce only extremely thin translucent films [99]. Alkaline electrolytes, such as sodium and calcium hydroxides, have a very low capacity to form the oxide layer, being the dynamic equilibrium tension between oxide dissolution and growth very low. On the contrary, sulfuric and phosphoric acids are the best electrolytes in terms of thickness and adhesion, presenting a high growth rate that exceeds the dissolution rate [101]; but really strong acids like HF or $HClO_4$ tend to eliminate the oxide.

  The characteristics of the electrolyte influencing the growth of the oxide are the ionic conductivity, the amount of oxygen available, the possibility of incorporating its ions in the film and the ability to dissolve the oxide itself. **Temperature** also plays an important role, as the oxidation of titanium is an exothermic reaction which is by definition favored at low temperatures. During anodization the temperature increases and this inhibits the growth of the oxide: at the same time, the electrolyte conductivity increases, reducing the voltage necessary for oxidation [74][101];

- the **agitation of the solution** is linked to the gas evolution of hydrogen and oxygen. This phenomenon leads to the formation of bubbles which create an interface between the anode and the electrolyte, hindering the ionic current and consequently increasing the anodic potential necessary for the formation of the film. The agitators

ensure that the bubbles do not remain on the surface, thus reducing the forming potential [101];

- the **duration** of the process influences not only the thickness of the oxide but also the surface structure; the study by Mizukoshi et al.[105] shows that polished traces could be observed on the Ti substrate for low process times, between 2 and 10 min; concave curvatures appeared over time with tens of micrometers in diameter which suggested the distension of the formed oxide; the polished traces between 30 and 60 minutes were no longer observed, but curved bends formed on the entire Ti substrate at the high magnification show that they are pores (Figure 1.3.6);
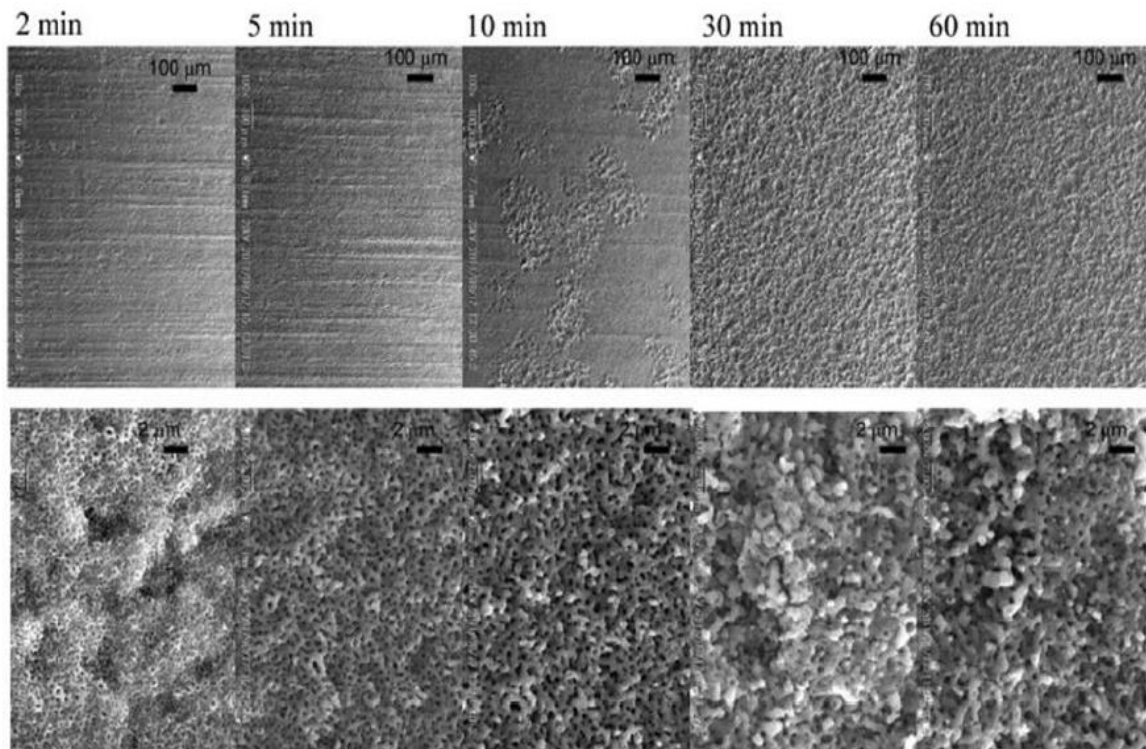
Figure 1.3.6 - SEM images of TiO$_2$ surface with the progress of anodization.[105]

- the **surface chemical composition** and its **finishing** also influence the development of oxide.[106]

1.3.6.1 – Anodic Spark Deposition

The anodizing process initially causes the oxide layer to grow almost linearly as the supply voltage increases, forming a compact and amorphous dielectric barrier that prevents the flow of the ionic current through the oxide itself. As the process proceeds, there is a slowdown in

the growth of the film and its blockage, but if a certain threshold is exceeded, this barrier can be overcome. This value is called dielectric breakdown potential and approximately corresponds to 100V for titanium depending on the electrolyte, the composition of the anode and the current density. In these particular conditions the anodic spark deposition (ASD) begins. The density current is concentrated in the weak points of the oxide layer, because the insulation is less effective, causing such high electric field values to start the ionization of the atoms and the localized microplasma state, hence also the name of micro-arc oxidation (MAO). At that point, a localized electric field of 10^6 V/m^2 causes the instant melting and solidification of the heated oxide layer up to 5000-6000 K [102]. The phenomenon is visible through the formation of sparks that move from the initial weak point along the entire surface creating electric arcs. The effects of this anodizing phenomenon are also visible in the morphology of the surface, as a matter of fact they show a glassy plane surrounded by the craters left by the sparks. The size of the craters varies from 200 nm to 2-3 µm and depends on the processing parameters, the longer the ignition process is, the greater the average pore size is [106]. Furthermore, the pores can take circular, ellipsoidal or irregular shape structured in a elongated way. The film passes from an amorphous structure of the oxide to a crystalline shape caused by the sparks breaking the oxide and inducing high temperatures [107]. The solidification is almost instantaneous and does not lead to complete crystallization. At the beginning, ASD forms crystals with anatase structure; proceeding with the process, the crystals undergo an allotropic transformation in rutile, induced by the maintenance of high temperatures with annealing effects [106]. A more uniform morphology and structure is carried out for long treatments. The change from amorphous phase to crystalline phase in TiO$_2$ can be detrimental for its anticorrosive properties and for the presence of pores; despite this, these new structures can generate unexpected applications [46][93]. For instance, the ionic conductivity, due to the porosity of the film, finds application mainly in the gas detection devices, as in the lambda probes for the detection of volatile organic compounds or oxygen. Another characteristic concerns the voids of oxygen at the interface between substrate and oxide, which induce a memresistive behavior depending on the polarization of the current.

Anodic spark deposition is a technique that has the ability to incorporate ions present in the electrolyte and to modify in this way the surface composition; this is due to the instantaneous localized melting and quenching of the surface. As a matter of fact, the electrical breaks of

an anodic film produce high temperatures and pressures in and around the discharge channels, which result in the thermolysis of the electrolyte components and their incorporation into growing coating structures. The possibility to tune the composition is a fundamental tool not only in corrosion resistance application, but also in biomedical and electronical applications. An example of early studies concerns the incorporation of sodium and silicon in the oxide layer by anodizing in Na_2SiO_3. A TiS_x formation was obtained in Na_2SiO_3 and Na_2PO_4, maintaining a voltage above 250V and producing an oxide more resistant to corrosion [88]. Another study by Hu et al.[108] offers a possible explanation: the electrolyte containing Na_2SiO_3 improves the corrosion resistance characteristics of the oxide due to the greater conductivity of these compounds, forming a denser and more compact microstructure than those not containing such a salt. However, it is also important to evaluate the performance potential of the ASD: at 400V the formed layer is composed of an external porous layer enriched with sodium and silicon, which does not contribute to corrosion resistance, and a compact internal oxide layer, composed mainly of TiO_2 [106]. If another element is considered, also the incorporation of zirconium is an important treatment: a first characteristic is the ability to increase the resistivity of the electrolyte and therefore the power of the microarc, thus increasing the pore size for low frequency pulsed ASD, while for high frequency the pores are uniformly distributed and with small size. Another effect concerns its oxide (ZrO_2), which has greater stability in aqueous solutions and increases resistance to corrosion [109]. The incorporation of chlorides is further important tool for modifying the roughness of the oxide film. A PEO treatment in HCl after a low alternating current pre-anodization creates a rough and thick oxide layer, important for applications that require surface roughness on several scales, such as the biomedical ones. On the other hand, the use of Cl-enriched electrolytes leads to the formation of the $TiCl_4$ complex which causes the cracking of the oxide and it must be avoided [110]. The incorporation of P^- and C^- ions in the oxide layer by ASD exhibits excellent osteointegration properties and it hinders the dissolution of titanium ions in the body fluid. Alumina has also recently become an important compound to be studied during incorporation. This compound can increase the corrosion resistance of the porous layer through its filling and impeding effect.[111]

A nanopores structure or titania nanotubes can be created using anodization in combination with the presence of fluorides in the electrolytes [112]. After the formation of the first compact oxide layer, the presence of fluorides has the effect of localized attacks on the

surface. In these penetration points there is oxide hexafluoride, which prevents the oxide from growing and at the same time the contours of the pore grow. This process continues until the dissolution and growth of the oxide are equivalent. The length and width of the nanotubes depends on the concentrations of the F⁻ ions. Anodization that forms nanotubular layers is usually performed by ramping up to a constant voltage normally between 1 and 150 V, in aqueous or non-aqueous electrolytes, and the presence of fluoride anions at concentrations ranging from 0.05–0.5 M. In order to limit the action of fluoride ions, which are very aggressive in aqueous solutions, new generations of electrolytes have been studied; among these non-aqueous solutions stand out the organic electrolytes, such as ethylene glycol, which allows to reach lengths of hundreds of micrometers (Figure 1.3.7) [113]. The development of this surface conformation is welcomed by different technological fields due to its semi-conductive properties; some examples are: dye-sensitized solar cell which has advantageous features, such as easy application with conventional roll-printing techniques, semi-flexibility, semi-transparency and low cost; photocatalysts to purify wastewater coming for example from the pharmaceutical industries to depollute the air in both industrial and urban areas as a coating with biocidal action and also in biomedical implants to improve bone integration or adhesion with cells.[114]
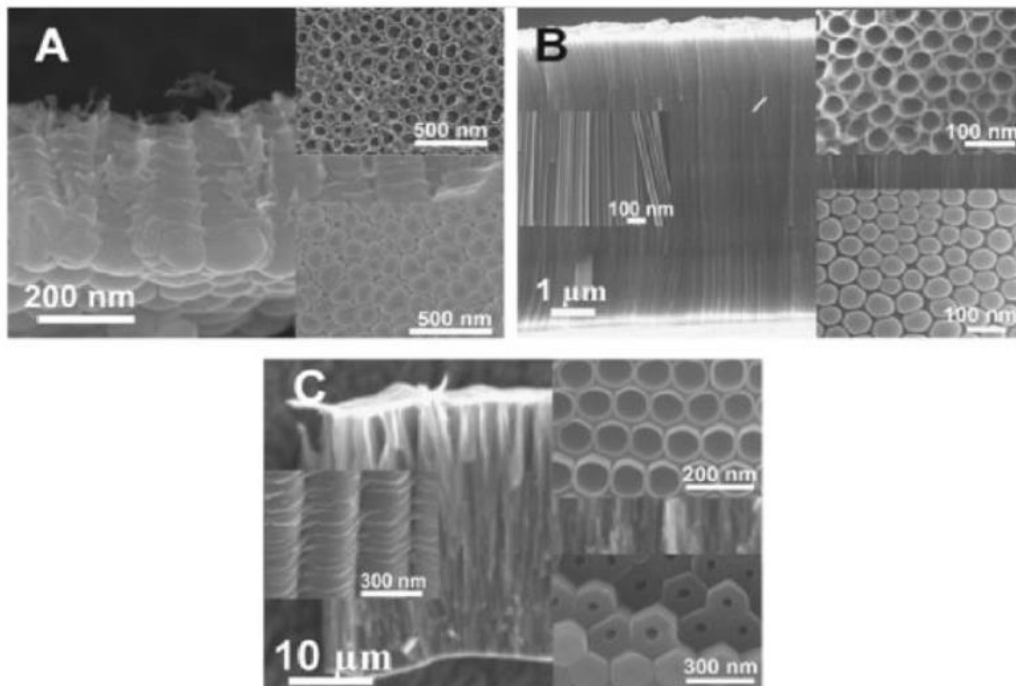
Figure 1.3.7 - SEM images showing TiO₂ nanotube in different electrolytes : A) in HF; B) in glycerol/fluoride electrolytes; C) in ethylene glycol/fluoride electrolytes.[114]

1.3.6.2 Pulsed Anodization

By the term "anodization" is meant a continuous process that is in direct current (DC) and this process can be traditional or spark. The **pulsed anodization (HA)** instead defines a discontinuous process, where the anode current shows a waveform that intersects the zero value, according to the imposed conditions. These discontinuous waveforms can be divided into two categories (Figure 1.3.8): **monopolar**, in which periods of on and off are alternated and **bipolar**, in which the current can assume values not only positive and equal to zero, but also negative. A further division of the last type of waveform into complete bipolar with the current always turned on with positive and negative values, and in bipolar with rest or hybrid pulsed anodization (HPA) is made, where the period is divided between positive, negative and even zero currents. The positive value phases are the anodic phases, in which there is the growth of the oxide film; the phases with negative values are the cathodic phases where the film does not grow, but other phenomena occur; finally, there are the off phases with the current equal to zero, which can also be called rest phases. The parameters in the pulsed process, that are added to the continuous one, are: duty cycle and frequency. The first, expressed as a percentage, defines the relationship between time of a phase (anodic, cathodic or rest) and the total time, while the second defines how many times per second the duty cycle is repeated. Figure 1.3.8 shows ideal duty cycles, where the current is maintained constant during anodic or cathodic phase; in real case, the instantaneous current density however varies with spikes over time, in correspondence with instantaneous rises and decreases of the potential (Figure 1.3.9-b).[96]
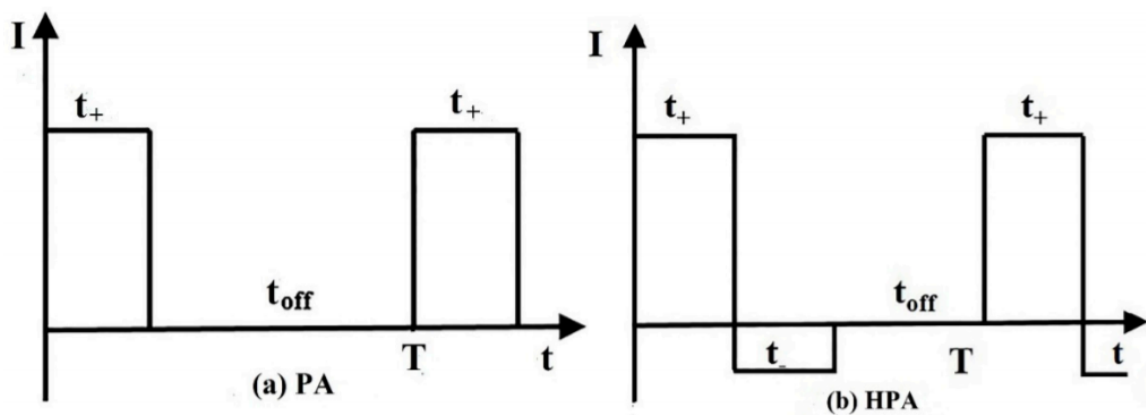
Figure 1.3.8 - Schematic diagram of two different current modes : a) monopolar pulsed anodization ; b) hybrid pulsed anodization.[115]

Pulsed anodization can be performed with two input signal control modes: in the first mode, the current density is an input signal and the voltage increases in accordance with the increasing coating resistance; in the second mode, the potential is an input signal which allows to limit the maximum current. In this case, it is possible to observe a current peak with the following current decay at the output, as the coating impedance increases.
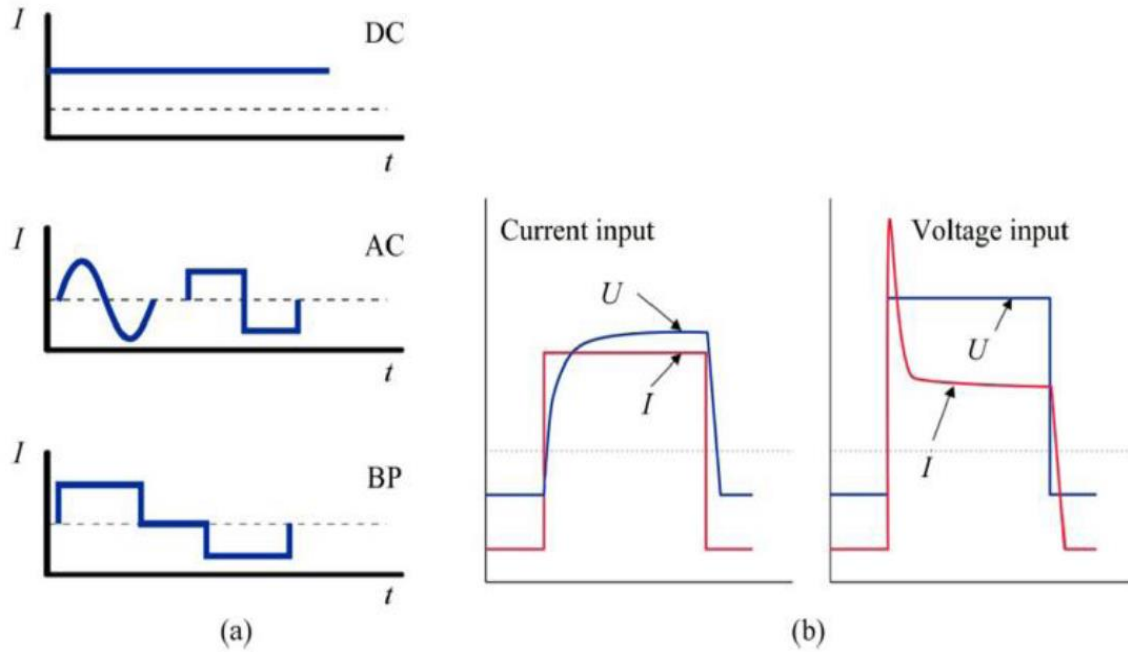
Figure 1.3.9 - PEO current applications a) and control modes b).[96]

A discontinuous anodizing process leads to a different development of the coating. Several studies have been carried out to understand what were the effects of duty cycle and frequencies on thickness, porosity and crystallinity. In the work of Williamson et al.[116], duty cycle was considered as a benchmark for a monopolar pulsed treatment on titanium grade 4. The treated samples showed a greater thickness for small work cycles (Fig. 1.3.10-A) and a higher degree of crystallinity. In addition, they exhibited a homogeneous distribution of nano-pores. As a result, the corrosion resistance was also improved.
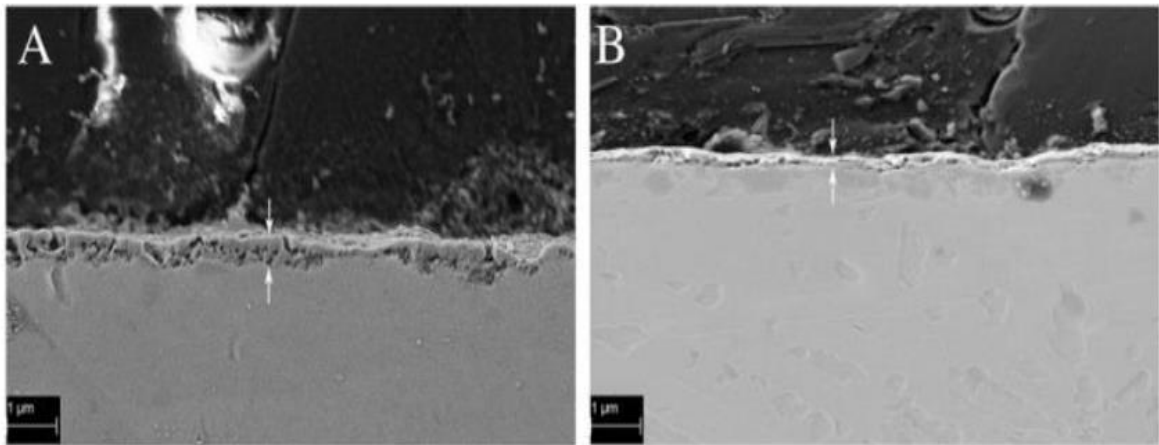
In another study [117], a multilayered nanoporous structure was found in the oxide, making it even more evident by prolonging the anodizing time. Another characteristic of the pulsed anodizing is the achievement of the desired potential in a shorter time than the continuous one. Frequency also plays a fundamental role in pore distribution and size. In fact, by increasing the frequencies, pores with reduced dimensions are obtained. This effect is shown in the study by D.A. Torres-Ceròn et al.[118] Titanium anodization is performed in an aqueous solution containing 8 g/L Na_3PO_4 and 0.4 g/L NaOH. The potential is set at 340V in pulsed mode for 10 minutes with a 10% duty cycle and frequencies of 1000 Hz, 1500 Hz and 2000 Hz. As the frequency increases there is a decrease in the size of the grains, going from 29 nm for 1000 Hz and 1500 Hz to 21 nm for 2000 Hz; on the contrary, the surface density of the pores has an incremental trend: from 0.15 μm^2 for 1000 Hz, 0.27 μm^2 for 1500 Hz to 0.32 μm^2 for 2000 Hz. This effect of reducing the pores can be justified by a shorter time of arcs discharge for the high frequencies, these being the reciprocal of the work cycle time [119]. Crystallinity is another parameter influenced by frequency and this is shown by Wang et al.[120] study. In this case, pure Ti is subject to a pulsed process with constant duty cycle and with frequencies in a range of 100-5000 Hz. The composition of TiO_2, for low frequencies, consists of rutile, anatase and hydroxyapatite. The pores are well separated and evenly distributed, with a size ranging from 0.2 microns to 5 microns. Instead, for high frequencies, the structure of the film is more amorphous and with larger pores, in which internal walls have smaller pores (Figure 1.3.11). The change of structure and morphology of the coating is due to the different number of electrical breakdowns; at 100 Hz, the time interval between one spark and another was about 10 ms, longer than the lifetime of the

spark and so the molten areas had enough time to be cooled and solidified before next pulse; at 5000 Hz, sparks interval was about 2×10^{-4} s, this time duration did not allow cooling and solidification of molten areas and a secondary breakdown happens, due to the higher conductivity of the hot oxide. Many small pores were produced by the secondary breakdown in the large pores produced by the primary breakdown.
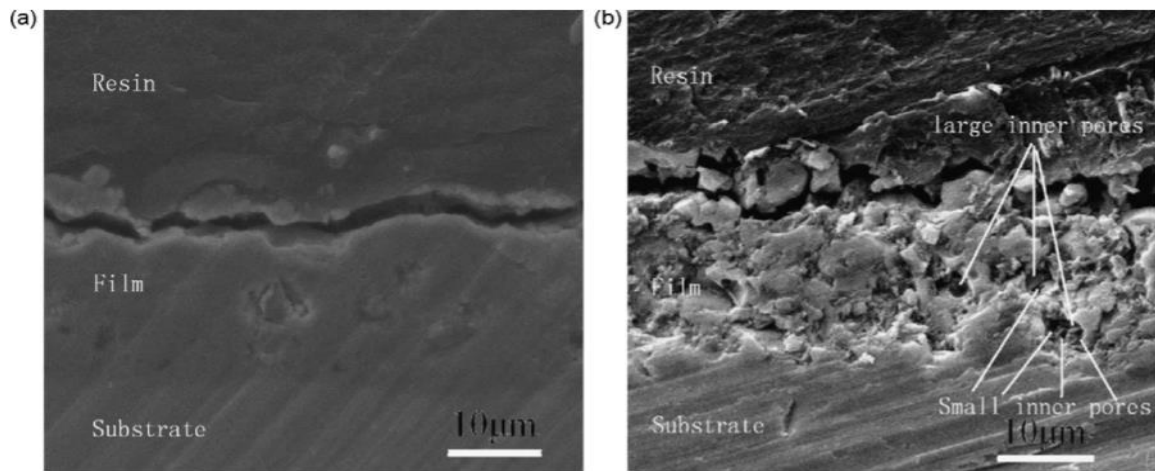
Figure 1.3.11 - SEM cross-sectional views of the Ti specimens treated with MAO at different frequencies: (a) 100 Hz and (b) 5000 Hz.[120]

The combination of duty cycle and frequency is shown in the work of S. Gowtham et al.[121]. The ASD coatings produced have 10% and 95% duty cycle, both performed at 50 Hz and 1000 Hz. The thickest oxides were detected for the 95% cycle, for both frequencies, and for the 10% cycle at 1000 Hz. This result underlines the importance of the anodic phase to obtain high film thicknesses. The pore size increases with the work cycle, with the onset of smaller pores within the main ones for the 1000 Hz frequencies. The Ti treated with 95% duty cycle at 1000 Hz shows the best corrosion behavior (Figure 1.3.12).
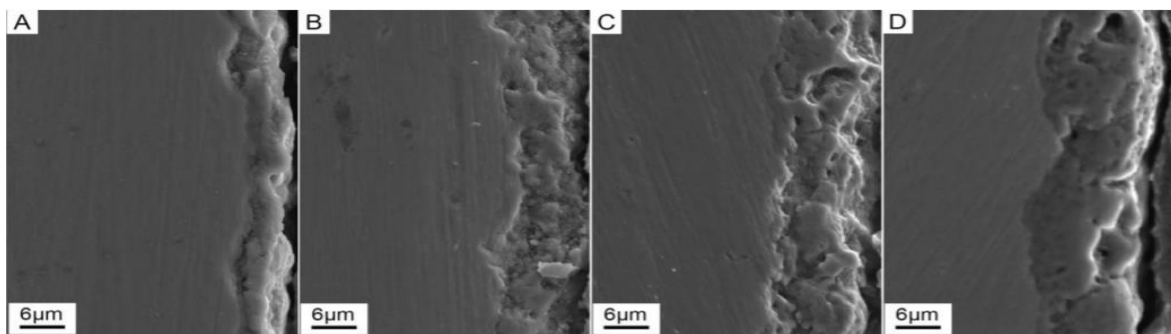
Figure 1.3.12 - SEM images of Ti coatings: 10% duty cycle A) at 50 Hz and B) at 1000 Hz; 95% duty cycle C) at 50 Hz and D) at 1000 Hz.[121]

Some studies have been conducted by combining the main parameters of the anodizing process with the new ones deriving from the pulsed process. An example comes from M. Babaei et al.[119], who at the same time observes the effects of frequency and electrolyte concentration on surface morphology. It is observed that the pore size decreases bringing the frequency to 1000 Hz, as it occurs in the previous cases. If the additives double in solution, the pores density is reduced, but with a larger size. This phenomenon is due to the lowering of the electrical resistivity of the electrolyte which causes an increase in spark intensity. On the other hand, in the samples treated at low frequencies (100 Hz), the differences in pore size, depending on the concentration, is no longer visible; this occurs because the greater fluidity of the fused substances on the surface eliminates the effect of micro-discharge which leads to a structure with large pore sizes.

Pulsed bipolar anodization introduces additional parameters that influence the development of the oxide: the intensity and duration of the cathodic phase. A first effect of the cathodic pulse is the occurrence of reducing reactions; a second effect is a partial dissolution of the oxide from the coating; and finally, it influences the surface state of the electrode. More titanium metal passes from the substrate to the surface, giving a positive effect in the formation of TiO_2. The benefit is valid for small intensity and duration of the cathodic pulse; but if it is strong and durable, it can lead to a reduction in the film thickness involving proton accumulation and so higher oxide conductivity.[122]

In conclusion, the discontinuous anodization of titanium is studied to control crystallinity and porosity in the structure of its oxide. The possibility of creating a highly ordered porous structure finds interest in the applications of solar cells, photocatalysis, photonic crystals and sensors (Figure 1.3.13)[123]. In the biomedical sector, the need for a bioactive structure is fundamental. This characteristic is accentuated in the titanium oxide by controlling its roughness and by the formation of anatase and rutile phases. The surfaces of dental and orthopedic implants benefit from a nanoporous structure which increases the antimicrobial effect and the osteoblast attachment. Furthermore, heat treatments, usually performed after a traditional anodization process to change the crystalline phase and morphology, are no longer necessary with appropriate waveforms.
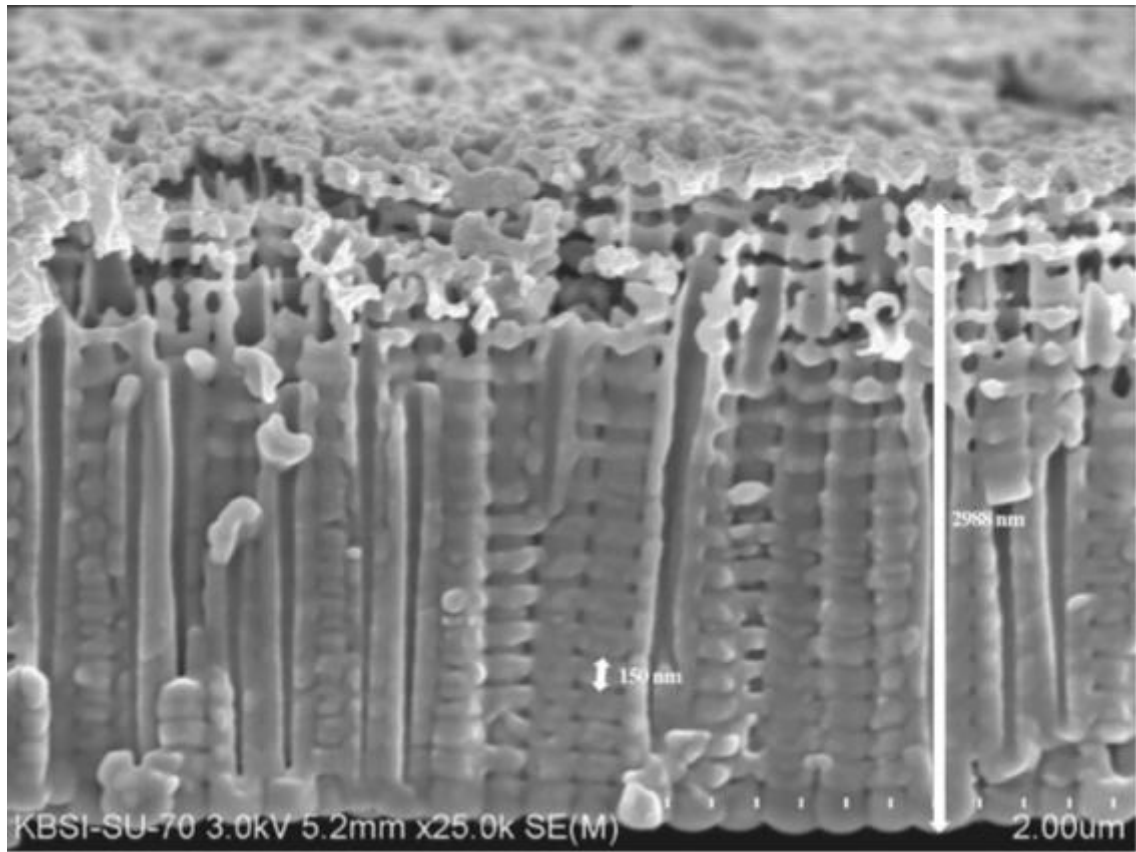
Figure 1.3.13 - TiO2 photonic crystal arrays FE-SEM image by Pulsed Anodization.[123].

CHAPTER 2 – Materials & Methods

In this chapter, the reasons and experimental procedures of this titanium study are explained in detail. The first paragraphs deal with the properties and characteristics of the Ti gr.2 and gr.7 samples and a description of their preparation, which included mechanical and chemical processes. The configuration of the equipment and waveform used in anodic spark deposition is further described. Surface analysis was investigated by optical microscopy, scanning electron microscopy (SEM) and X-ray diffraction (XRD). Finally, the corrosion resistance was then evaluated with immersion and potentiodynamic tests, the latter both from an anodic and cathodic scan.

2.1 – Materials

The experiments were performed on commercially pure titanium Grade 2 (CP-Ti Grade 2), also referred to as ASTM Grade 2 [20] or USN R50400. Corrosion tests were also performed on the CP-Ti Grade 7, that is titanium gr.2 alloyed with palladium (USN R52400). In the Table 2.1.1, their compositions and mechanical properties are shown.

Table 2.1.1 - Chemical composition and mechanical properties of CP-Ti Grade 2 and 7.[20]

	Grade 2	Grade 7
Nitrogen	0.03	0.03
Carbon	0.08	0.08
Hydrogen	0.015	0.015
Iron	0.30	0.30
Oxigen	0.25	0.25
Aluminum	-	-
Vanadium	-	-
Palladium	-	0.12-0.25
Titanium	Balance	Balance
Mechanical properties		
Rm (MPa)	345	375
Rp 0.2 (MPa)	275	345
Elongation (%)	20	20
Hardness	160HB/30	160HB/30
Modulus of elasticity (GPa)	103	107
Poissons Ratio	0.37	0.37

The samples used were obtained from a slab of Ti Grade 2 and have a square shape of the average size 10x10x1.6 mm^3.

The initial preparations for the elimination of grease and dust consist of ultrasonic washing in ethyl alcohol for 5 minutes, then rinsing in distilled water.

The samples for the ASD process were also mechanically cleaned to uniform the surface conditions on one face, with 100, 320 and 600 grit SiC papers. The first paper was used to remove the natural oxide and to ensure a planar surface, the second and the third paper to remove excessive scratches; the values of roughness of the so-prepared samples resembles the titanium roughness as received from the producer, so allowing the reproduction of the implementation conditions in field. Polishing was followed again by EtOH ultrasonic baths and water rinsing.

2.2 – Plasma Electrolytic Oxidation setup

The electrochemical cell is shown in the Figure 2.2.1: the cathode is an active titanium network, also called MMO (mixed metal oxide) that is composed of noble metal oxides such as ruthenium and iridium; the electrolyte used is H_2SO_4 0.5M, as the previous research has shown itself to be the best solution for a thick oxide [103]. The sample, represented by the anode, is immersed through a titanium clip covered with insulating tape, excluding the points of contact with the anode and the external circuit.
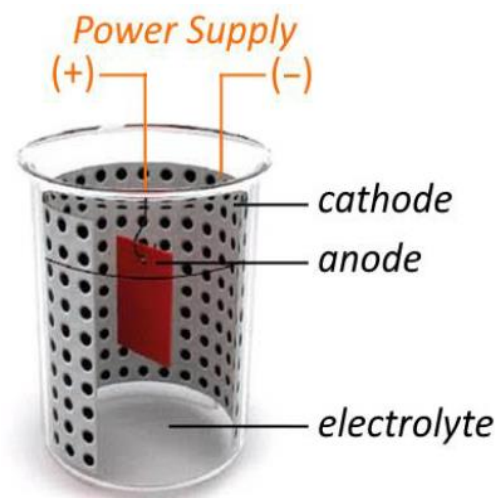
Figure 2.2.1 - Schematic representation of electrochemical cell for anodization.

Asterion AST 751 is the power supply. The instrument allows to anodize both in DC and AC regimes and also to combine them. It can work in galvanostatic or potentiostatic regime; For the current dissertation work, the second possibility has been chosen. The frequencies can vary from 16 Hz to 1000 Hz and the maximum voltage selected can vary up to 200V in the case of AC in order to avoid limitations in the currents that stop the process. The potential waveform was generated through a spreadsheet pre-set by previous studies; this excel file sets the phases of the duty cycle (anodic, cathodic and off) and, in the case of a bipolar process, even the power of the cathodic process in percentage with reference to the power of the anodic phase. A conversion parameter is also provided in order to convert the RMS value of the tuned waveform to the forming voltage applied to the cell (Figure 2.2.2). In this work, a 160V potential with a 0.5 V/s ramp has been chosen; the process takes 320 seconds and it is performed at 20 Hz and 1000 Hz. The Asterion software can also continuously represent the waveforms of potentials, currents and powers.
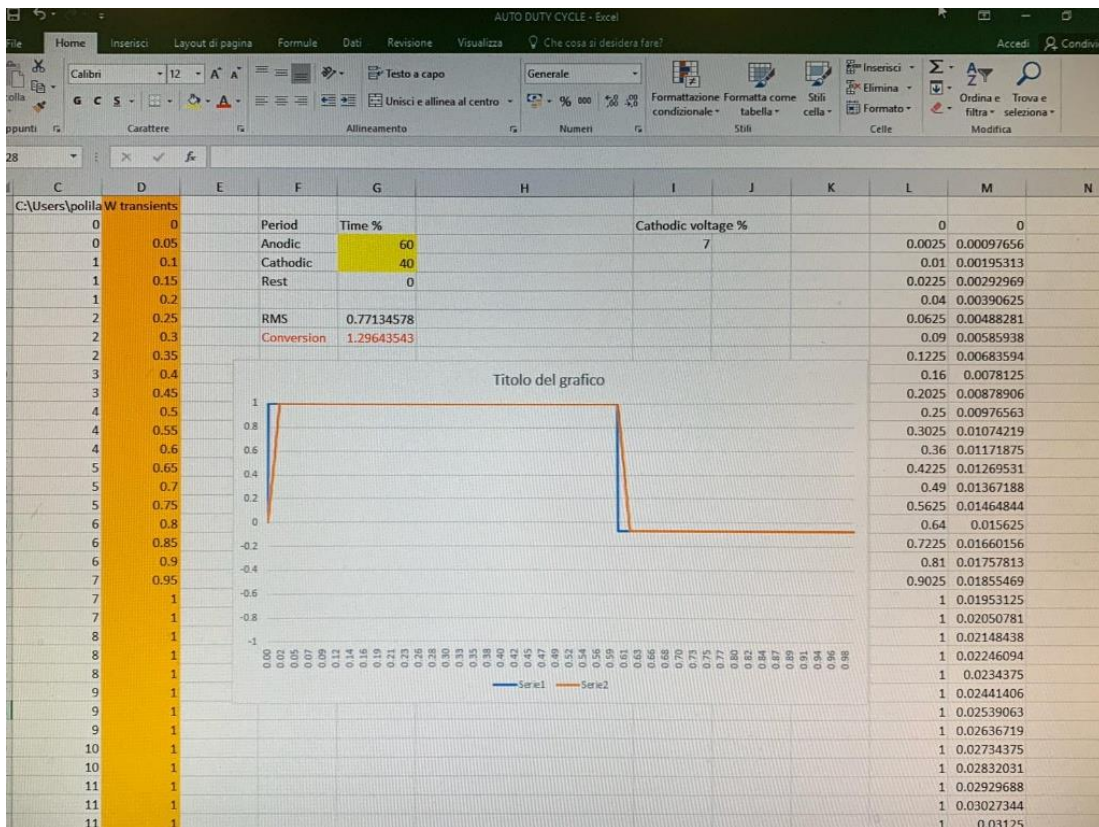
Figure 2.2.2 - Waveform spreadsheet.

Bipolar pulsed anodization induces dissolution phenomena of the oxide coating depending on the intensity and duration of the cathodic phase. The first objective of this research was

to find the duty cycles that led to an opaque gray color of the sample. The color of anodized titanium is due to phenomena related to interference between the light scattered from the oxide surface and the ray reflected at the metal-oxide interface and depend on the thickness of the film which is of the order of a few hundred nanometers in the traditional anodization process. The opaque gray color, on the other hand, identifies the impediment of electromagnetic radiation to be reflected in the visible by the titanium metal in the substrate. This means a high TiO_2 thickness (around a few micrometers).

The waveform design applied to the electrochemical cell is imposed by the power supply. The three parameters that define it completely are (Figure 2.2.3):

- % anodic (%A) is % of anodic polarization;
- % cathodic (%C) is % of cathodic polarization;
- % cathodic peak (%C peak) is % of cathodic peak with respect to the anodic one.
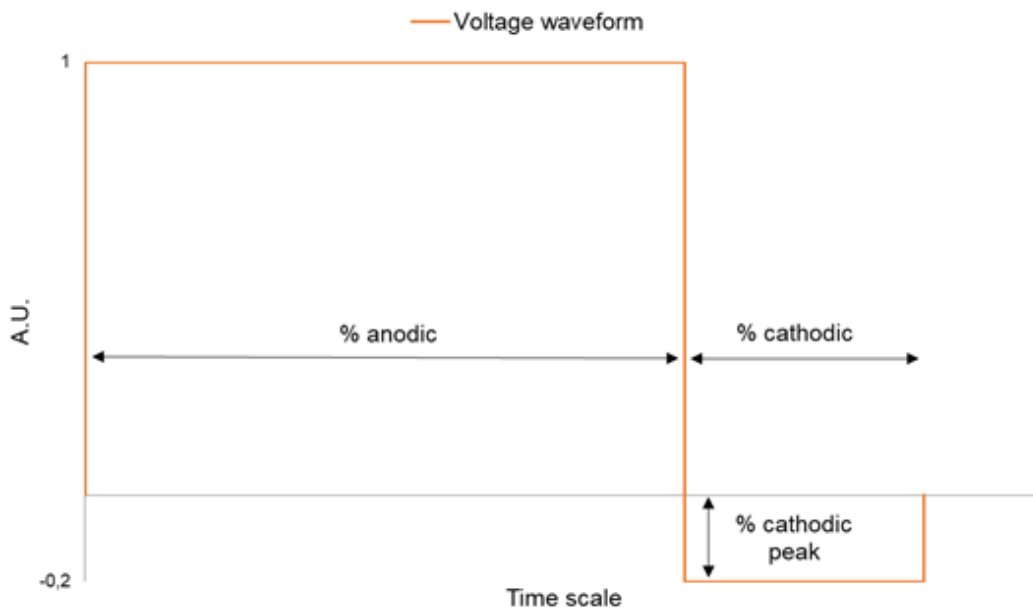
Figure 2.2.3 - Duty cycle parameters descriptions (i.e. 20% cathodic peak).

In the Table 2.2.1, the tested cycles are reported, varying the phases and the amount of the cathodic polarization.

Table 2.2.1 - Pre-anodization treatments for the selection duty cycles.

Cycles	Cathodic peak	
	7%	10%
10%A90%C – 20Hz		
10%A90%C – 1000Hz		
20%A80%C – 20Hz		
20%A80%C – 1000Hz		
30%A70%C – 20Hz		
30%A70%C – 1000Hz		
40%A60%C – 20Hz		
40%A60C – 1000Hz		
50%A50%C – 20Hz		
50%A50%C – 1000Hz		
60%A40%C – 20Hz		
60%A40%C – 1000Hz		
70%A30%C – 20Hz	-	-
70%A30%C – 1000Hz	-	-
80%A20%C – 20Hz	-	-
80%A20%C – 1000Hz	-	-
90%A10%C – 20Hz		
90%A10%C – 1000Hz		

Anodizing tests were not carried out for cathodic peaks at 2% and 5%, as a common duty had already been found with minimum anodic phase and with an opaque color for the most severe cycles (at 7% and 10%). The duty cycles chosen were 90%A - 10%C and 60%A - 40%C for the cathode peaks equal to 2%, 5%, 7% and 10%. The first waveform was selected because the anodic phase percentage is close to the percentage of a DC treatment. The second waveform was the one with the highest amount of cathodic polarization compatible with the desired colour and so a high enough thickness.

2.3 – Corrosion Tests

2.3.1 – Immersion test

Titanium tends to corrode uniformly in strong reducing acids. The oxide growth process allows to increase its corrosion resistance, but different anodizations lead to different TiO_2 formations in terms of thickness, porosity and structure. Plasma electrolytic oxidation leads to a thick ceramic film with greater porosity than the colored process. Sulfuric, phosphoric, hydrochloric, oxalic and sulfamic acids have been investigated on pure Ti gr. 2 and 7 and on the Ti treated with bipolar pulsed anodization.

The immersion test follows the ASTM G1 [124] and G31 [125] standards. The preparation of the samples involved the washing in deionized water, the picking in Kroll's solution (2% v/v HF + 4% v/v HNO_3) for 30 second in order to remove any trace of contaminants and to expose metallic titanium directly towards the aggressive solution, the weighing and the dimensions measurement in order to calculate the area of the sample exposed to the acidic solution (Figure 2.3.2). The weight of the samples was taken with GIBERTINI balance (precision of 0.1 mg) before (W_1) and after the pickling (W_2) to evaluate the effect.

The test equipment (Figure 2.3.1) is composed of a five-neck spherical balloon, the Liebig refrigerant connected to an external circulation thermostat (JULABO CD-200F) and the heated magnetic stirrer (AREX VELP) connected to a digital thermoregulator (VTF VELP).
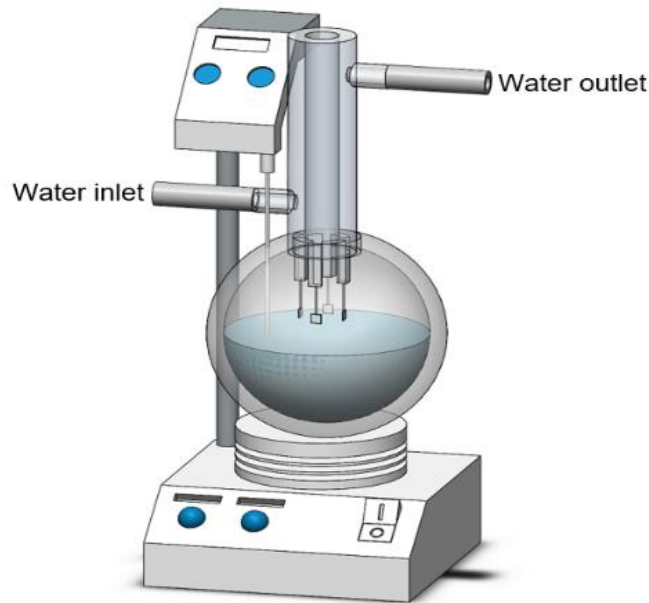
Figure 2.3.1 - Schematic immersion test set-up.

The duration of the immersion test is strictly correlated with the sensibility of the balance used to assess the mass loss per each sample. The minimum amount of time required for the test is given by equation from ASTM G31 standard:

$$hours = \frac{2000}{CR\ (mpy)}$$

Corrosion rates (C.R.) have been taken from the literature data. The solutions, capable of inducing a significant loss of mass at defined temperatures and concentrations, are sulfuric, sulfamic, phosphoric, hydrochloric and oxalic acids.

Table 2.3.1 - Tested acids at different temperature and concentrations.

Acid	Concentration [v/v %]	Temperature [°C]
Oxalic	1	50
	10	60
Sulfamic	10	60
H₃PO₄	30	60
	40	35
	50	35
	60	35
H₂SO₄	10	50
	10	60
HCl	2	60
	6	50
	10	60

The test involves immersion in the solution at set temperature and concentration conditions of three samples (10x10x1.6 mm^3) at the same time; these are extracted individually after 24 h, 48 h and 72 h. After the removal of the third sample happening after 72 hours, a fourth sample is introduced into the solution for 24 h. The test so planned permit to understand how change metal corrodibility with time and also to evaluate if the corrosion ability of the solution varies.

Occurrence	Status	Criteria
Liquid corrosiveness	Unchanged	$A_1=B$
	Increased	$B>A_1$
	Decreased	$B<A_1$
Metal corrodibility	Unchanged	$A_{t+1}=A_t$
	Increased	$A_{t+1}>A_t$
	Decreased	$A_{t+1}<A_t$

Being:

A_1 = corrosion damage of the sample immersed for 24 h

A_t = corrosion damage of the sample immersed for 48 h

A_{t+1} = corrosion damage of the sample immersed for 72 h

B = corrosion damage of the sample immersed after 72 h and removed after 24 h

The extracted samples were washed and dried to be weighed (W_3). An additional weight (W_4) was made after a stay in the dryer for 24 h, in order to evaluate the effect of residual water. A cathodic process was performed for the removal of possible surface corrosion products, that affect the real value of corrosion rate. The equipment used for the electrochemical treatment was the same as in the anodizing process, but the sample to be treated was made the cathode by applying a current density of 300 A/m^2. A one liter solution containing 20 g of NaOH was used. Finally, the samples were cleaned in deionized water, dried by compressed air and weighted (W_5). The final mass (W_6) was evaluated with correction parameter that consider undesired metal dissolution during corrosion product removal. This parameter was obtained by the same cathodic process applied to Ti gr. 2.

The Figure 2.3.2 summarizes the different steps taken by the samples before, during and after the test and shows the mounted equipment.
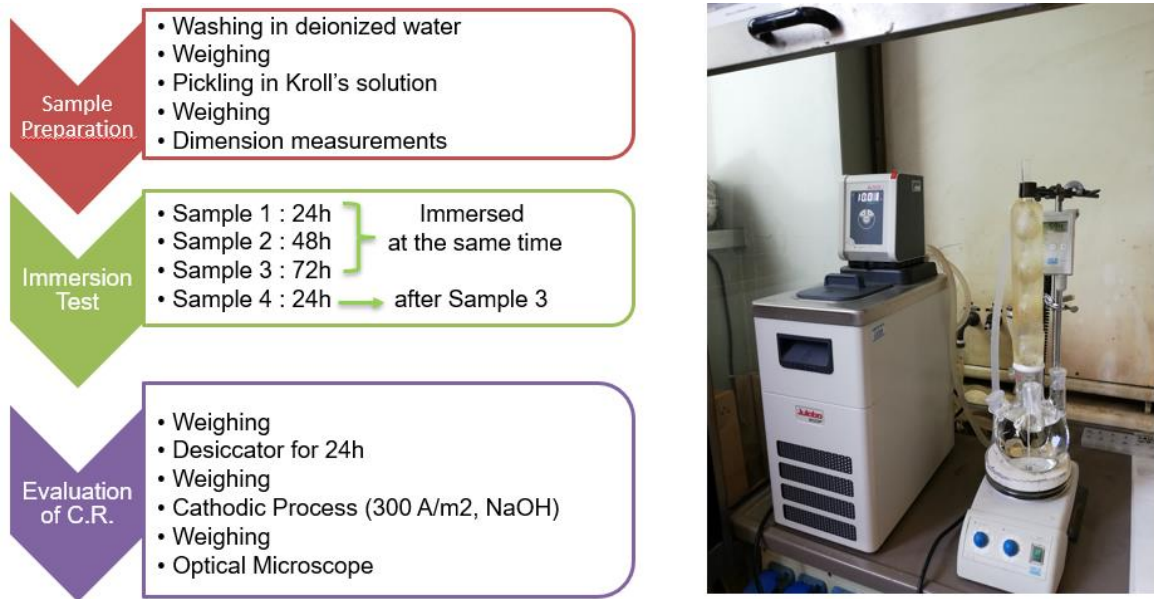
Figure 2.3.2 - On the left, schematic samples steps for immersion test. On the right, assembled equipment.

In the preparation of the anodized samples, the pickling was not performed. The test, which was not at programmed intervals as in pristine Ti, had a duration of 24 h in the 10% v/v sulfuric acid at 60°C.

The average corrosion rate was calculated by the following equation:

$$C.R. = (K \times \Delta W) / (A \times T \times D)$$

Where: $K=8.76 \times 10^4$; $\Delta W = W_2 - W_6$ mass loss in [g] ; A=area in [cm^2] ; T=time of exposure in [h] ; D=density in [g/cm^3].[124]

2.3.2 – Potentiondynamic test

In the literature, it has been reported that among all the possible halide anions, titanium tends to undergo anodic dissolution of the passive layer only in bromides. This phenomenon is an effect that has been attributed to the absorption in the sites associated with the inclusions of impurities containing Al and Si or Fe. In a previous work of the group, all the halides were tested to find out which was more aggressive [126]. As matter of facts, all the halide anions were introduced as sodium salts in order to guarantee the total independence of the cation

corrosion resistance. The corrosion resistance behavior of the oxide layer followed the indications of the literature and the sodium bromide was an optimal aggressive solution with a concentration of 0.5M.

Potentiodynamic tests were performed with MetroOhm Autolab Potentiostat M204 in 1L solution of NaBr 0.5M at 50°C.The greater temperature, respect the previews research, was chosen to increase the aggressivity of the solution. The cell, as prescribed by the ASTM G5 [127], is shown in the Figure 2.3.3: WE represents the working electrode, i.e. the metal, with only one face of 1 cm^2 exposed to the solution; RE is the reference electrode (Ag/AgCl); CE is the counter electrode made of activated titanium. Open Circuit Potential is initially searched by the machine in about 60 minutes. Subsequently, potential has been scanned from 100 mV below the OCP up to 8V SSC at 20 mV/min. Anodic current and potential difference between metal and reference electrode have been registered with Nova® 2.1.1 software.
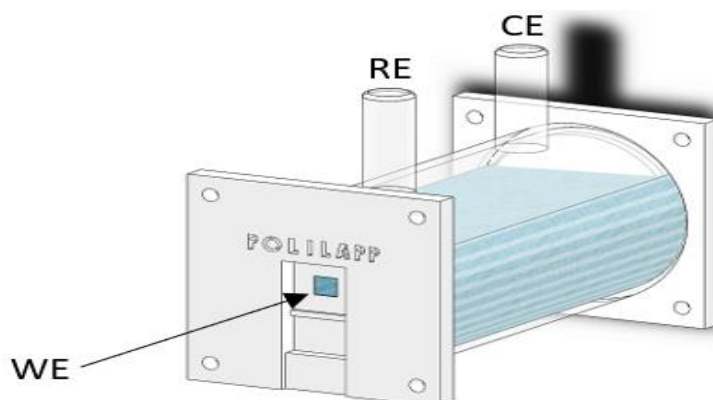
Figure 2.3.4 - Schematic Three electrode electrochemical cell (WE= working electrode, RE= reference electrode, CE= counter electrode).
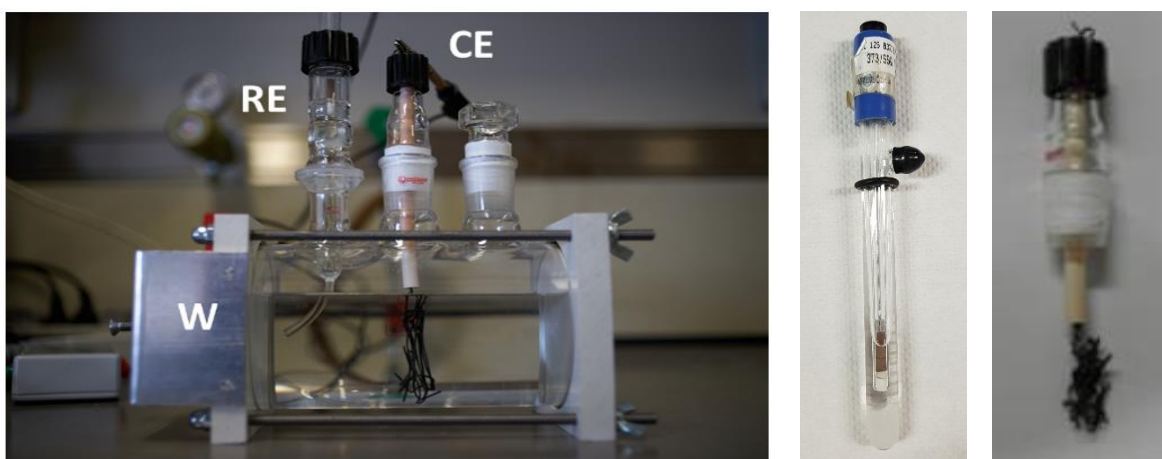
Figure 2.3.3 - Potentiodynamic test cell on the left. Reference electrode (SSC) and counter electrode (Ti) on the right.

In this study, cathodic potentiodynamic tests were performed in an acid environment. Particularly, a solution of H_2SO_4 0.5M at 25°C was used. Potential has been scanned from 100 mV above the OCP up to -2.5V below the OCP at 20 mV/min. The equipment coincides with the one used during the anodic polarization test in NaBr, except for the cell, a spherical balloon, and a support completely covered with Teflon as prescribed by the ASTM standards for introducing the sample into the solution. The surface exposed was also in this case of 1 cm². The Figure below shows the working cell and the sample support.
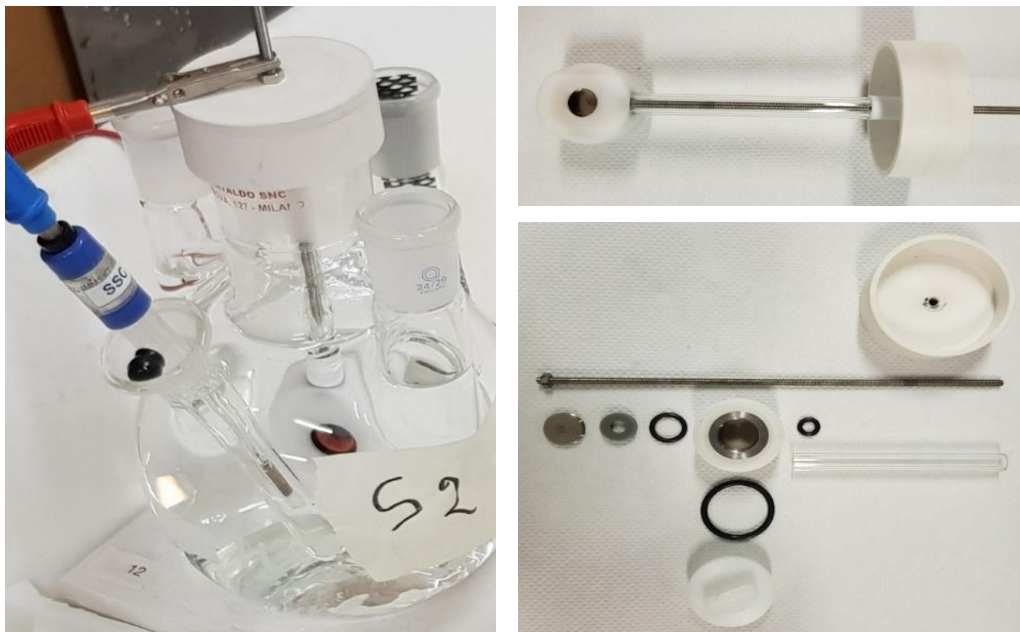
Figure 2.3.5 - On the left, cathodic potentiodynamic test at work. On the right, sample's support assembled (up) and not assembled (down).

2.4 – Surface Analysis

2.4.1 – SEM

A scanning electron microscope SEM StereoScan 360 was used to photograph and determine the TiO_2 surface morphology. Surface conductivity for analysis was provided by gold-sputtered technique. Five pictures for each anodization condition were acquired and an average pore number per image and surface porosity were evaluated by software. ImageJ (Figure 2.4.1) is a Java-based image processing program developed at the National Institutes

of Health and the Laboratory for Optical and Computational Instrumentation (LOCI, University of Wisconsin).
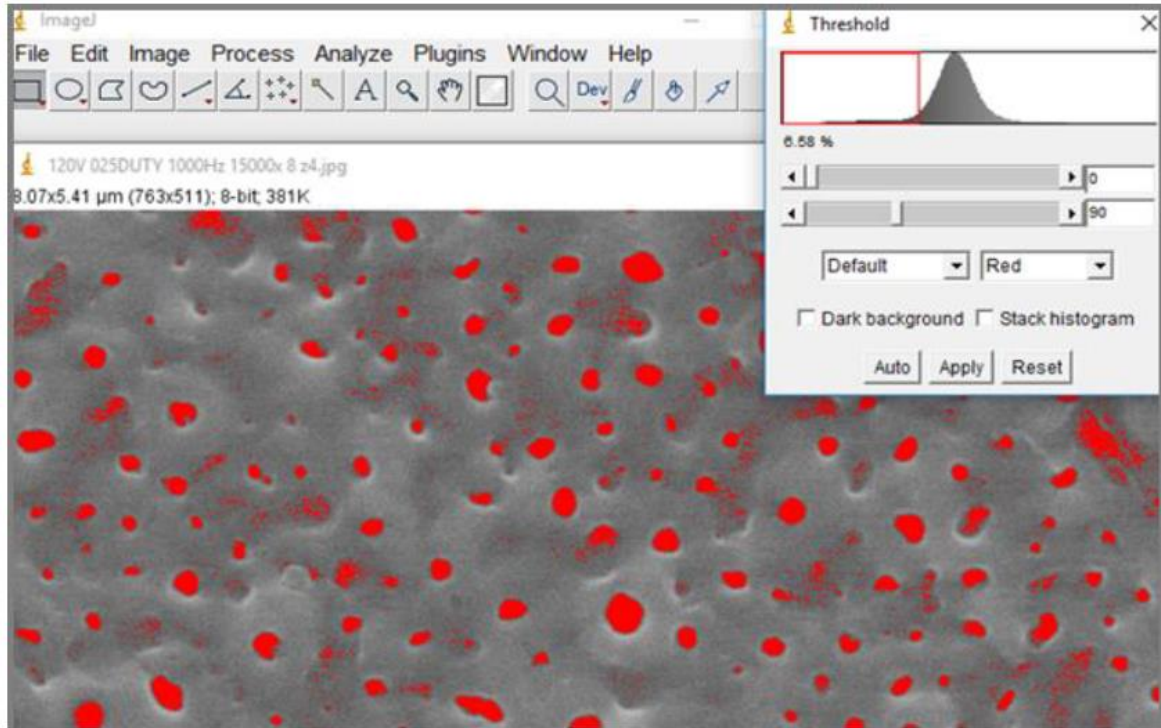
Figure 2.4.1 - View of the ImageJ software processing SEM picture of an anodized sample.

The surface porosity was estimated by the formula:

$$\frac{area\ covered\ by\ pores\ per\ image}{total\ area\ of\ the\ image} * 100$$

The SEM was also used as a direct method to measure the oxide thickness. The sample was sectioned and then incorporated, by hot pressing, into a phenolic resin. Finally, the exposed lateral surface was lapped with silicon carbide papers and alumina particles to obtain surface finishing like a mirror (around 0.8 microns). The average film thickness was evaluated by performing five measurements per image, for a total of 5 images collected in different zones of the deposit.

2.4.2 – XRD

The presence of crystalline structure in the oxides was detected using the XRD technique with a diffractometer model Phillips PW 1830, able to generate a Cu-Kα radiation with a

wavelength of 0.154 nm. The oxide spectra were acquired from 2ϑ angles, in a range between 20° and 40°, knowing that the main peaks for anatase and rutile can be found at $2\vartheta = 25.5°$ and $2\vartheta = 27.5°$ respectively.

2.4.3 – GDOES

The concentration of the elements, specifically hydrogen and sulfur, retained in the oxide during the anodization process were evaluated with Glow-Discharge Optical Emission Spectroscopy (GDOES). In this technique, the surface layers are removed by sputtering with argon ions. The removed atoms pass into the plasma drifted by the applied voltage between the cathode (our sample) and the anode. Photons are emitted with excited waves and have characteristic wavelengths which are recorded by means of a downstream spectrometer and subsequently quantified.

2.4.4 – Optical Microscope

In order to observe the morphology of the corrosion and possible corrosion product on the surface, the optical microscope LEICA DL ML has been used to capture a magnified image of the samples. Due to the intrinsically bi-dimensional nature of the images obtainable in this fashion, a 3D qualitative reconstruction of the surface was carried out moving the focus of the microscope lenses slowly closer to and further from the surface, so that "valleys" and "peaks" on the surface were clearly distinguishable.

2.4.5 – Roughness analysis

The surface roughness induced by uniform corrosion tests was measured by laser profilometry technique. The pure titanium samples taken into consideration were those after 24 h and 72 h of test, for each acid tested. Each sample was subjected to three roughness measurements, to then evaluate the average mean roughness (Ra), max roughness (Rmax), Rq, Rz and Rt. Rz values is the distance between two lines parallel to the average line drawn at a distance equal to the average of the 5 highest peaks and to the average of the 5 lowest valleys in the interval of the base length. Rz roughness provides, in practice, a measure of the maximum irregularity averaged over five peaks and five valleys. Rt is the maximum distance between the major peak and the deepest valley in the base length L.

CHAPTER 3 – Results & Discussion

3.1 – Anodization parameters

Plasma electrolytic oxidation was performed in a potentiostatic fashion, that is, the controlled variable was the voltage. The profile of the current generally has followed the same of the voltage but with the presence of spikes in correspondence of the rise and falls fronts. This phenomenon is derived from the fact that initially the system required more current to change the polarization, after which it stabilized by showing a plateau (Figure 3.1.1).
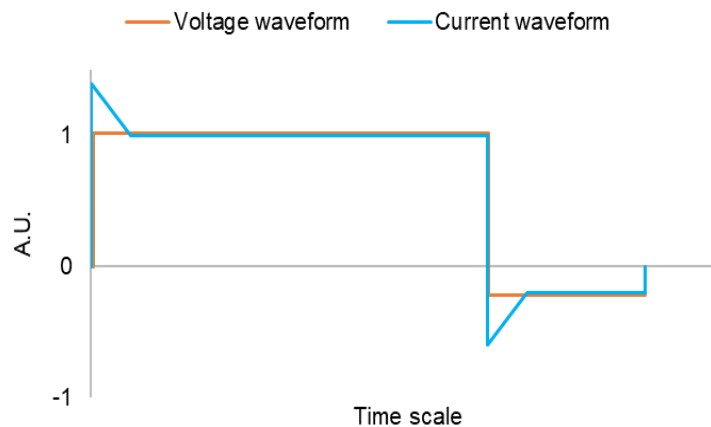
Figure 3.1.1 - Voltage-current waveforms.

The selected duty cycles, according to the criteria imposed in paragraph 2.2, were 90%A - 10%C and 60%A - 40%C at different cathode peaks: 2%, 5%, 7% and 10%. These were performed at two extreme frequencies, 20 Hz and 1000 Hz. The voltage to be reached was 160V with a 0.5 V/s ramp leading to a treatment time of 320 seconds. The initial and final temperature, and the current, anodic and cathodic, has been marked for each anodizing treatment (Table 3.1.1). The temperature increase comes from the joule effect due to the passage of current through all the impedances composing the circuit, as like the impedance of the electrolyte and the overvoltage localized on the metal electrodes.

Table 3.1.1 - Temperature and electrical parameters of each anodization condition tested.

Sample n°	Waveform	ΔT [°C]	I_{ANODIC} [A]	$I_{CATHODIC}$ [A]
1	90%A-10%C - 20Hz - 2%	3	0.224	-0.267
2	90%A-10%C - 1000 Hz- 2%	2	0.487	-2.575
3	60%A-40%C - 20Hz - 2%	2	0.265	-0.155
4	60%A-40%C - 1000Hz - 2%	4.5	0.516	-0.470
5	90%A-10%C - 20Hz - 5%	3	0.220	-2.080
6	90%A-10%C - 1000Hz - 5%	2	0.150	-0.984
7	60%A-40%C - 20Hz - 5%	2	0.116	-1.679
8	60%A-40%C - 1000Hz - 5%	16	0.844	-3.000
9	90%A-10%C - 20Hz - 7%	2.5	0.240	-3.210
10	90%A-10%C - 1000Hz - 7%	3	0.173	-2.042
11	60%A-40%C - 20Hz - 7%	3.5	0.221	-2.600
12	60%A-40%C - 1000Hz - 7%	19.5	1.088	-3.740
13	90%A-10%C - 20Hz - 10%	2.5	0.457	-6.565
14	90%A-10%C - 1000Hz - 10%	4	0.163	-2.485
15	60%A-40 %C- 20Hz - 10%	7.5	0.386	-4.000
16	60%A-40%C - 1000Hz - 10%	8	0.349	-3.660

The duty 60%A - 40%C showed higher heating of the electrolyte than the duty 90%A - 10%C, for all the cathodic peaks used. This is because the currents, both anodic and cathodic, involved in the process were huge. Sample 12 induced the highest temperature rise in electrolyte, showing highest I_A and reasonable high I_C. Another special case was condition 2, in which the plateau of the cathodic current was the highest among the cycles with peak at 2%; the explanation is because more current needed to reverse the polarization 1000 times per second (1000 Hz) from a 90% anodic contribution. In conclusion, an increase of the cathodic peak generally increases the plateau of cathodic current involved into the anodization process, while the anodic contribution showed a non-linear trend.

3.2.1 – Morphology

The morphology of the treated samples was investigated by the SEM analysis, capturing five photos for each anodization condition. The images were processed by ImageJ software to estimate the number of pores, surface porosity and coefficients of variation, that are reported in Table 3.2.1.

$$\frac{area\ covered\ by\ pores\ per\ image}{total\ area\ of\ the\ image} * 100$$

The coefficients of variation (C.V.) represent the difference in the number of pores or surface porosity measurements that were taken at different positions along the surface. These values give us indications regarding the homogeneity of the coating.

$$CV\ (\%) = \left(\frac{Standard\ deviation}{Mean}\right) \times 100$$

Table 3.2.1 - Surface porosity and number of pores per image, for each anodization condition tested. C.V.= coefficient of variation.

Sample n°	Waveform	Pores n°	C.V. [%]	Porosity [%]	C.V. [%]
1	90-10-20Hz-2%	256	12.6	9.71	6.9
2	90-10-1000Hz-2%	220	14.2	7.3	23.1
3	60-40-20Hz-2%	249	15.5	14.4	17.5
4	60-40-1000Hz-2%	238	29	10.34	12
5	90-10-20Hz-5%	198	6.3	17.25	4.5
6	90-10-1000Hz-5%	188	11.3	13.38	11.2
7	60-40-20Hz-5%	175	13.9	15.29	16.4
8	60-40-1000Hz-5%	510	11.5	13.21	19.9
9	90-10-20Hz-7%	198	4.7	13.92	13.8
10	90-10-1000Hz-7%	173	3.9	9.71	13
11	60-40-20Hz-7%	491	13.2	16.1	28.9
12	60-40-1000Hz-7%	182	5.7	25.55	6.1
13	90-10-20Hz-10%	412	2.8	16.73	15.1
14	90-10-1000Hz-10%	151	15.1	13.35	15.8
15	60-40-20Hz-10%	733	6.4	19.56	11.1
16	60-40-1000Hz-10%	86	15	18.50	6.9

In general, the surface porosity has a decreasing trend with increasing frequencies, with the exception of duty 60%A - 40%C with cathodic peak at 7%. In fact, sample 12 shows that high frequencies favor an increase in surface porosity even if there is a drastic decrease in the number of pores. Moreover, this condition has the highest degree of porosity (25.55%), but with low variation coefficients (5.7% for pores number and 6.1% for surface porosity). The lowest value of porosity, on the other hand, belongs to condition 2 with only 7.3% with the second highest value of C.V. (23.1%).

The Figure 3.2.1 display how the evolution of the surface porosity is influenced by the variation of the cathodic peak. It is interesting to point out that the duty 90%A - 10%C, at the two frequencies (red curves), show the same behaviour upon cathodic peak variation, where the use of a frequency of 1000 Hz allowed to obtain a lower surface porosity for all the conditions tested. Despite the decrease in porosity with respect to the frequency increase, the trend of variation coefficients is the opposite, with the exception of cycles 9 and 10, indicating an uneven surface distribution. Conversely, the duty 60%A - 40%C behave differently with the frequencies: for 20 Hz there is a monotonically increasing trend, with the maximum at 10% cathodic peak but with maximum C.V. for condition 11 (28.9%), that means high inhomogeneities; while, for 1000 Hz there is a maximum at 7% cathodic peak with a sharp decrease bringing the peak to 10%.
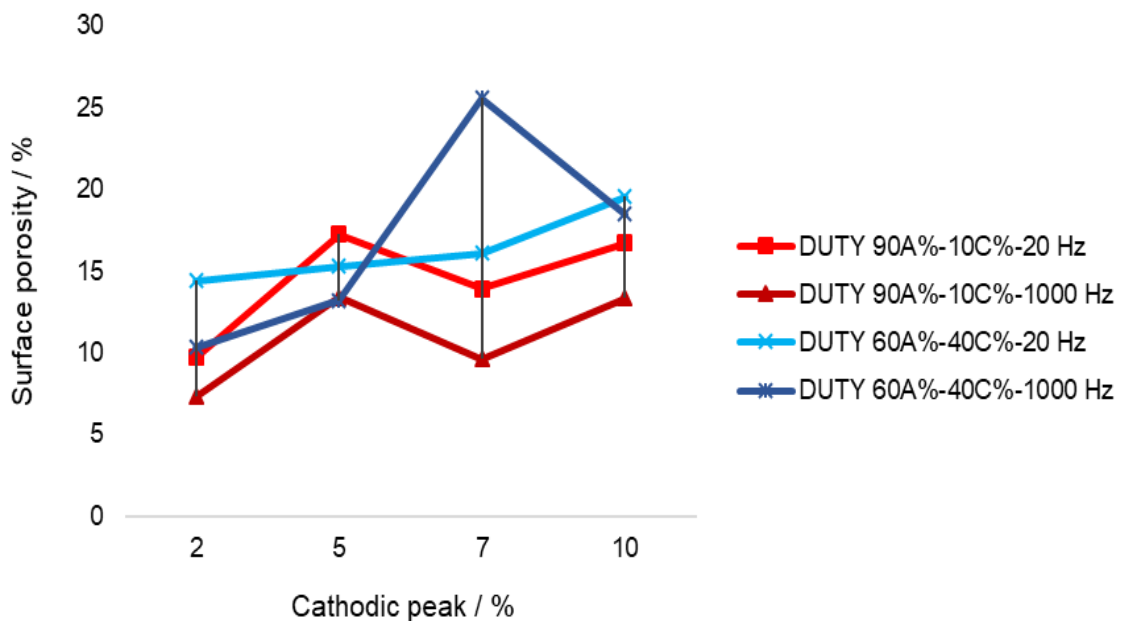
Figure 3.2.1 - Surface porosity evolution at different cathodic peaks.

Figure 3.2.2 shows the influence of frequency and cathode peak on the number of pores. This appears to be little affected in the cycles 90%A - 10%C from the frequency and from the cathode peaks, with the exclusion of the sample 13 (10%C peak) for which the low frequencies lead to a high number of pores (412) evenly distributed. Duty 60%A - 40%C, on the other hand, show opposite trends. The transition from low to high frequencies tends to favor the reduction of porosity. The most notable case is at samples 15 and 16 with a cathodic peak at 10%, where the number of pores goes from 733 to 83. While, a deviation of this behavior is exhibited under conditions 7 and 8, with the increase in the pores number at 1000 Hz.
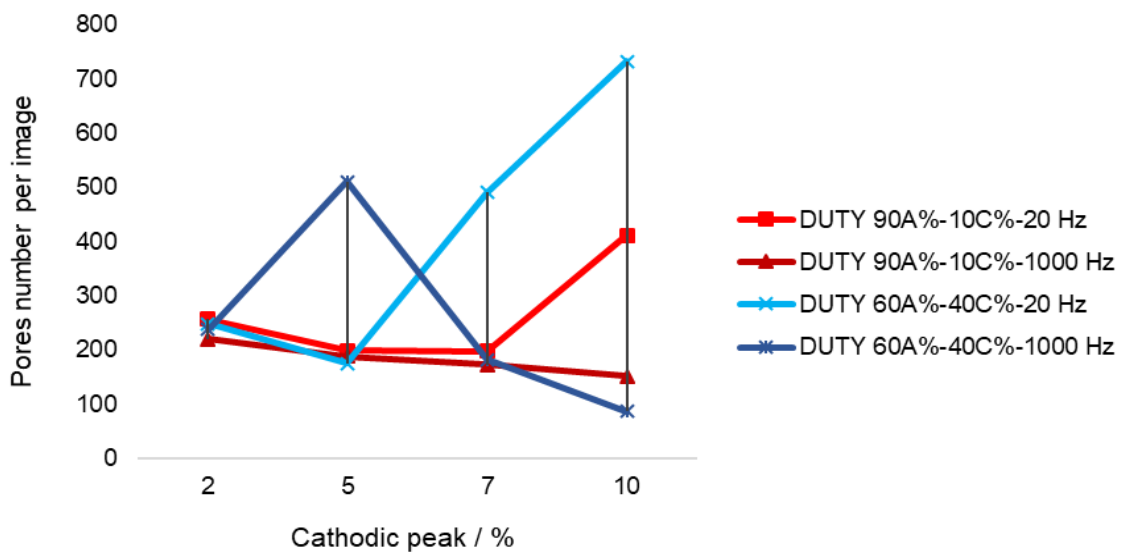
Figure 3.2.2 - Pores number evolution at different cathodic peaks.

The SEM images for all anodized samples are collected in Figure 3.2.3. It is possible to notice the different morphology in the samples 2 and 16, which show the lower porosity among all the specimens. In condition 2 there is a greater number of pores but with a smaller size, about 0.01 μm^2, while in condition 16, with the lowest number of pores, the average size of these latter is 8 times greater (0.085 μm^2).

Furthermore, the pictures highlight five different morphologies:

- Surface characterized by a high number of small pores: samples 8, 11 and 13. In these conditions, unlike what has been elaborated by other authors [128], high frequencies

do not necessarily produce smaller pores, even if the overall surface porosity seemed to diminish. In fact, for the 60%A - 40%C duty, apart from the one designed with a cathodic peak of 5%, the opposite is true. An increase in frequency leads to an increase in pore size. Condition 11 shows a particular formation of deposits, distributed in a non-homogeneous way, which give a certain surface roughness, with pores having a diameter between 95 and 343 nm.

- Surface characterized by a few very large pores: sample 12. This condition, which has the highest percentage of surface porosity, is also the one that induces the largest heating of the electrolyte during the anodizing treatment. The cause of this increase is probably due to prolonged sparks, which degrade the coating, causing a high level of porosity, and heating the solution by the development of high current.

- Surface characterized by deposits and high roughness: samples 2, 4 and 15. The duty cycles with cathodic peak at 2% and with frequencies at 1000 Hz lead to the formation of small deposits that are distributed over the entire surface. These deposits affect the roughness, increasing it, and sealing some pores. In condition 15, instead, rather than small deposits, one must speak of cluster of materials above the surface with very small pores.

- Surface relatively flat characterized by small pores and same surface porosity: samples 1 and 10. The specimens were produced with the same work cycle (90%A - 10%C) and show the same surface porosity of 9.71%. Furthermore, the coverings appear flat and without deposits. The differences of these conditions reside in the frequencies (20 Hz for the sample 1 and 1000 Hz for the sample 10) and in the cathode peak used (2% for the sample 1 and 7% for the sample 11). The latter has hindered the effect of frequency variation.

- The surfaces of the remaining samples (3, 5, 6, 7, 9, 14 and 16) coincide similarly with those already encountered in other studies concerning monopolar anodes spark deposition.
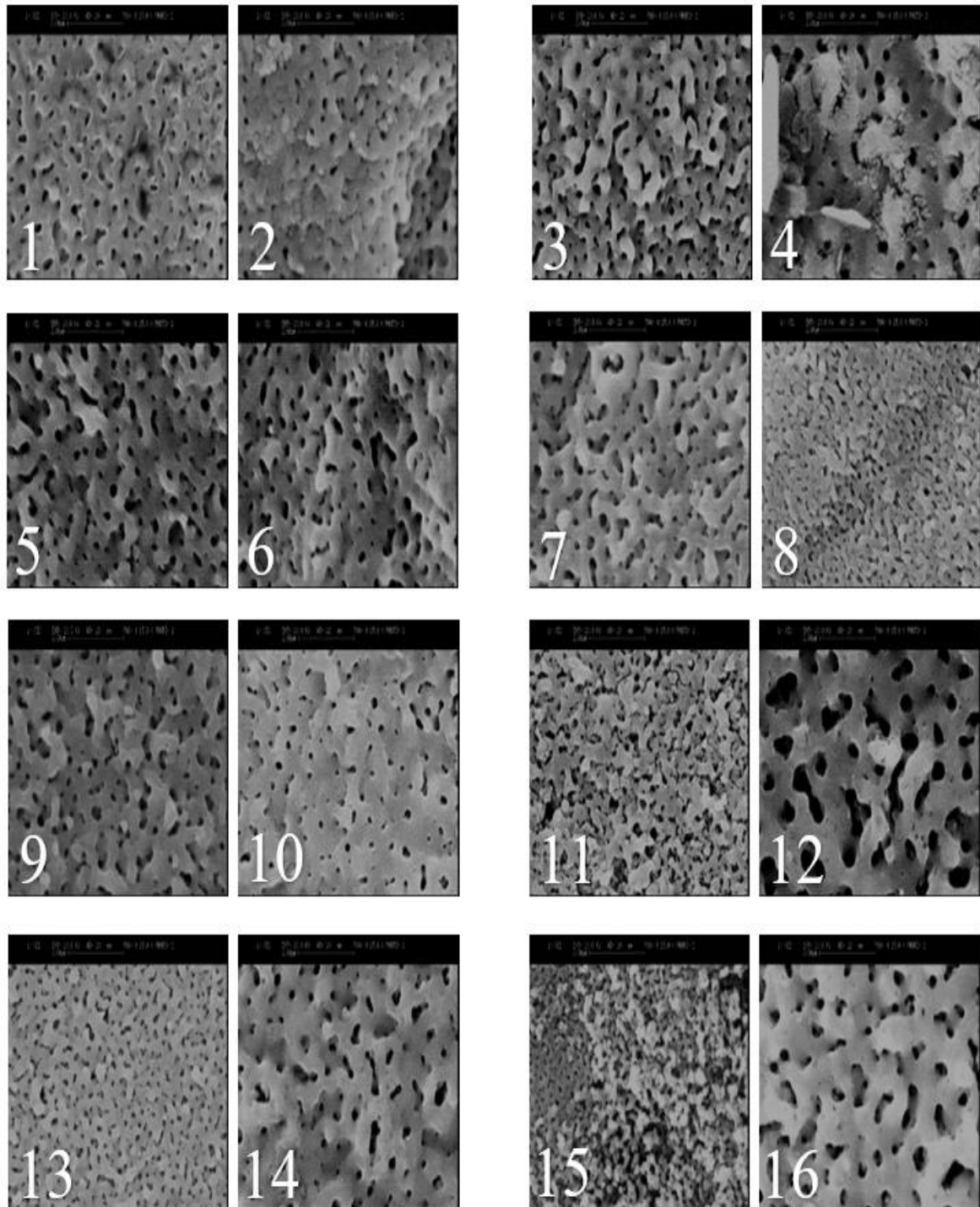
Figure 3.2.3 - Cambridge Stereoscan 360 SEM images, from sample 1 to 16.

3.2.2 – Oxide thickness

The thickness of the TiO$_2$ coating is also measured with the SEM analysis. Initially, the preparation of the anodized samples involves a cut along one side and then incorporation, by hot pressing, into a phenolic resin. The next step was a mechanical lapping with silicon carbide paper and alumina particles to obtain a mirror finish surface with an average roughness of approximately the order of 0.8 μm. In Table 3.2.2 their average, minimum and maximum values are collected. The average thickness of a coating is evaluated by performing 5 measurements per image, for a total of 3 images collected in different areas of the deposit.

As can be seen from the Figure 3.2.4, the duty 90%A - 10%C at 1000 Hz results to have an almost constant thickness with the increase of the cathode peak. While at low frequencies, it has an increasing trend up to 7% but obtaining the minimum thickness with cathodic peak at 10%, even with respect to high frequencies. In the waveform 60%A - 40%C - 20 Hz the variation of the cathode peak shows an alternating trend in the average thickness of the oxide. At a frequency of 1000 Hz, this work cycle allowed the thickness to be increased for all the conditions tested, with sample 16 showing the highest average value of 4.2 μm. The less thick oxide films were reached by conditions 7 and 15, also showing the lower amount of both crystalline phases, as shown in the next paragraph. This correlation appears reasonable since the smaller amount of crystalline structure could be interpreted as a less aggressive ASD deposition regime. Less sparks lead to less heating of the solution and less oxide growth. On the contrary, the thicker samples had a high level of rutile phase, indicating the presence of more intense spark events. Figure 3.2.5 is an SEM image of the sample 9, which has about 3 microns of thickness, uniformly distributed along the thickness shown in the image.
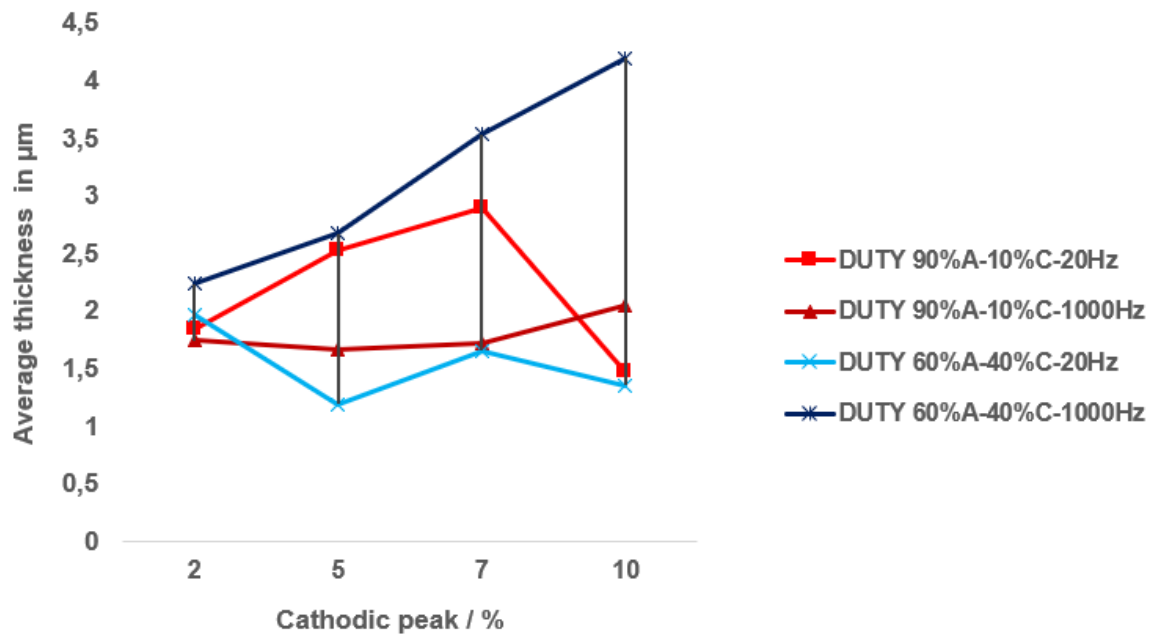
Figure 3.2.4 - Oxide thickness trend at different cathodic peak.

Table 3.2.2 - Minimum, maximum and average thickness values for each anodization condition tested.

Sample n°	Average [μm]	Min [μm]	Max [μm]
1	1.85	1.41	2.1
2	1.75	1.36	2.31
3	1.97	1.54	2.34
4	2.24	1.51	2.78
5	2.53	1.78	3.14
6	1.67	1.49	1.83
7	1.20	1.04	1.57
8	2.68	1.79	3.82
9	2.90	2.56	3.48
10	1.72	1.14	2.62
11	1.66	1.34	2.07
12	3.54	3.20	3.82
13	1.48	1.25	1.86
14	2.05	1.5	2.45
15	1.36	1	1.85
16	4.2	3.47	4.75
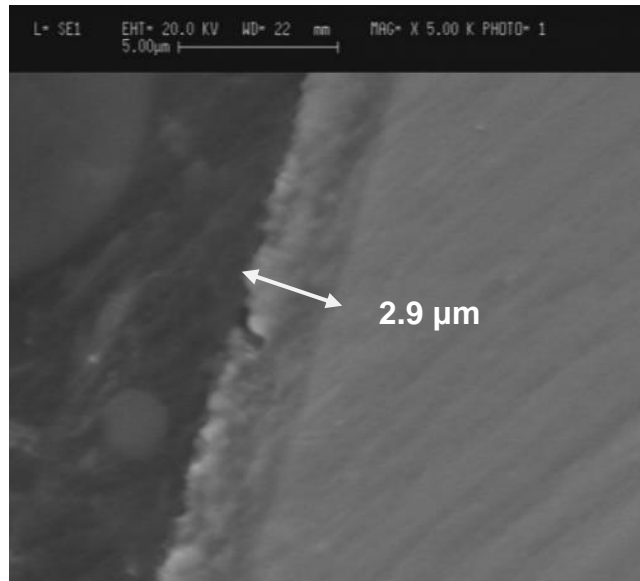
*Figure 3.2.5 - Cross-section image of condition 9 (90A%-10C%-20 Hz-7%) acquired by
SEM 360 Stereoscan Cambridge Analytica.*

3.2.3 – XRD analysis

Titanium dioxide can occur in two crystallographic forms, anatase and rutile, which can be analyzed with X-ray diffraction.
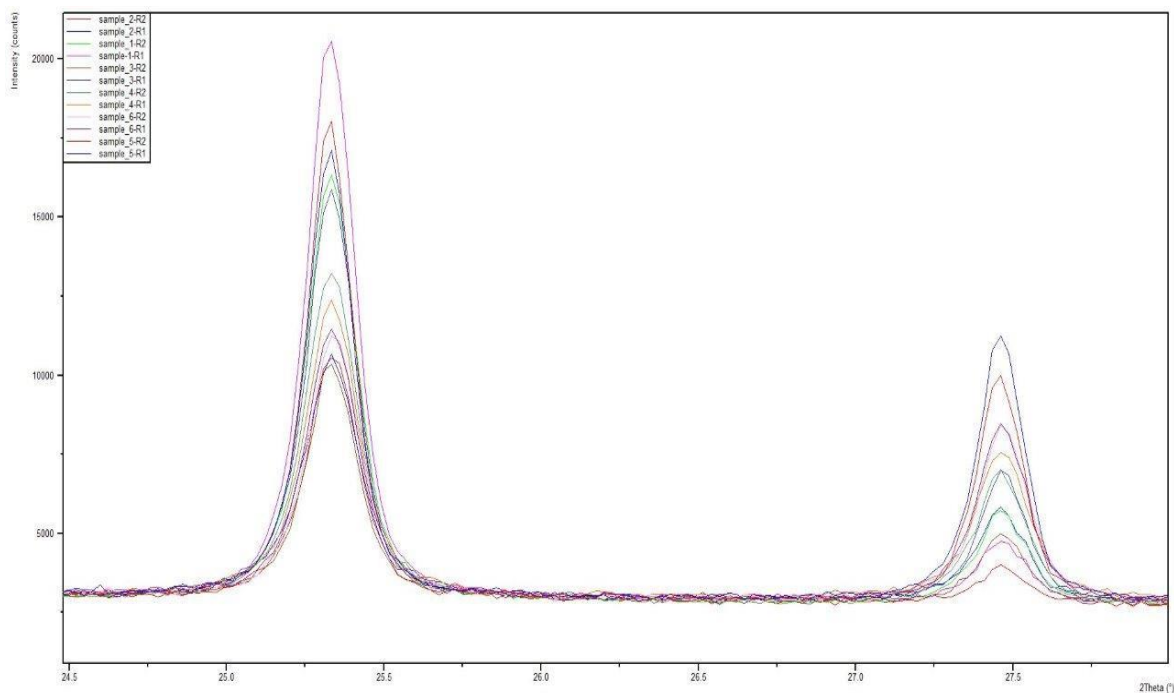
Figure 3.2.6 - XRD diffraction spectrum of samples 1,2,3,4 and 5.

In the Figure 3.2.6, an example of the diffraction spectrum is represented, for samples 1,2,3,4 and 5, with the intensity as a function of the 2ϑ, in which $2\vartheta=25.5°$ correspond to anatase phase and $2\vartheta=27.5°$ to rutile phase. In order to better compare the structures of the different conditions, the Intensity vs 2ϑ graphs in Figure 3.2.6 have been replaced with histograms representing the underlying areas of the main anatase and rutile peaks.
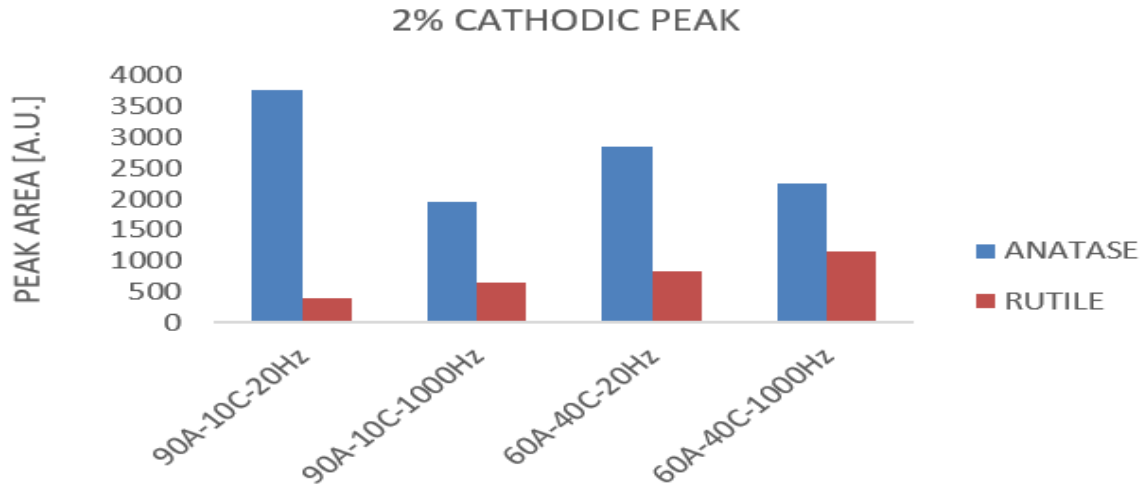
Figure 3.2.7 - Comparison between work cycles with cathode peak at 2% of anatase and rutile phases.

In Figure 3.2.7 the data concerning the crystalline phases of the anode regimes with cathodic peak at 2% are collected. It is observed that the increase in frequency for both work cycles 1 and 3 has allowed to reduce the quantity of anatase phase, while increasing that of rutile. Moreover, as the cathodic phase increases, there is an increase in rutile phase.
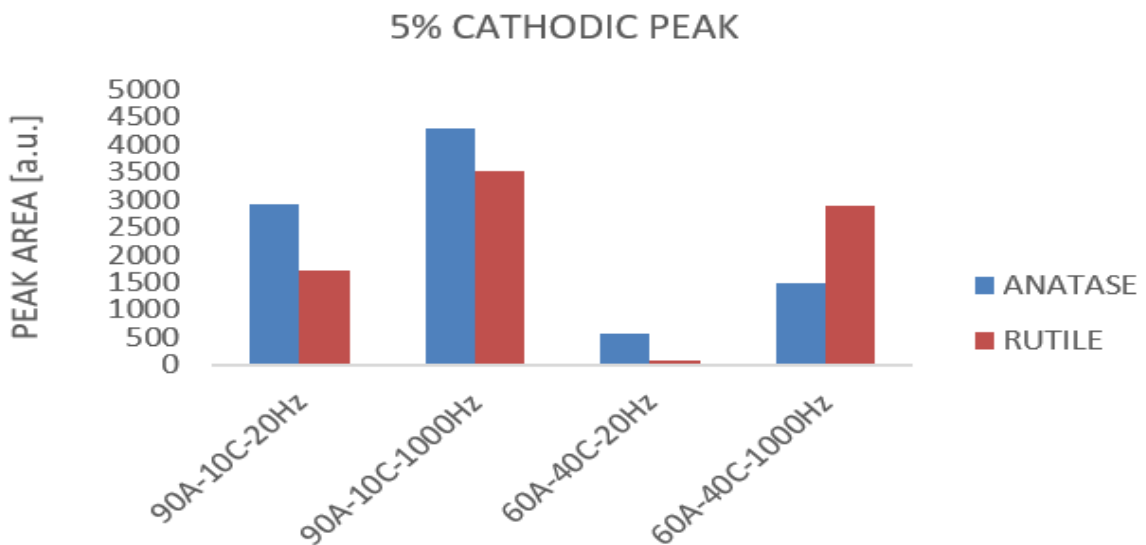
Figure 3.2.8 - Comparison between work cycles with cathode peak at 5% of anatase and rutile phases.

In the case of the 5% cathodic peak (Figure 3.2.8), both duty cycles increase the frequency leading to the formation of a greater quantity of anatases and rutile crystal phases. The maximum quantity of both structures was reached by sample 6 (90%A - 10%C at 1000 Hz), making it interesting for photocatalytic applications. On the other hand, the lowest amount of crystallinity was obtained under condition 7 (60%A - 40%C at 20 Hz). A high degree of amorphous material is required in the field of corrosion, where the lower conductivity of the amorphous phase is highly appreciated.
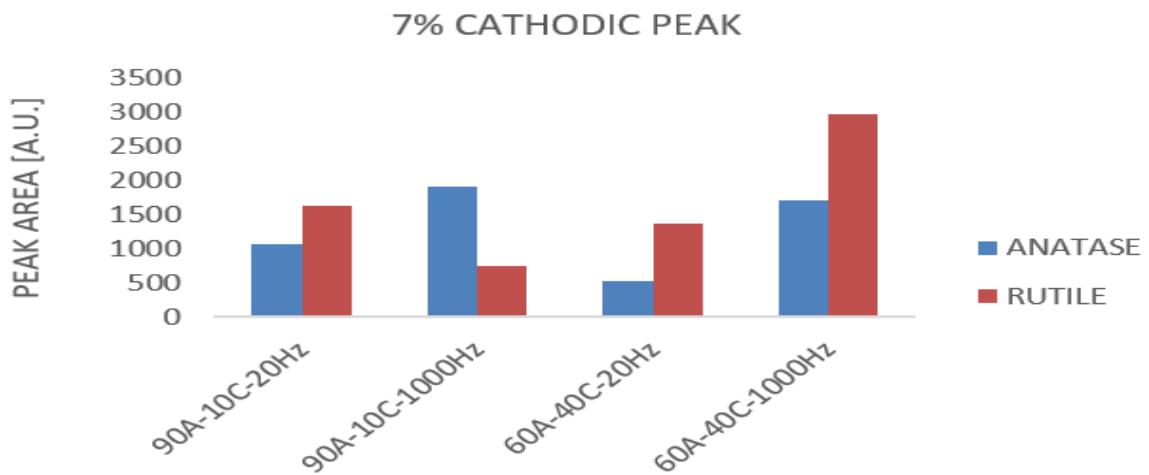
Figure 3.2.9 - Comparison between work cycles with cathode peak at 7% of anatase and rutile phases.

The cathodic peak of 7% (Figure 3.2.9) shows a different trend depending on the selected waveform. The increase in frequency for duty 90%A - 10%C reverses the production of crystalline phases: there is an increase in anatase and a decrease in rutile. Instead, this is not valid for duty 60%A - 40%C. Comparing conditions 11 and 12, the higher frequency of sample 12 induced a considerable increase in both crystal structures.
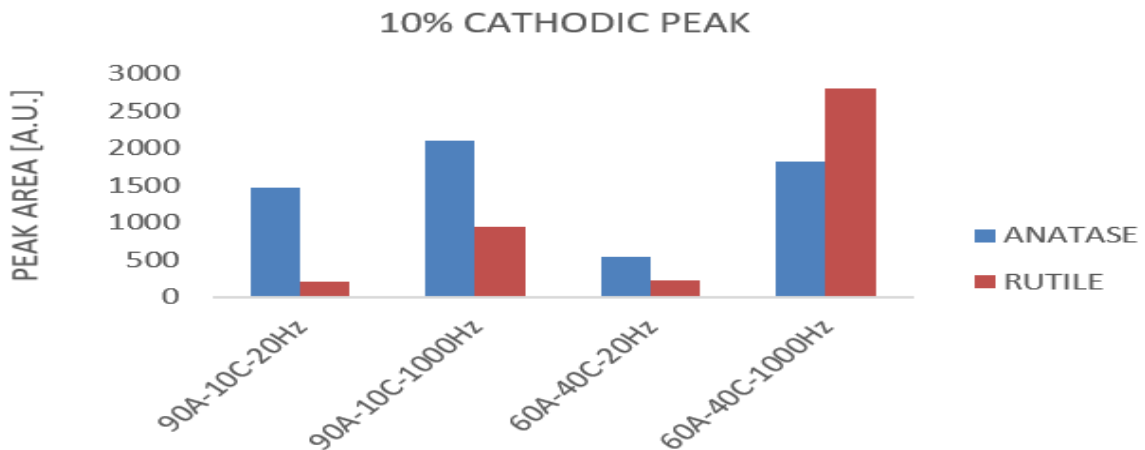
Figure 3.2.10 - Comparison between work cycles with cathode peak at 10% of anatase and rutile phases.

Finally, Figure 3.2.10 shows that using the cathodic peak at 10%, the quantity of anatase and rutile phases is increased for both work cycles at higher frequency.

The graph below (Figure 3.2.11) contains the crystalline peak areas of all the samples. This overview shows that the anatase phase is totally predominant only in cycles with a 2% cathode peak. Another peculiarity lies in the regime 60%A - 40%C at 1000 Hz for the remaining cathode peaks (5%, 7% and 10%), which show an equal ratio between the crystalline phases and equal areas of peaks, with the domain of the rutile phase.

| n°	A%	C%	Hz
1	90	10	20
2	90	10	1000
3	60	40	20
4	60	40	1000
5	90	10	20
6	90	10	1000
7	60	40	20
8	60	40	1000
9	90	10	20
10	90	10	1000
11	60	40	20
12	60	40	1000
13	90	10	20
14	90	10	1000
15	60	40	20
16	60	40	1000
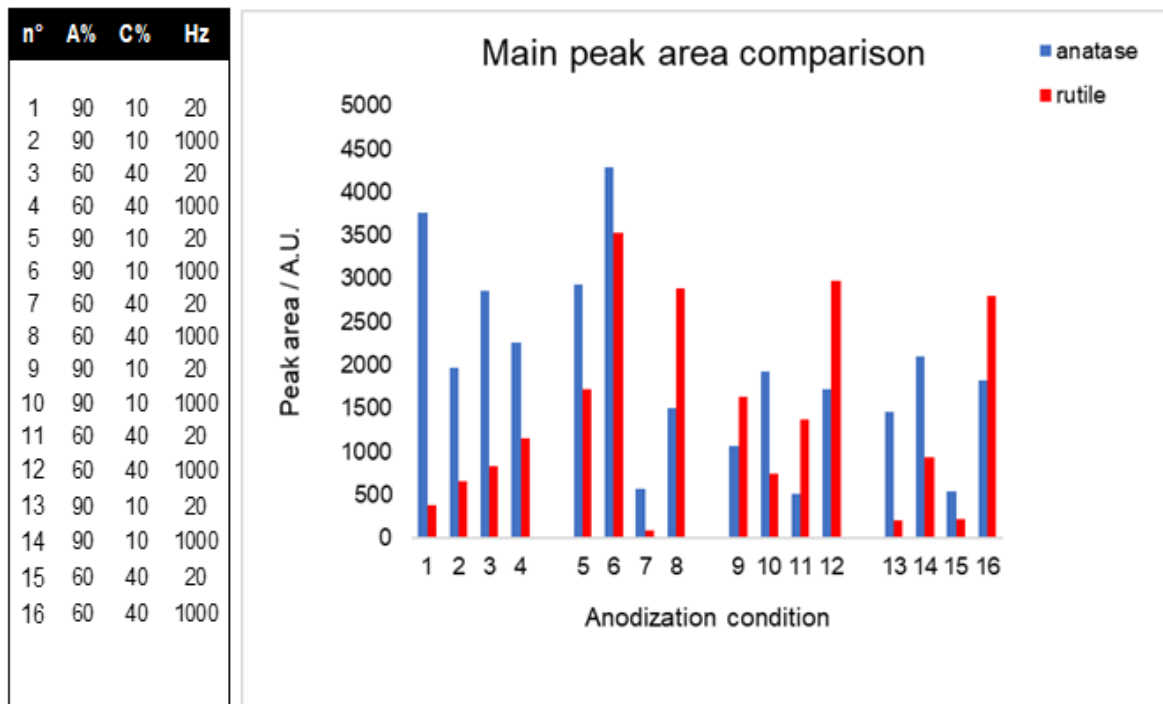
Figure 3.2.11 - Comparison among the structures of all anodized samples.

3.2.4 – Hydrogen retention

The use of the GDOES technique allows to evaluate the concentration profile of the species present in the TiO_2 coating. This analysis technique was performed on sample 16, as it presents the condition with the highest level of cathodic contribution (60%A - 40%C at 1000 Hz with 10% cathode peak), and on a sample with the same work cycle and frequency but monopolar type. The chemical profiling of the coatings along the thickness is concentrated on hydrogen and sulfur retention. In Figure 3.2.13, it is possible to understand from the trend of oxygen (blue line) and titanium (purple line) that the oxide has a thickness greater than 3.5 µm, quite according to the SEM analysis (4.2 µm). The hydrogen (H) and sulfur (S)

profiles, after a high signal from the surface of the film, decrease until the proximity of the interface between the oxide and the metallic titanium. This increase in concentration of H and S agrees with other studies [129]. It can be deduced that the hydrogen permeates the oxide during the cathodic part of the duty cycle, while the sulfur during the anodic part, in the form of sulphates. The presence of a compact barrier layer, formed during the anodizing process, induces an accumulation of elements at the interface between the coating and the metal. This is explained by the fact that hydrogen has a diffusion coefficient in titanium oxide (10-13 cm^2/s) of at least 3 orders of magnitude lower than that of the metal [130].
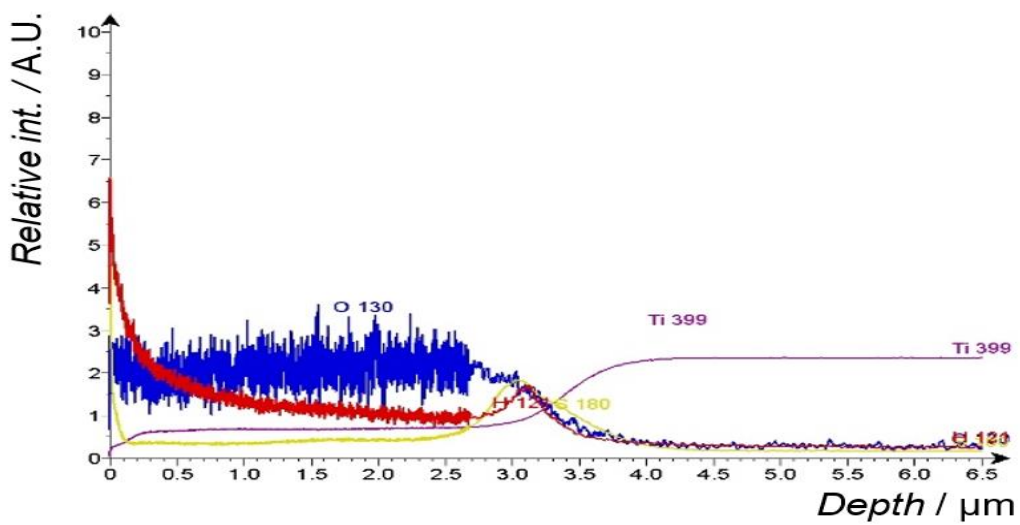
Figure 3.2.13 - GDOES chemical profiling of sample anodized in bipolar ASD regime (60A%-40C%-1000Hz-10%).
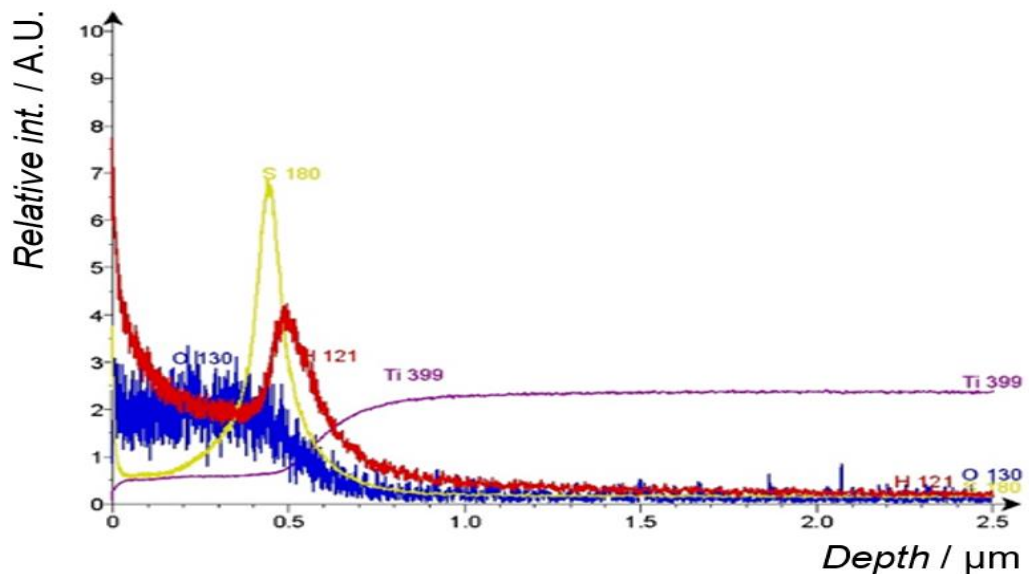
Figure 3.2.12 - GDOES chemical profiling of sample anodized in monopolar ASD regime (60A%-40R%)

In the monopolar regime (60%A, Figure 3.2.12), the same peak occurs at the interface between the metal and the oxide, but with a higher signal. The second test was performed immediately after the previous one, allowing to maintain the same calibration of the instrument. In this configuration, it is possible to notice that the bipolar cycle has allowed a lower retention of sulfur and hydrogen with respect to the monopolar regime and that hydrogen retention has occurred independently of the applied cathodic polarization. Comparing Figure 3.2.13 and Figure 3.2.12 shows that the use of a bipolar process produced a thickness at least 6 times greater than that obtained by a monopolar regime, about 0.6 μm, using the same amount of applied anodic polarization (60%) and at the same frequency (1000 Hz). This result found discrepancies compared to previous studies (note), which show low thickness coatings using a bipolar signal on titanium gr.5 in a solution of sodium aluminate of 8 g/L and sodium phosphate 1 g/L. Other authors have established that probably the high cathodic polarization applied to the sample has allowed an increase in the conductivity inside the oxide due to the introduction of cations, decreasing the potential barrier and favoring the kinetics of oxide growth [131]. However, apart from the interface of the metal coating, hydrogen was not detected in the titanium metal sample for both the monopolar and bipolar process, thus avoiding possible phenomena of hydrogen embrittlement of the substrate material.

3.3 – Corrosion

3.3.1 – Immersion tests

Uniform corrosion was evaluated with immersion tests (ASTM G1 and G31) in solutions of sulfuric, sulfamic, phosphoric, hydrochloric and oxalic acids, as explained in paragraph 2.3.1. The programmed tests for pure titanium had a total duration of 5 days using 4 samples: three immersed at the same time and extracted after 24 h (A_1), 48 h (A_t) and 72 h (A_{t+1}); one entered the third day for 24 h (B).

The first results following the tests concerned the corrosion rates. In addition, it was analyzed whether and how the corrodibility of the metal and the aggressiveness of the solution changed during the test.

Table 3.3.1 - Corrosion rate of Ti gr. 2 in sulfamic acid (10%v/v , 60°C).

Acid	Sample	C.R. [mm/y]	Solution aggressivity	Metal corrodibility
Sulfamic **10% v/v** **60°C**	A_1	0.35	$A_1 << B$ (↑)	$A_t < A_{t+1}$ (↑)
	A_t	0.34		
	A_{t+1}	0.47		
	B	1.92		

Table 3.3.2 - Corrosion rate of Ti gr.2 in phosphoric acid at different temperature and concentrations.

Acid	Sample	C.R. [mm/y]	Solution aggressivity	Metal corrodibility
H_3PO_4 **30% v/v** **60°C**	A_1	2.59	$A_1 = B$	$A_t = A_{t+1}$
	A_t	2.57		
	A_{t+1}	2.65		
	B	2.38		
H_3PO_4 **40% v/v** **35°C**	A_1	0.71	$A_1 > B$ (↓)	$A_t = A_{t+1}$
	A_t	0.47		
	A_{t+1}	0.43		
	B	0.39		
H_3PO_4 **50% v/v** **35°C**	A_1	1.58	$A_1 >> B$ (↓)	$A_t < A_{t+1}$ (↑)
	A_t	0.10		
	A_{t+1}	0.33		
	B	0.29		
H_3PO_4 **60% v/v** **35°C**	A_1	0.41	$A_1 < B$ (↑)	$A_t > A_{t+1}$ (↓)
	A_t	0.69		
	A_{t+1}	0.52		
	B	0.65		

Table 3.3.3 - Corrosion rate of Ti gr.2 in hydrochloric acid at different temperature and concentrations.

Acid	Sample	C.R. [mm/y]	Solution aggressivity	Metal corrodibility
HCl	A_1	0.05		
	A_t	0.07		
2% v/v	A_{t+1}	1.13	$A_1 << B$ (↑)	$A_t << A_{t+1}$ (↑)
60°C	B	1.76		
HCl	A_1	0.80		
	A_t	1.05		
6% v/v	A_{t+1}	0.98	$A_1 < B$ (↑)	$A_t = A_{t+1}$
50°C	B	0.98		
HCl	A_1	3.97		
	A_t	5.64		
10% v/v	A_{t+1}	6.65	$A_1 << B$ (↑)	$A_t < A_{t+1}$ (↑)
60°C	B	6.40		

Table 3.3.4 - Corrosion rate of Ti gr. 2 in oxalic acid at different temperature and concentrations.

Acid	Sample	C.R. [mm/y]	Solution aggressivity	Metal corrodibility
Oxalic	A_1	1.89		
	A_t	1.83		
1% v/v	A_{t+1}	2.09	$A_1 = B$	$A_t < A_{t+1}$ (↑)
50°C	B	1.74		
Oxalic	A_1	5.67		
	A_t	8.45		
10% v/v	A_{t+1}	9.75	$A_1 < B$ (↑)	$A_t < A_{t+1}$ (↑)
60°C	B	6.46		

Table 3.3.5 - Corrosion rate of Ti gr.2 in sulfuric acid (10%v/v , 60°C).

Acid	Sample	C.R. [mm/y]	Solution aggressivity	Metal corrodibility
H_2SO_4	A_1	8.08		
	A_t	11.17		
10% v/v	A_{t+1}	14.16	$A_1 < B$ (↑)	$A_t < A_{t+1}$ (↑)
60°C	B	14.4		

The above tables show the corrosion rates obtained from the different acid solutions for titanium grade 2. The acids with more corrosive power are HCl, oxalic and H_2SO_4 at 10% v/v and 60°C. Sulfamic acid solution, despite of the low corrosion rate respect others, shows a significant increase in aggressivity, about 5 times as it was verified by the immersion of a fourth sample after 72 h from the first one. The corrosion rates of the phosphoric acid appear to be more influenced by the temperature than by the concentration, in fact the higher values are recorded for the condition 30% v/v and 60°C, while progressively increasing the concentrations, but maintaining the temperature at 35°C, the C.R. do not vary markedly. The aggressiveness of the H_3PO_4 solution at 50% v/v and 35°C exhibits a considerable reduction, of about 5 times. The corrosion of the HCl has an incremental trend in all the studied conditions. It is interesting to note that the case of the lowest concentration (2% v/v), the corrodibility of pure titanium and the aggressiveness of the solution increase drastically. Up to 48 h, the corrosion rates remain below the acceptable limit value (0.13 mm/y), while for longer uses of the solution they exceed it by almost 10 times. Oxalic acid as in literature appears to be a very aggressive organic acid, with a corrosive attack greater than HCl. The most corrosive acid is sulfuric acid, with the maximum corrosion rate for sample B of 14.4 mm/y.

Titanium grade 7 was tested with oxalic and sulfuric acid at 10% v/v and 60°C, which were the strongest acids, organic and inorganic, against titanium grade 2. Table 3.3.6 shows the corrosion rates of the two acids.

Table 3.3.6 - Corrosion rate of Ti gr. 7 in sulfuric and oxalic acid.

Acid	Concentration [%v/v]	Temperature [°C]	Sample	C.R. [mm/y]	Metal Corrodibility
H_2SO_4	10	60	A_1	0.54	$A_t > A_{t+1}$ (↓)
			A_t	0.29	
			A_{t+1}	0.22	
Oxalic	10	60	A_1	0.12	$A_t < A_{t+1}$ (↑)
			A_t	0.15	
			A_{t+1}	0.22	

Titanium grade 2 samples, exposed to the worst conditions for each acid (sulfamic 10% v/v at 60°C, H_3PO_4 30% v/v at 60°C, HCl 10% v/v at 60°C, oxalic 10% v/v at 60°C and H_2SO_4 10% v/v at °C), were treated with a cathodic process to remove possible surface corrosion products. Subsequently, the surfaces were studied under an optical microscope, to evaluate

the area and depth of the craters distributed on them, and with the laser profilometer, to obtain the roughness (Ra, Rq, Rz, Rt and Rmax).

The following images represent the surfaces of the samples at 24 h (A_1) and at 72 h (A_{t+1}) obtained with the optical microscope, with indications over the crater areas.

Figure 3.3.1 - Surface of the sample A_1 (24h) tested in sulfamic acid.

Figure 3.3.2 - Surface of the sample A_{t+1} (72h) tested in sulfamic acid.

Figure 3.3.3 - Surface of the sample A$_1$ (24h) tested in H$_3$PO$_4$.
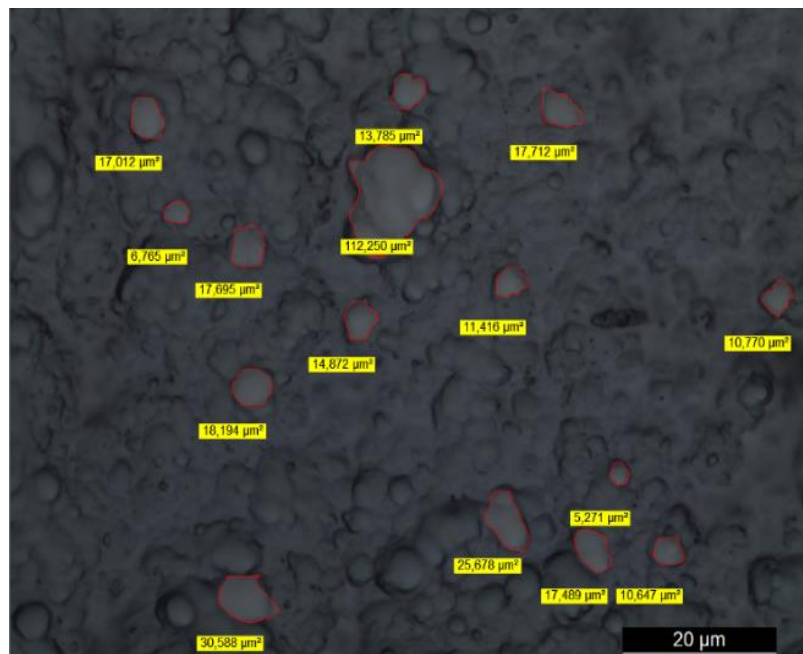
Figure 3.3.4 - Surface of the sample A$_{t+1}$ (72h) tested in H$_3$PO$_4$.
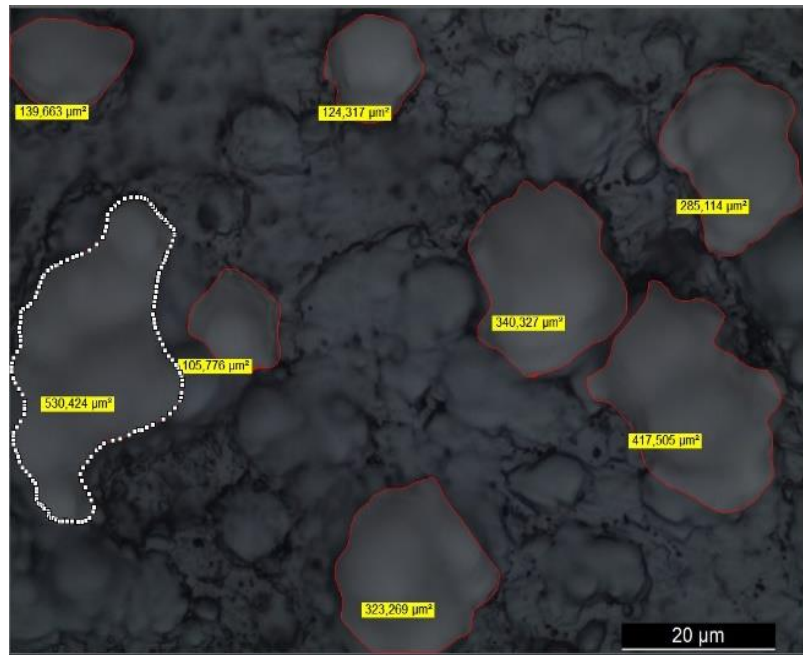
Figure 3.3.5 - Surface of the sample A₁ (24h) tested in HCl.

Figure 3.3.6 - Surface of the sample Aₜ₊₁ (72h) tested in HCl.

Figure 3.3.7 - Surface of the sample A_1 (24h) tested in oxalic acid.

Figure 3.3.8 - Surface of the sample A_{t+1} (72h) tested in oxalic acid.
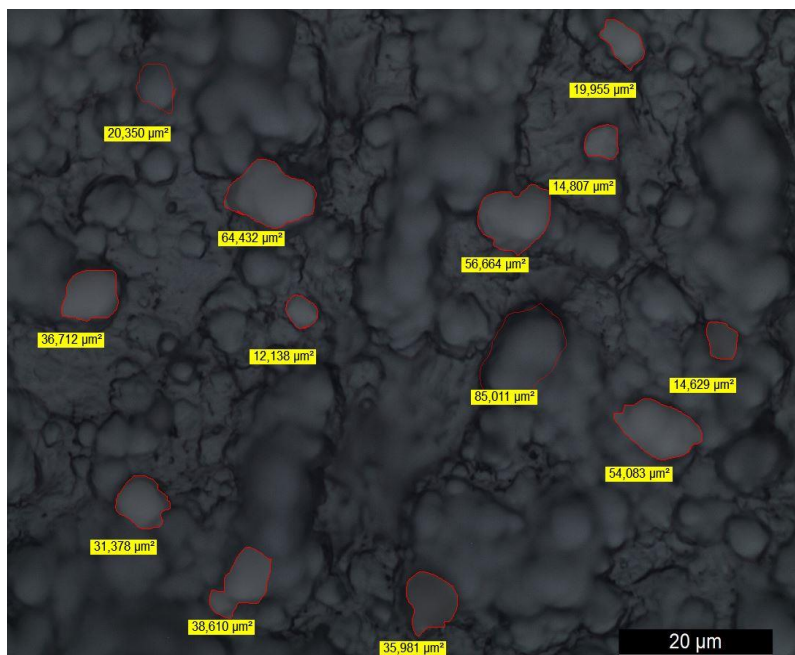
Figure 3.3.9 - Surface of the sample A₁ (24h) tested in H₂SO₄.
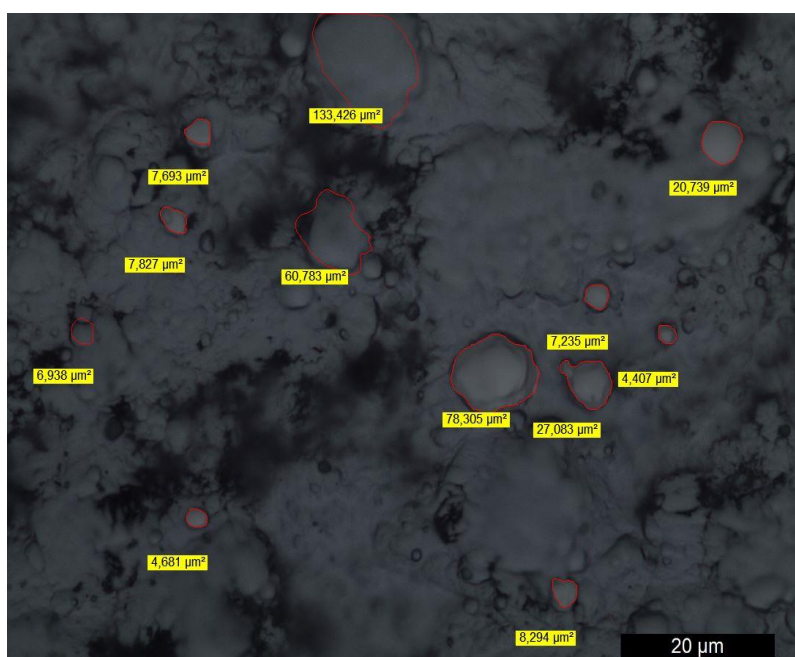
Figure 3.3.10 - Surface of the sample A$_{t+1}$ (72h) tested in H₂SO₄.

In Table 3.3.7, the values of the depths and average areas of the craters are collected together with the average roughness values (Ra, Rmax, Rq, Rz and Rt), since each sample was profiled 3 times by the laser profilometer.

Table 3.3.7 - Roughness and craters size of titanium grade 2 in reducing acids (24 h and 72 h).

Acid	Sulfamic		H_3PO_4		HCl		Oxalic		H_2SO_4	
Conc.[%v/v]	10		30		10		10		10	
T [°C]	60		60		60		60		60	
Sample	A_1	A_{t+1}	A_1	A_{t+1}	A_1	A_{t+1}	A_1	A_{t+1}	A_1	A_{t+1}
Ra [µm]	0.617	0.774	0.466	0.506	1.022	1.813	1.895	2.550	0.723	0.828
Rq [µm]	0.758	0.973	0.587	0.638	1.284	2.577	2.390	3.243	0.960	1.187
Rz [µm]	4.094	5.432	3.372	3.739	7.019	14.29	12.42	17.06	6.158	7.371
Rt [µm]	4.516	6.202	3.831	4.404	8.351	16.16	14.21	19.19	7.119	11.48
R_{max} [µm]	4.216	5.900	3.556	4.241	8.265	15.37	13.58	17.70	7.030	11.42
A.C. Area [µm²]	94.85	177.84	22.81	313.1	283.3	3503.2	113.62	336.6	37.29	30.62
Depth Crater [µm]	0.8	3	0.2	0.7	2	8	1.5	5	0.5	1.5

The general trend is an increase in roughness with increasing exposure time in acid solutions. HCl is the worst case considering the depth and the average area of the craters, of which the latter with an increase of an order of magnitude from the sample A_1 to the sample A_{t+1}. The roughness profiling data, on the other hand, show that the oxalic acid has the most irregular surface, also visually confirmed by Figure 3.3.11.

Figure 3.3.11 - Sample of Ti grade 2 after 24 h in 10% v/v oxalic acid at 60°C.

The graphs of the roughness profile are shown below, one for each condition tested.
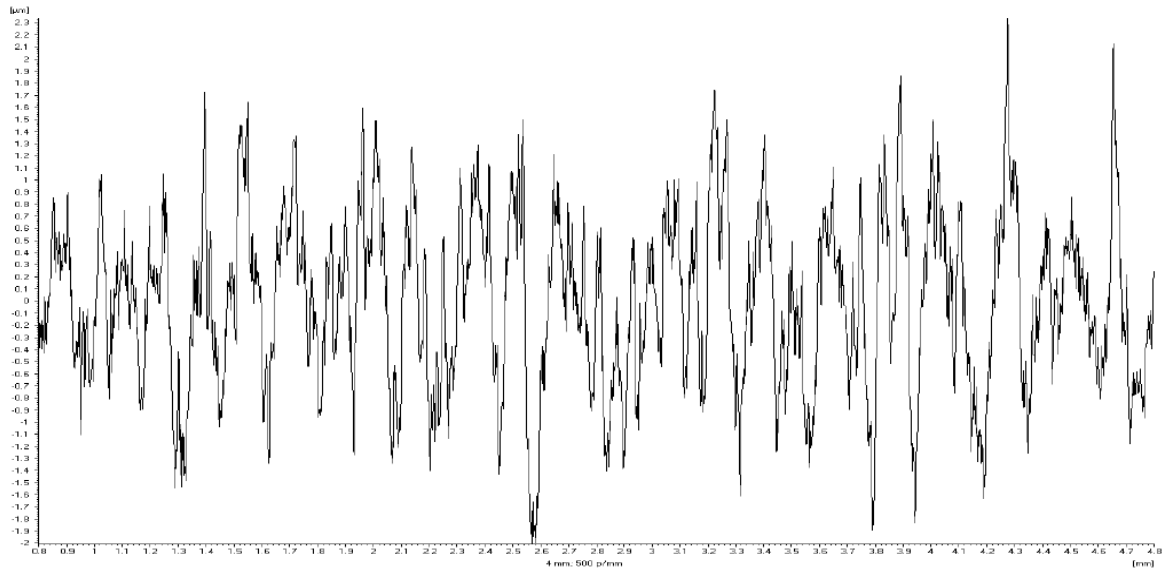
Figure 3.3.12 - Roughness profile of sample A$_1$ (24h) in sulfamic acid.
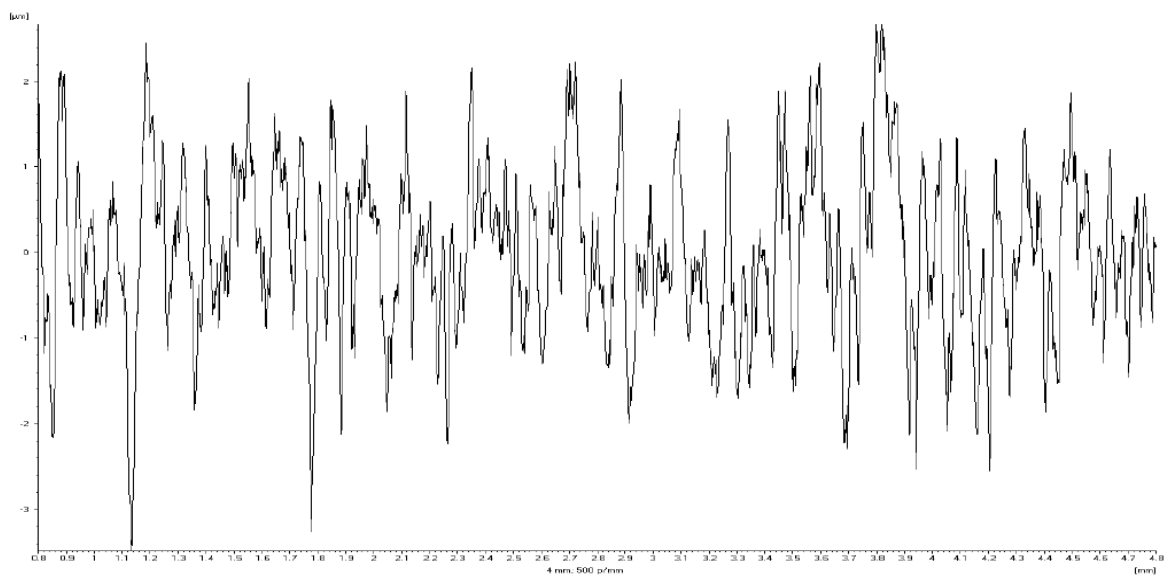
Figure 3.3.13 - Roughness profile of sample A$_{t+1}$ (72h) in sulfamic acid.
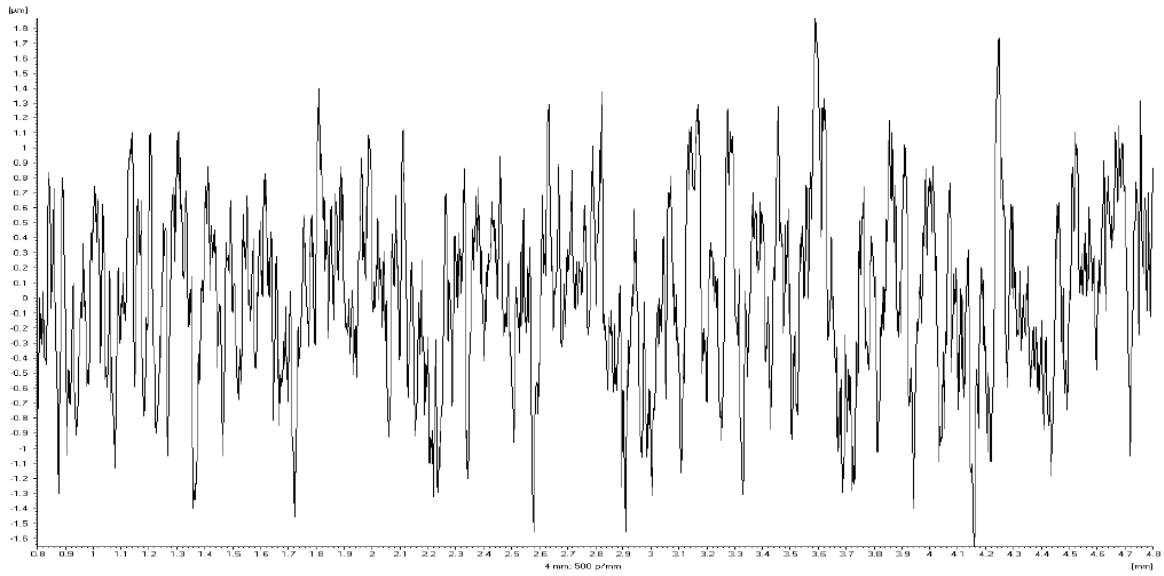
Figure 3.3.14 - Roughness profile of sample A₁ (24h) in H₃PO₄.
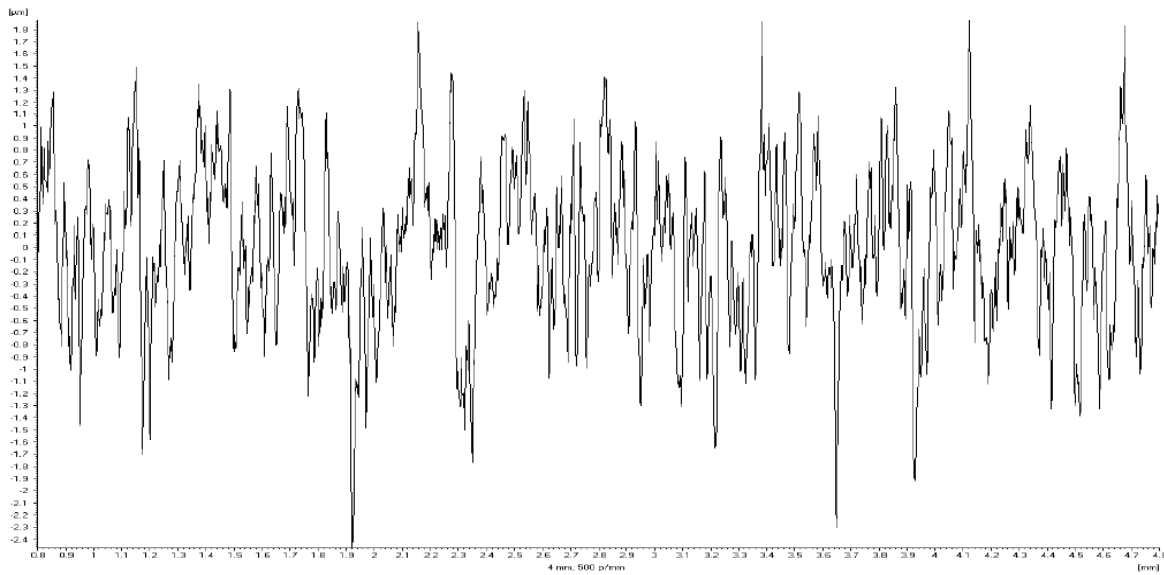
Figure 3.3.15 - Roughness of sample Aₜ₊₁ (72h) in H₃PO₄.
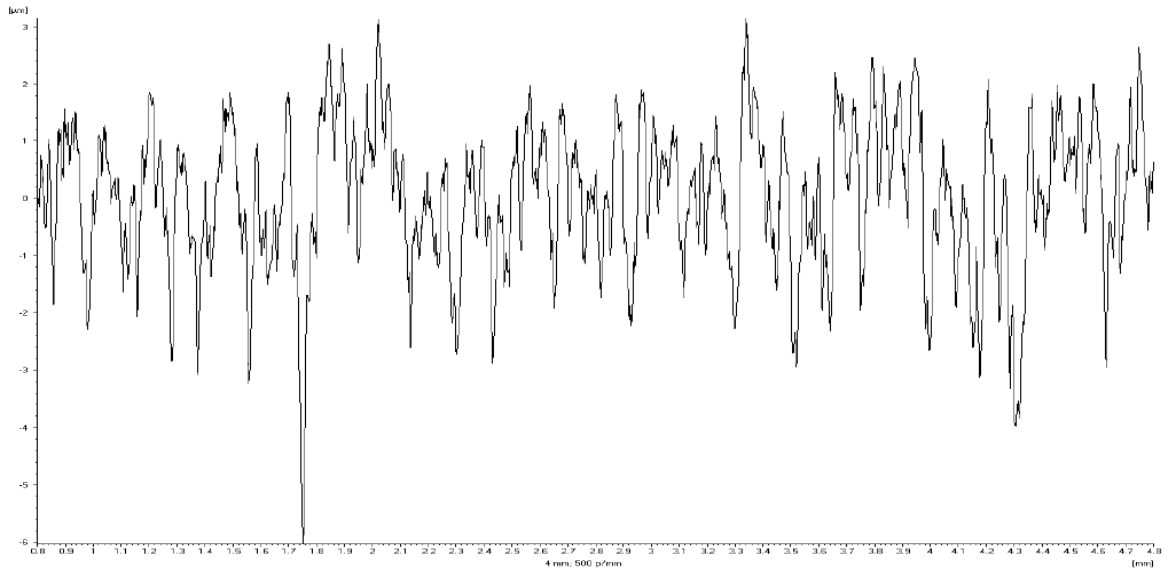
Figure 3.3.16 - Roughness of sample A₁ (24h) in HCl.
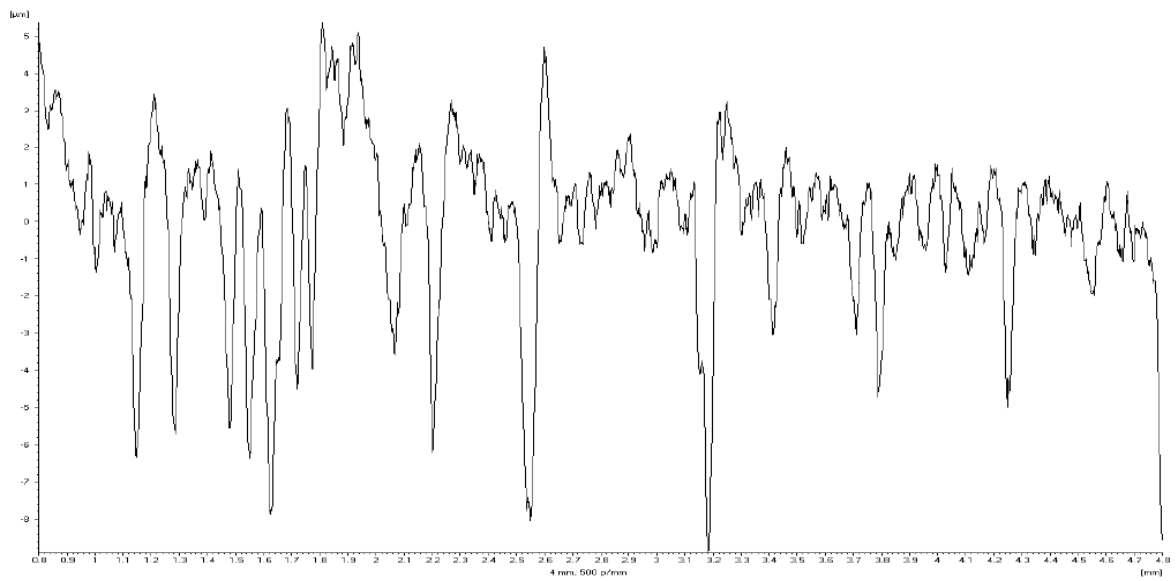
Figure 3.3.17 - Roughness of sample A_{t+1} (72h) in HCl.
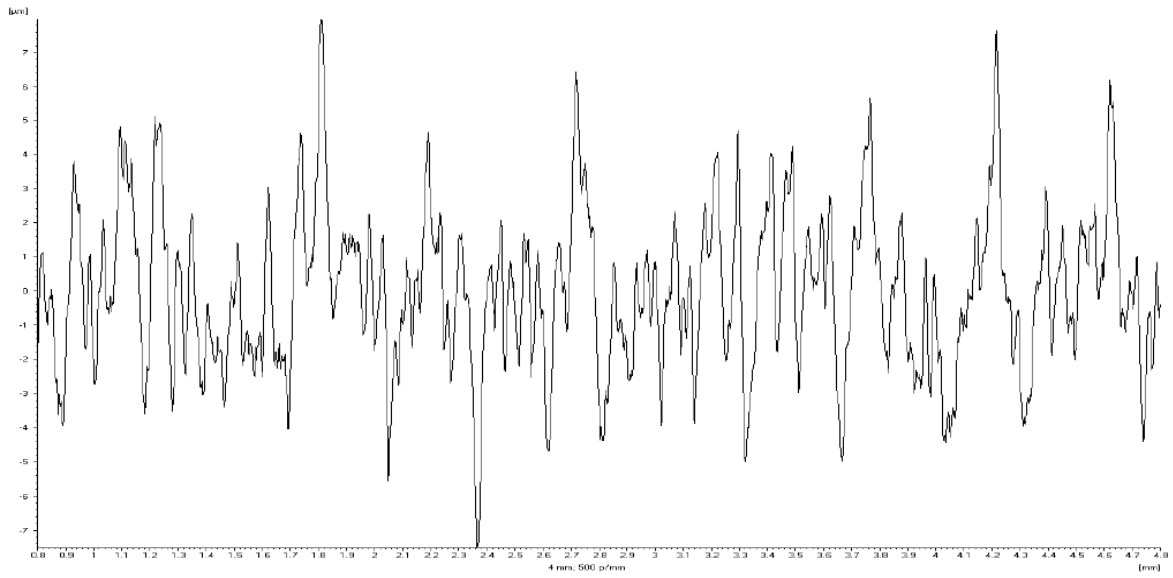
Figure 3.3.18 - Roughness of sample A$_1$ (24h) in oxalic acid.
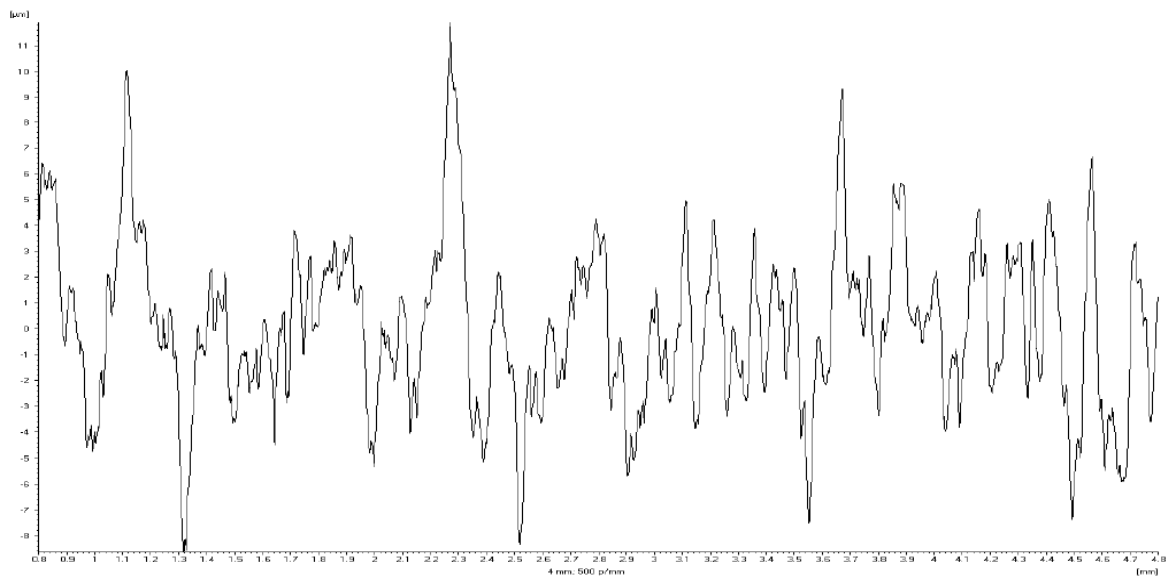
Figure 3.3.19 - Roughness of sample A$_{t+1}$ (72h) in oxalic acid.
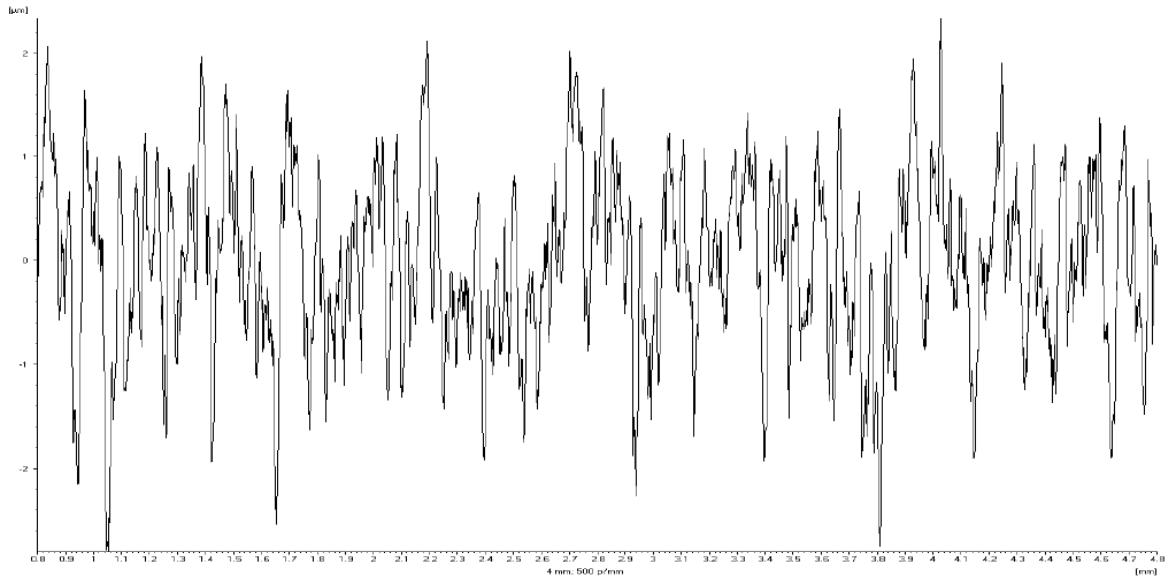
Figure 3.3.20 - Roughness of sample A_1 (24h) in H_2SO_4.
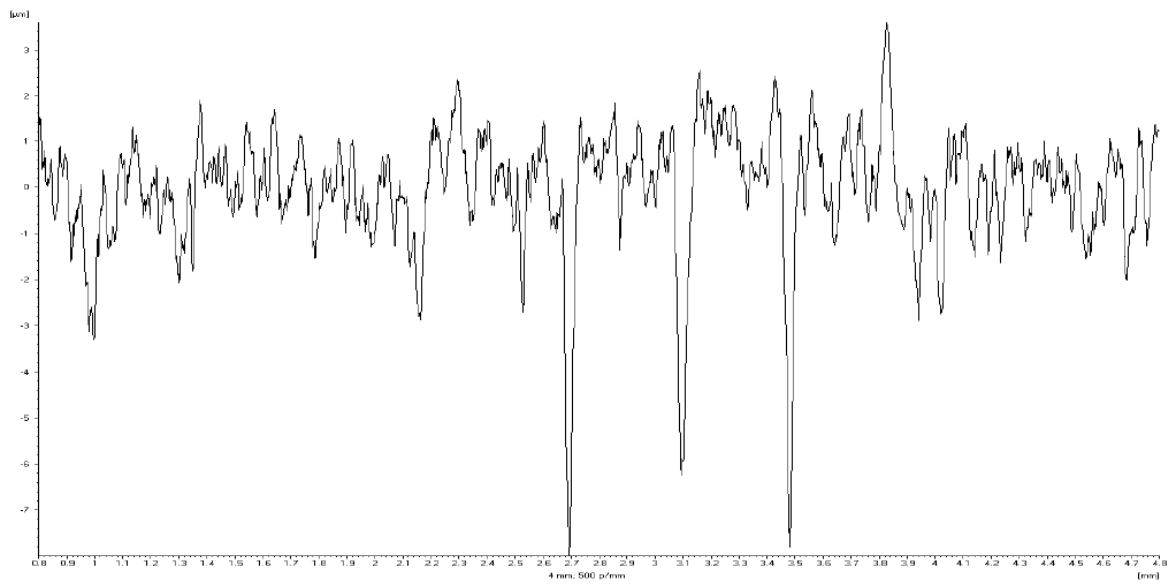
Figure 3.3.21 - Roughness of sample A_{t+1} (72h) in H_2SO_4.

Sulfuric acid, at 10% v/v and 60°C conditions, was the most aggressive acid, for this reason it was chosen to be tested on anodized samples. Two immersion tests were performed for all the treated specimens, with a duration of 24 h. Table 3.3.8 shows the corrosion rates and its average value for all the conditions, in addition, with reference to the previous data of Ti gr.2 (8.1 mm/y for 24 h), the improvement in corrosion resistance was calculated by the formula:

$$Improv. \% = \frac{C.R.(Ti\ gr.2) - C.R.(Ti\ anodized)}{C.R.(Ti\ gr.2)} * 100$$

Table 3.3.8 - Immersion test results of titanium anodized samples in 10% v/v H_2SO_4 at 60°C.

Sample n°	Waveform	C.R. [mm/y]	Mean C.R. [mm/y]	Improv. [%]
1	90-10-20 Hz-2%	5.25 - 7.81	6.5	19.4
2	90-10-1000 Hz-2%	8.23 - 5.04	6.6	18.1
3	60-40-20 Hz-2%	7.36 - 4.89	6.1	24.4
4	60-40-1000 Hz-2%	4.98 - 7.09	6.0	25.5
5	90-10-20 Hz-5%	5.76 - 5.66	5.7	29.5
6	90-10-1000 Hz-5%	5.73 - 6.91	6.3	22.0
7	60-40-20 Hz-5%	5.73 - 5.83	5.8	28.6
8	60-40-1000 Hz-5%	5.25 - 6.81	6.0	25.5
9	90-10-20 Hz-7%	5.93 - 7.44	6.7	17.4
10	90-10-1000 Hz-7%	6.11 - 10.52	8.0	-
11	60-40-20 Hz-7%	4.75 - 7.29	6.0	25.7
12	60-40-1000 Hz-7%	0.09 - 0.00	0.04	99.5
13	90-10-20 Hz-10%	6.44 - 7.69	7.1	12.8
14	90-10-1000 Hz-10%	6.85 - 7.44	7.1	11.8
15	60-40-20 Hz-10%	6.23 - 5.98	6.1	24.6
16	60-40-1000 Hz-10%	0.18 - 0.53	0.35	95.6

The coating of the samples, during the test, was completely detached after a few hours from the beginning, apart for conditions 12 and 16. Nevertheless, the film of the sample 16 was partially removed during the process of washing and drying with compressed air (Figure 3.3.22 a). This pull-off mechanism may be due to the recombination of the hydrogen at the metal-oxide interface, it is shown in SEM images with different magnification (Figure 3.3.23). Only the oxide of the sample 12 survived completely after all the steps (Figure 3.3.22 b).

Figure 3.3.22 - Sample 16 on the left (a) and sample 12 on the right (b).
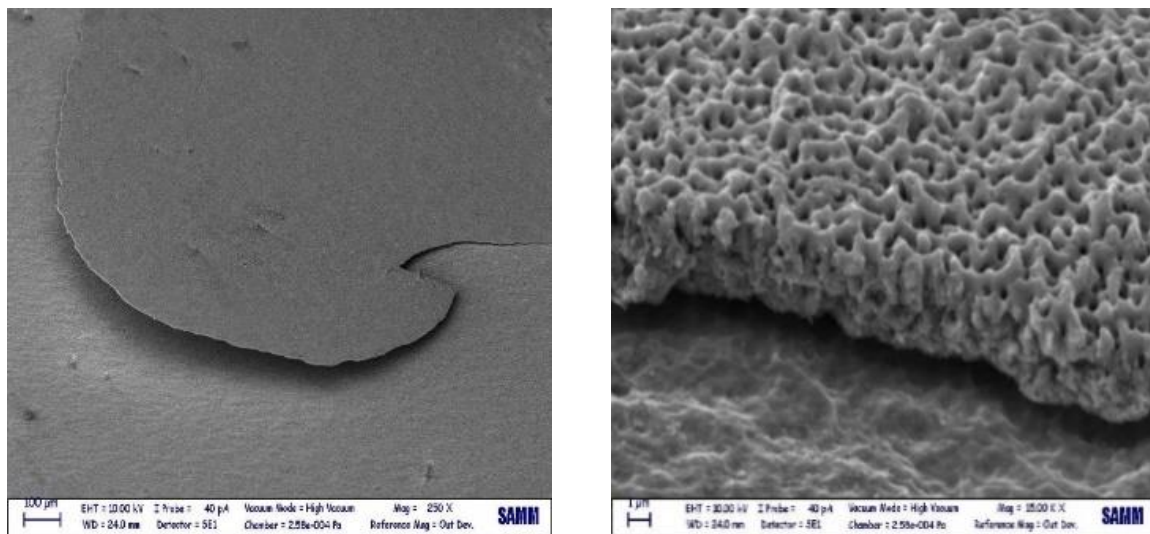
Figure 3.3.23 - SEM images of titanium oxide coating (condition 16) pulled-off from the metallic substrate at different magnitude.

The average corrosion rates were plotted with respect to the variation of the cathode peak in Figura 3.3.24, in order to understand its influence. It is interesting to note that increasing the cathodic peak did not prove an advantage in corrosion resistance for all cycles, with the exception of the condition 60%A - 40%C with 7% C peak at 1000 Hz. Sample 12 not only

proves to be the best among the samples treated with an average corrosion rate of 0.04 mm/y, but also shows a coating that performs better than titanium grade 7, which has a corrosion rate of 0.21 mm/y under the same test conditions. The sample 10, on the other hand, showed the worst result in terms of corrosion, in fact it showed no improvement compared to the bare titanium grade 2. The rapid detachment of the coating from the metal substrate leads to no protection.
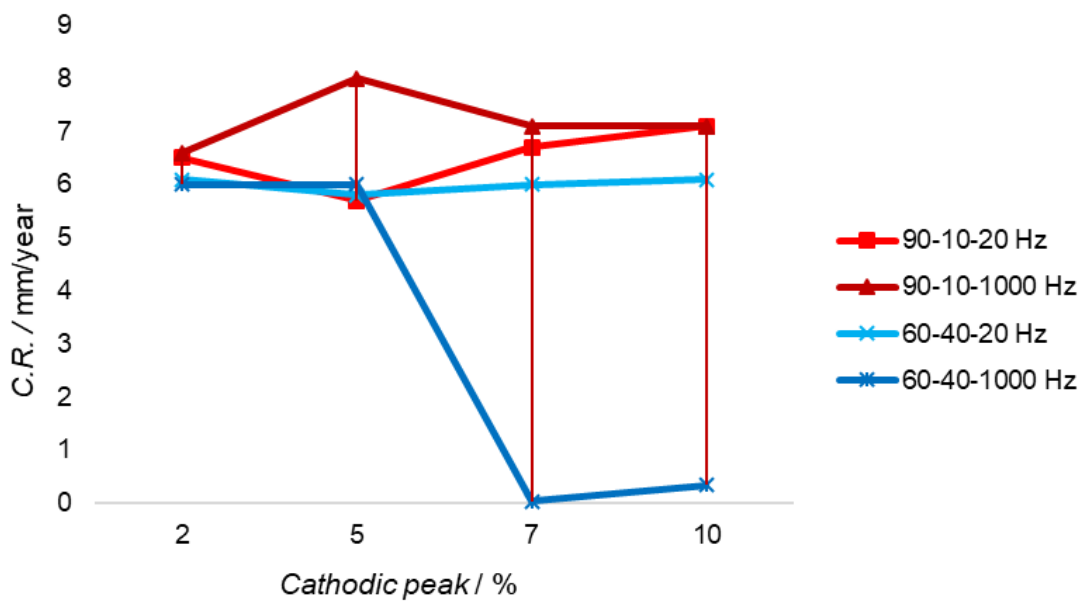
Figure 3.3.24 - Effect of cathodic peak on C.R. of anodized samples for different waveforms.

In Figure 3.3.25, the average corrosion rates were plotted against the different anodization cycles. Duty cycles and frequency changes do not affect the corrosion rates of samples treated with cathodic peaks at 2% and 5%. On the contrary, using the cycle with higher cathodic phase (60%A - 40%C) and bringing the frequency to 1000 Hz, for the conditions with cathodic peak 7% and 10%, the best performances are obtained in sulfuric acid tests.
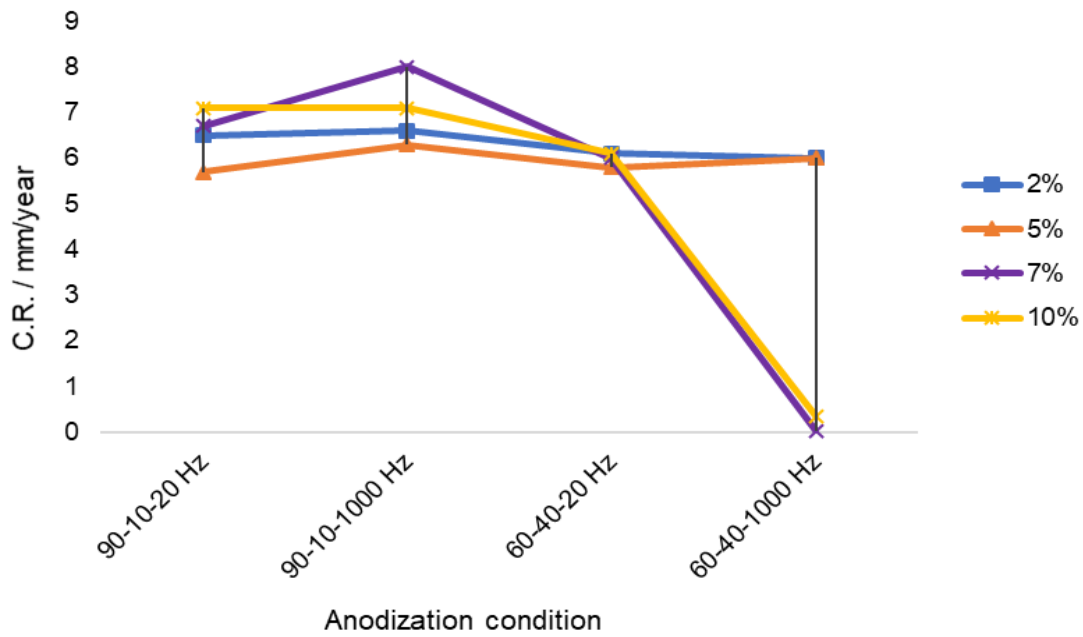
Figure 3.3.25 - Effect of duty cycle and frequency on the generalized corrosion ability of anodized samples.

Table 3.3.9 compares the results obtained from the immersion tests and the previously evaluated titanium dioxide characteristics. This representation makes it possible to distinguish the signals that reduce or increase the resistance to corrosion with reference to an average corrosion rate of 6 mm/y. Samples 10, 13 and 14 do not prove a useful improvement to corrosion. Of these treatments, condition 10 has underperformed compared with the others, despite having the same relative low thickness and quantity of crystalline phases. Investigating porosity along the entire thickness or an adhesion test could help to clarify why sample 10 shows worse behavior. The best results were obtained with the 60%A - 40%C cycle at 1000 Hz with cathodic peak at 7% and 10%. A first look points out that both show the highest oxide thicknesses, 3.54 μm for sample 12 and 4.2 μm for sample 16. It should be emphasized that condition 12 also has the highest surface porosity (25.55%). The crystalline structure of the above-mentioned conditions was prevalently made of rutile, with a medium level of anatase phase, relatively to other anodization conditions. As in the previous cases, the TEM analysis could help to clarify the spatial distribution of the crystalline phases, to understand if the presence of a certain phase, rutile or anatase, in contact with the aggressive solution would prove a benefit during a corrosive attack.

Table 3.3.9 - Summary of sample (from 1 to 16) characterized for generalized corrosion, thickness, structure (L=low; M=medium; H=high content), porosity.

Sample n°	C.R. [mm/y]	Thickness [μm]	Anatase	Rutile	Porosity [%]
1	6.5	1.85	H	L	9.71
2	6.6	1.75	M	L	7.3
3	6.1	1.97	H	L	14.4
4	6.0	2.24	M	L	10.34
5	5.7	2.53	H	M	17.25
6	6.3	1.67	H	H	13.38
7	5.8	1.2	L	L	15.29
8	6.0	2.68	L	H	13.21
9	6.7	2.9	L	M	13.92
10	8.0	1.72	M	L	9.71
11	6.0	1.66	L	M	16.1
12	0.04	3.54	M	H	25.55
13	7.1	1.48	M	L	16.73
14	7.1	2.05	M	L	13.35
15	6.1	1.36	L	L	19.56
16	0.35	4.2	M	H	18.50

3.3.2 – Potentiodynamic tests

3.3.2.1 – Localized corrosion

The anodic potentiodynamic test was performed in a 0.5M NaBr solution at 50°C, with two repeatability for each anodizing condition and also for untreated titanium (grade 2 and grade 7). The graphs, which will be presented below, are subdivided by cathode peak and always show the reference curves of pure titanium, grade 2 and grade 7. Despite CP-Ti gr.7 shows an incredible increase in the resistance to uniform corrosion with respect to CP- Ti gr.2, thanks to the presence of around 0.2% of palladium, which increases its passive behavior, the localized corrosion resistance does not have the same trend. The increase in pitting potential is only 0.5 V, with a slight decrease in anodic current along all the potential scan verified. (Figure 3.3.26)
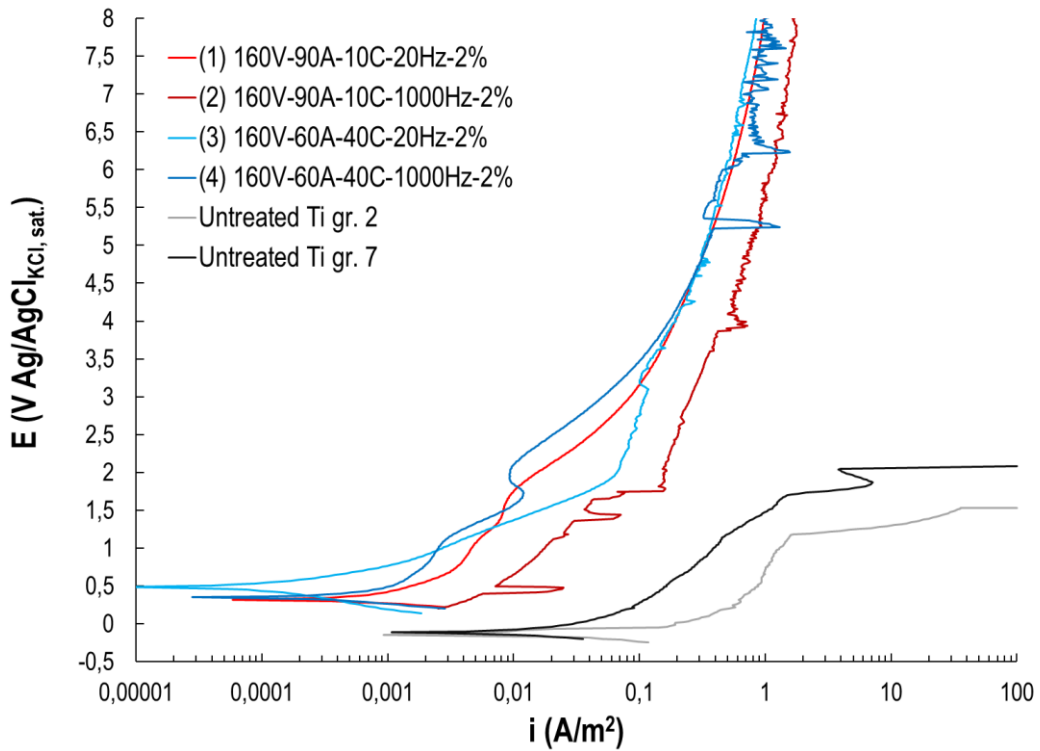
Figure 3.3.26 - Potentiodynamic results for samples anodized with waveforms at 2% cathodic peak.

Figure 3.3.26 shows the samples treated with a 2% cathode peak. Each of these conditions does not show a pitting potential on the entire anodic scan and the anodic currents are just below 1 A/m^2. The potentiodynamic curves of these samples exhibit a comparable behavior, probably due to similar morphologies and structures (i.e. porosity, thickness and crystal phase amount).

The anodized samples with cathodic peak at 5% are compared in Figure 3.3.27, showing only one condition for which there is a pitting potential. Sample 7 (60%A - 40%C at 20 Hz) has E_{pitt} at 4.9 V with an average anodic current density of 0.39 A/m^2. It should be noted that this condition has the lowest amount of total crystalline phase relative to the cathodic peak of 5% and also the lowest thickness (1.2 µm). Sample 6 has similar characteristics in terms of thickness (1.67 µm) and porosity, but a decidedly higher amount of crystalline phase. The behavior, however, turns out to be different, in fact it can be seen that there is no pitting potential and the anodic current density is slightly less than 1 A/m^2. An in-depth investigation of the development of porosity along the thickness of titanium dioxide could clarify the influence of the crystalline phase on localized dissolution.
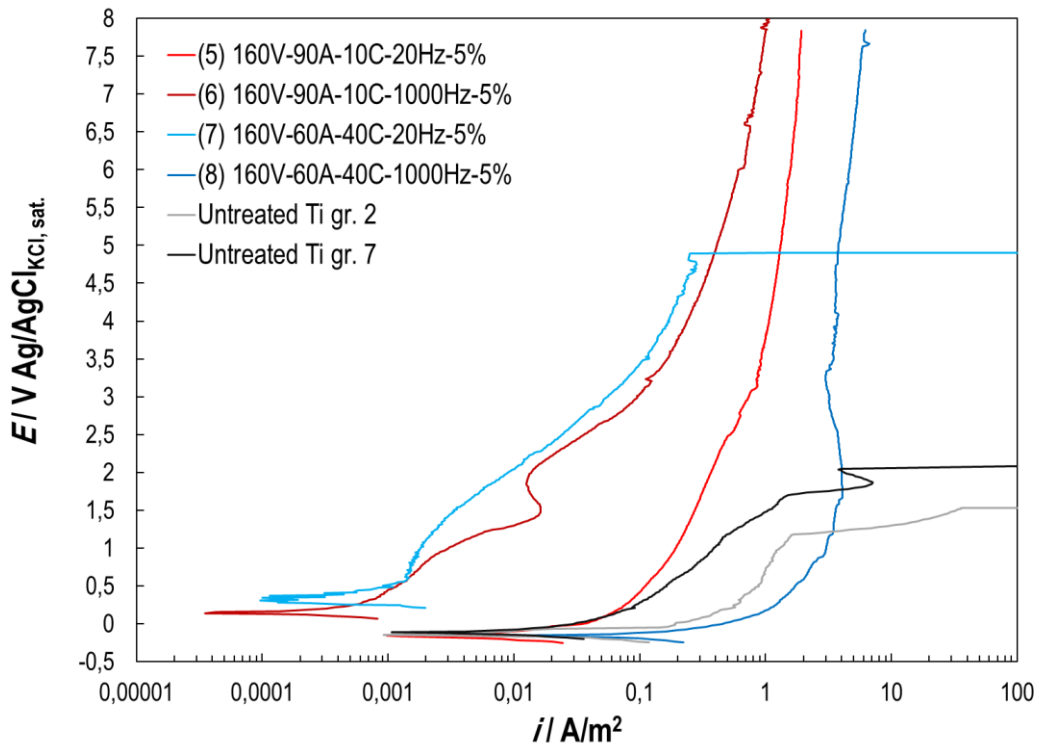
Figure 3.3.27 - Potentiodynamic results for samples anodized with waveforms at 5% cathodic peak.
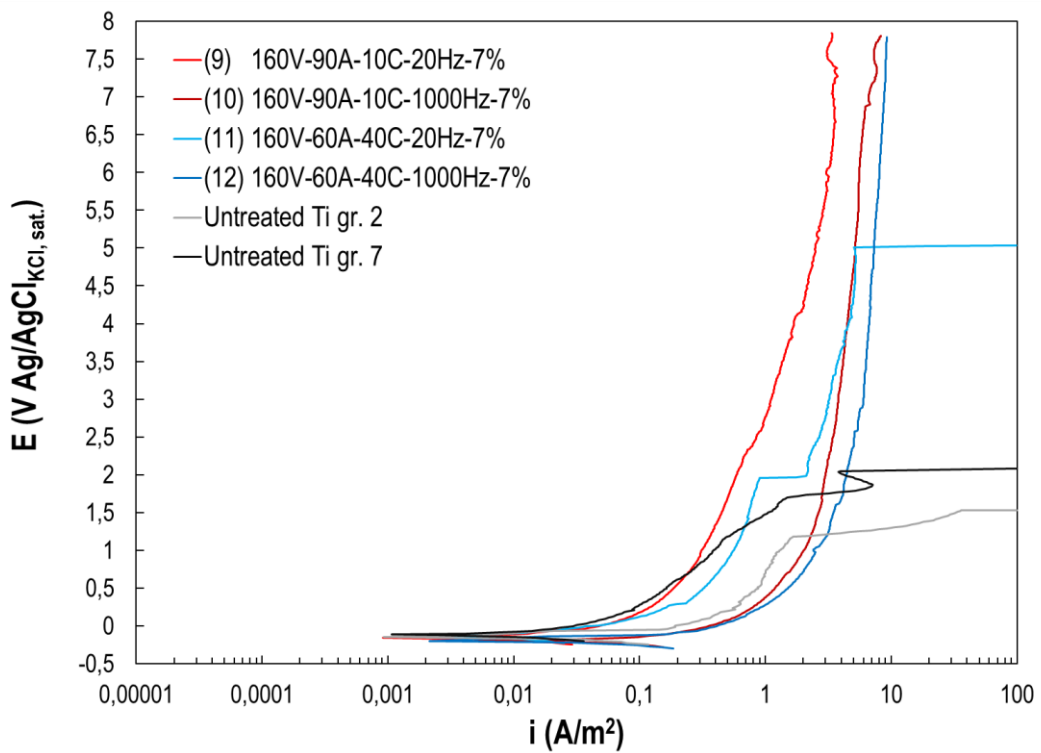
Figure 3.3.28 - Potentiodynamic results for samples anodized with waveforms at 7% cathodic peak.

103

Figure 3.3.28 refers to the potentiodynamic curves for samples treated with a 7% cathode peak. Similar to the previous case, condition 11 (60%A - 40%C at 20 Hz) shows a pitting potential (5 V SSC) and a higher current density (about 98 A/m^2). Other similarities between sample 11 and 7 are the thin thickness (1.66 µm) and the high porosity, both around 16%. In contrast, the 7% cathode peak condition shows a morphology composed of small pores and presence of deposits, and a higher total crystalline phase value compared to the same condition with 5% cathode peak.
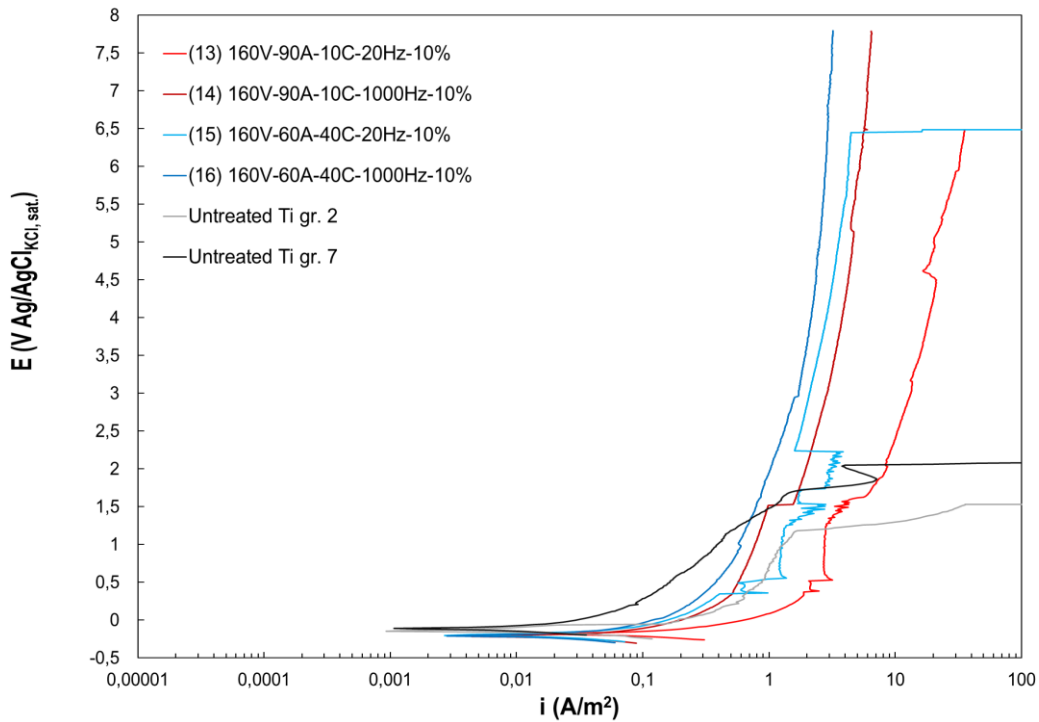
Figure 3.3.29 - Potentiodynamic results for samples anodized with waveforms at 10% cathodic peak,

Finally, Figure 3.3.29 shows the anodized samples with cathodic peak at 10%. The work cycles 14 and 16 at high frequencies (1000 Hz) do not have E_{pitt} and in particular the latter has a lower anodic current density (about 1 A/m^2). This is probably due to the high thickness of the oxide film (4.2 µm) combined with a relative low surface porosity. Samples 13 and 15, on the other hand, which are treated at low frequency (20 Hz) and which have thicknesses of 1.48 µm and 1.36 µm respectively, show pitting at potentials 6.48 and 6.45 V SSC. This behavior, in addition to minor thicknesses compared to minor cathodic peaks, is due to the greater surface porosity (16.73% for sample 13 and 19.56% for sample 15).

Before presenting the results for cathodic potentiodynamic tests it is useful to understand how curves are interpreted and what are the phenomena that govern the process.

In cathodic processes there are two fundamental reactions: the first concerns the reduction of oxygen (Eq. 1), with a reduction potential of +1.23 V SHE (Standard Hydrogen Electrode), which corresponds to 1 V SSC (Silver Silver Chloride) used in our experiments; the second concerns the reduction of hydrogen (Eq. 2), or evolution of hydrogen, with a reduction potential by definition of +0 V SHE, which corresponds to -0.2 V SSC.

$$O_2 + 4H^+ + 4e^- \rightarrow H_2O \qquad \textbf{(Eq.1)}$$

$$2H^+ + 2e^- \rightarrow H_2 \qquad \qquad \textbf{(Eq.2)}$$
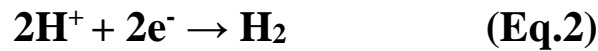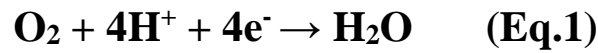
These reactions determine the shape of the cathodic potentiodynamic curves, since starting from the above potentials (1 V SCC for oxygen and -0.2 V SCC for hydrogen) there will be cathodic current increases caused by them. The current density, as the potential decreases, will not increase to infinity, but rather it will be limited initially by the frictions (overvoltage) that the charges (ions and electrons) undergo in the passage between electrolyte/metal electrode and it is called activation control; after which the current will be limited by mass transport, that is by the diffusion of ions from the oxide to the electrolyte.
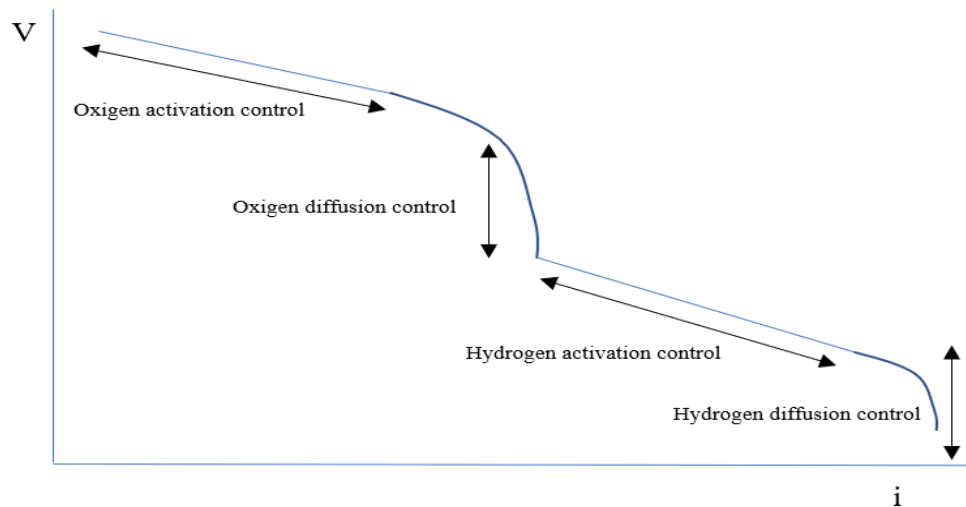
Figure 3.3.30 - Schematic representation of cathodic potentiodynamic curve.
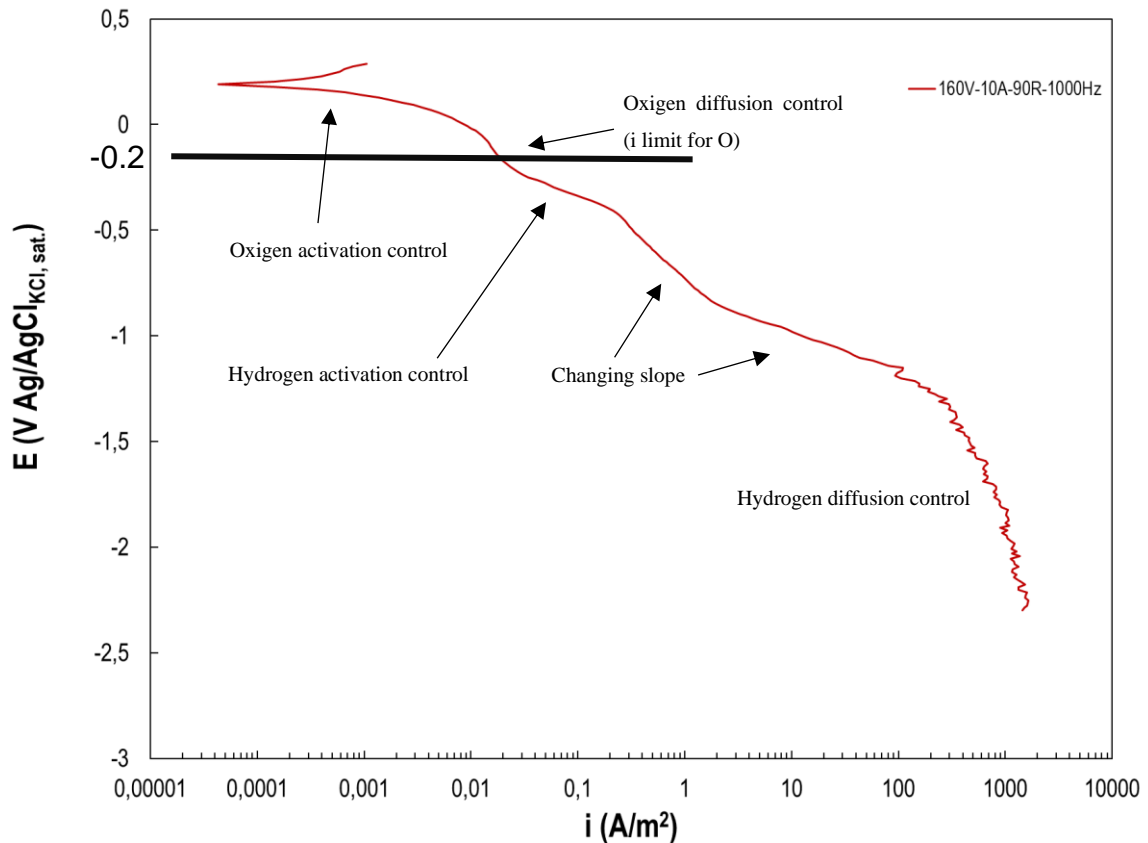
Figure 3.3.31 - Phenomenas that influence the cathodic curve in real example.

Figure 3.3.31 shows a real cathodic curve. Following the curve, the activation of oxygen controls the current increase up to a change of the slope, whereby the cathodic current is controlled by the diffusion of O_2 in the oxide; at that same point, the evolution of hydrogen begins, partially masking the limit of current due to the diffusion of oxygen; from this new slope, the process is in hydrogen activation control. The presence of slope variations may be due presence of the oxide which opposes a greater overvoltage than Ti gr.2 to the evolution of hydrogen [132]. Subsequently, the slope decreases again and this is attributable to two causes: the dissolution of the coating, thus exposing titanium metal, and TiH_2 formations, presented below [133]. Finally, the curve has a rapid decrease for current values tending to a limit, here the current is limited by the diffusion of the hydrogen ions.

In this thesis, the solution used for cathodic potentiodynamics test is 0.5M sulfuric acid at room temperature (25°C). The study by J.M.Casas et al [134] shows pH = 0.3. The Pourbaix diagram of the Ti-SO$_4$-H$_2$O system (Figure 3.3.32) is an important tool to evaluate how the

potential variation combined with the pH value, influences the stability of the specie studied. When the potential decreases below -0.2 V SSC (ie 0 V SHE), it induces titanium corrosion with Ti^{3+} formation which complexes with sulfates forming $TiSO_4^+$ ion. This reaction can cause sudden increases in cathodic currents at this potential threshold. Moreover, from the graph it is possible to notice that at -0.8 V SSC (-0.6 V SHE) titanium hydrides are formed (TiH_2).
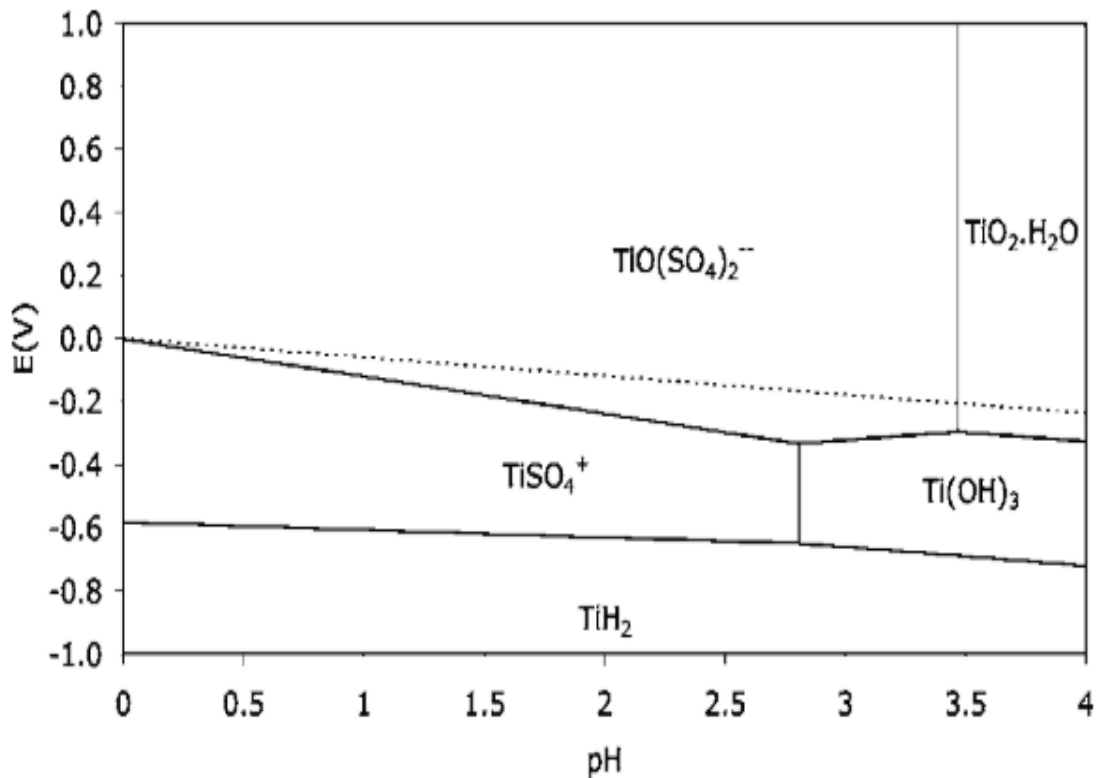
Figure 3.3.32 - Pourbaix diagram for the system Ti-SO₄-H₂O.

The results of the potentiodynamic tests are presented below. As in the anodic case, the curves of the treated samples are grouped by cathode peak together with the curves of pure titanium (grade 2 and grade 7). In general, CP-Ti gr.7 will show values of final currents greater than Cp-Ti gr.2, this is due to palladium which favors the process of hydrogen evolution. Each cathode graph was flanked by a table with the structural and morphological characteristics of the samples.
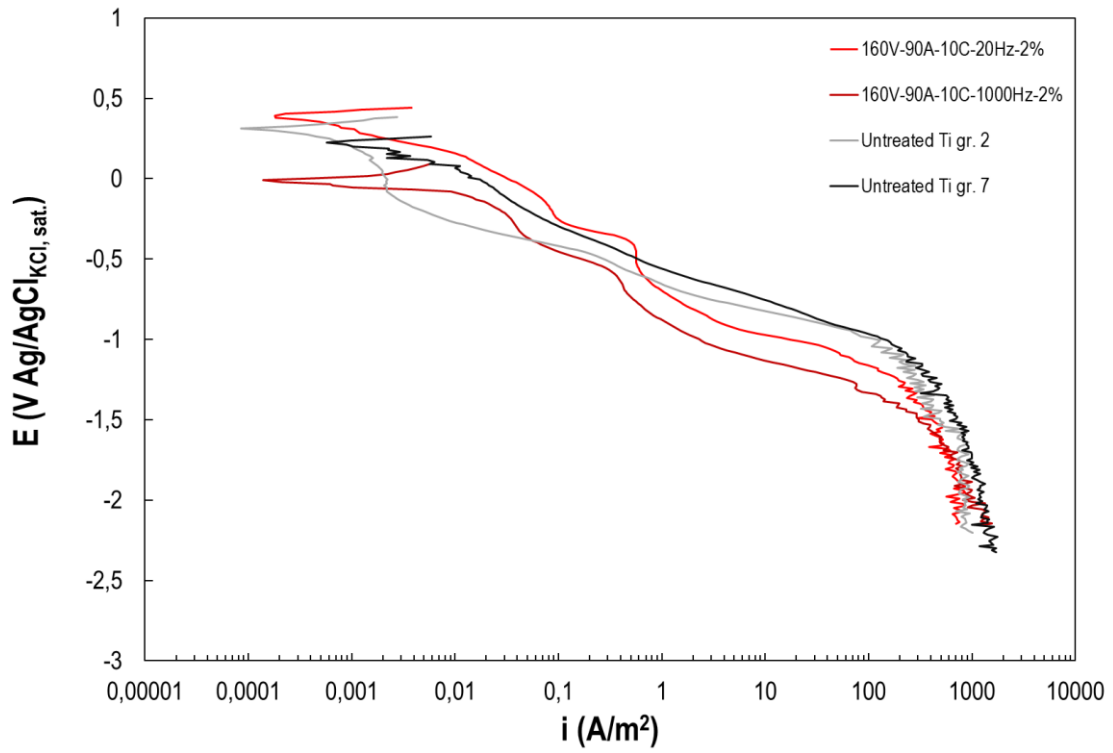
Figure 3.3.33 - Cathodic potentiodynamic results for samples anodized with waveforms 90%A – 10%C at 2% cathodic peak.
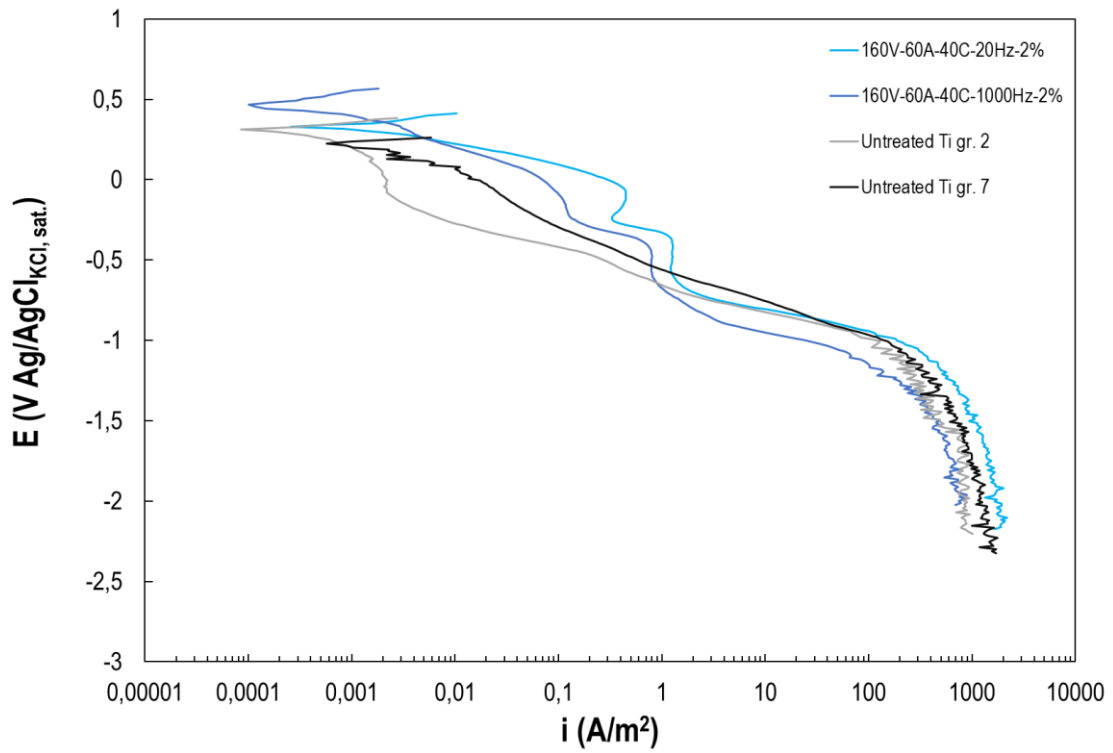
Figure 3.3.34 - Cathodic potentiodynamic results for samples anodized with waveforms 60%A – 40%C at 2% cathodic peak.

Table 3.3.10 - Structure, morphology and uniform corrosion behavior of duty cycles with cathodic peak at 2%..

Sample n°	C.R. [mm/y]	Thickness [μm]	Anatase	Rutile	Porosity [%]
1	6.5	1.85	H	L	9.71
2	6.6	1.75	M	L	7.3
3	6.1	1.97	H	L	14.4
4	6.0	2.24	M	L	10.34

Figures 3.3.33 and 3.3.34 show the cathodic curves for duty cycles with cathodic peak at 2%. The treated samples compared to the Ti gr.2 curve have a current with a more or less vertical slope at -0.2 V, this is due to oxygen diffusion limit. A particular "nose" conformation is exhibited by sample 3 (60%A - 40%C at 20 Hz) with recess at -0.3 V SCC. This phenomenon is given by the sum of the anodic curve of the material with the cathodic curve of the reagents (H_2 and O_2). The indentation of the "nose", in particular, is due to the potential of first passivation (E_{pp}). Moreover, condition 3 also presents the worst hydrogen limiting current, even with respect to Ti gr.7. This may be due to the greater porosity (14.4%) than the other cycles. An investigation with TEM could clarify this behavior. Condition 4 exhibits the best behavior between cycles at 2% C peak, with the highest OCP (0.5 V SCC) and lower limit currents at low voltages.

In Figures 3.3.35 and 3.3.36, the anodization conditions with cathodic peak at 5% are represented. Sample 6 (90%A - 10%C at 1000 Hz) has the "nose" shape around -0.3 V SCC, as seen above for sample 4, but with much lower current density. Also the condition 60%A - 40%C at 1000 Hz has a curvature, but less accentuated than the others, with current values equal to condition 6.

Table 3.3.11 - Structure, morphology and uniform corrosion behavior of duty cycles with cathodic peak at 5% (H=high, M=medium, L=low)..

Sample n°	C.R. [mm/y]	Thickness [μm]	Anatase	Rutile	Porosity [%]
5	5.7	2.53	H	M	17.25
6	6.3	1.67	H	H	13.38
7	5.8	1.2	L	L	15.29
8	6.0	2.68	L	H	13.21
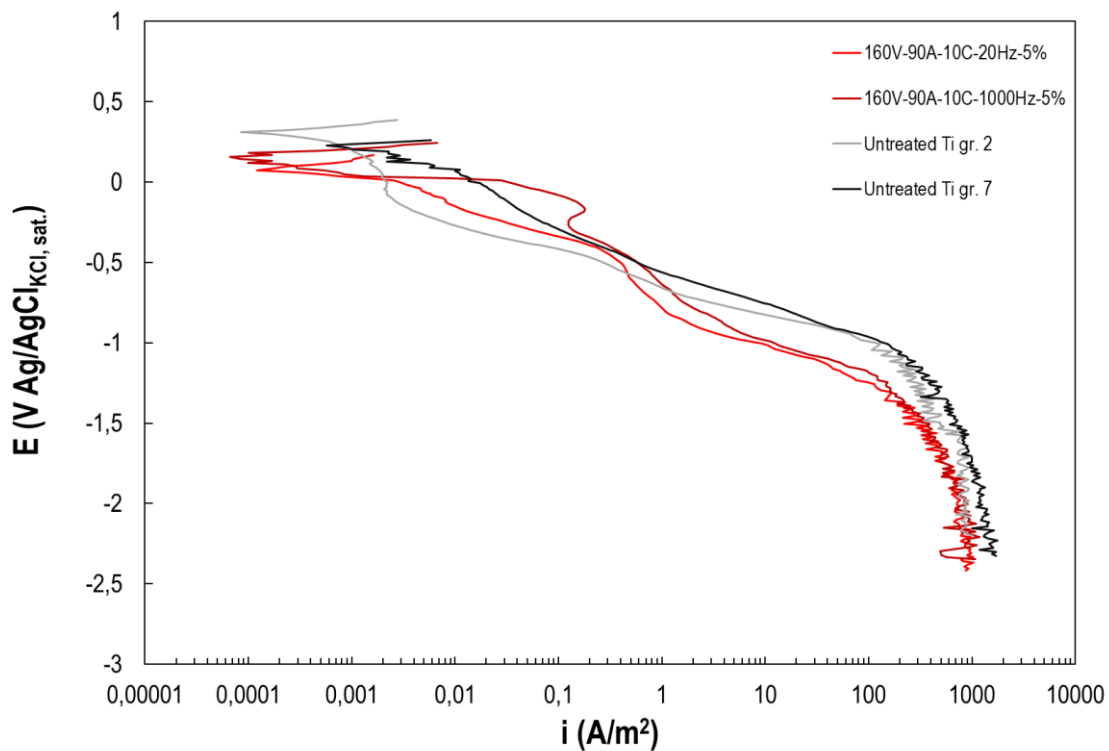
Figure 3.3.35 - Cathodic potentiodynamic results for samples anodized with waveforms 90%A – 10%C at 5% cathodic peak.
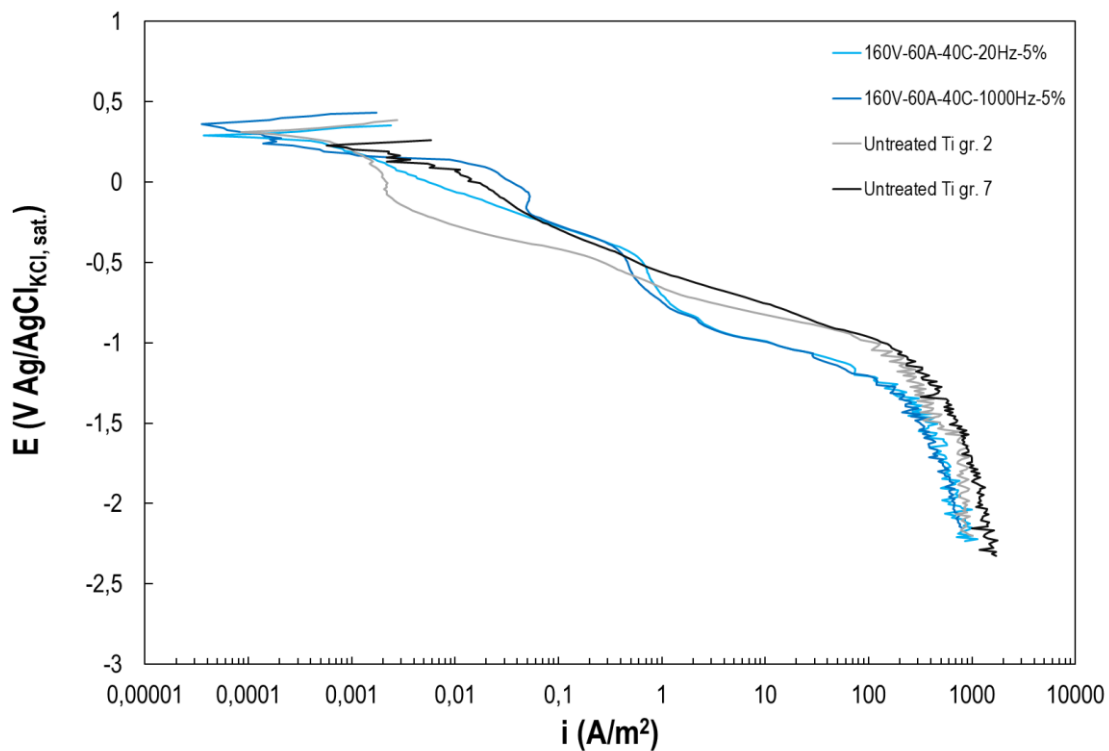
Figure 3.3.36 - Cathodic potentiodynamic results for samples anodized with waveforms 60%A – 40%C at 5% cathodic peak.
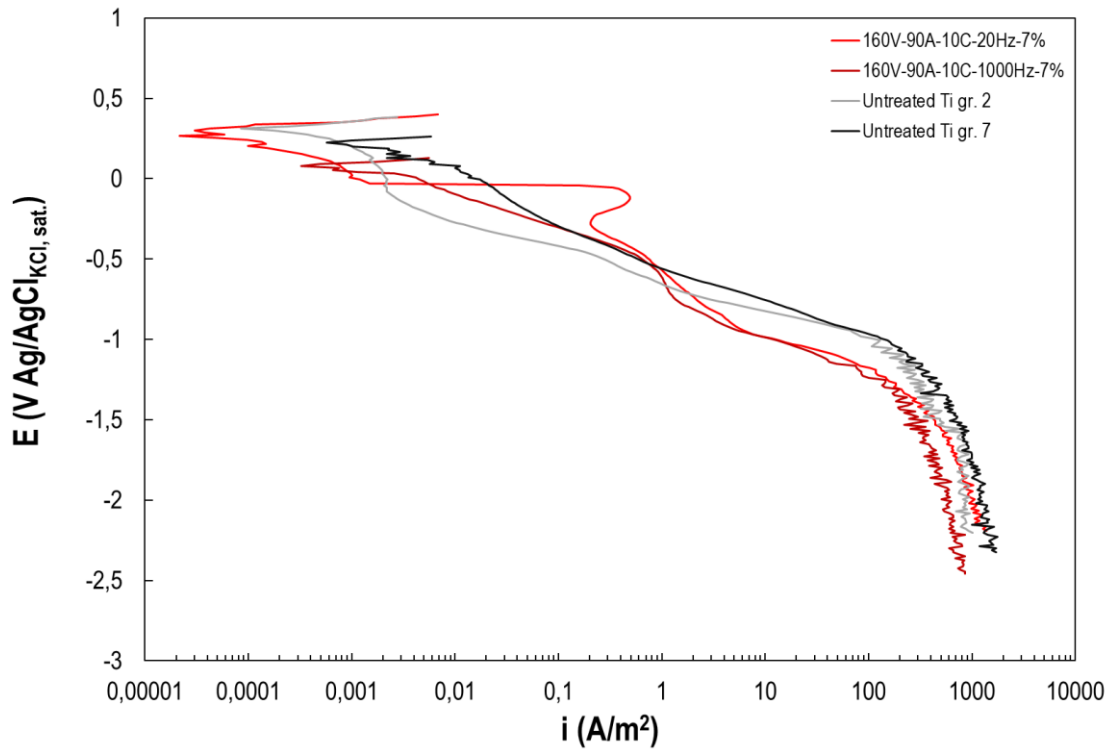
Figure 3.3.37 - Cathodic potentiodynamic results for samples anodized with waveforms 90%A – 10%C at 7% cathodic peak.
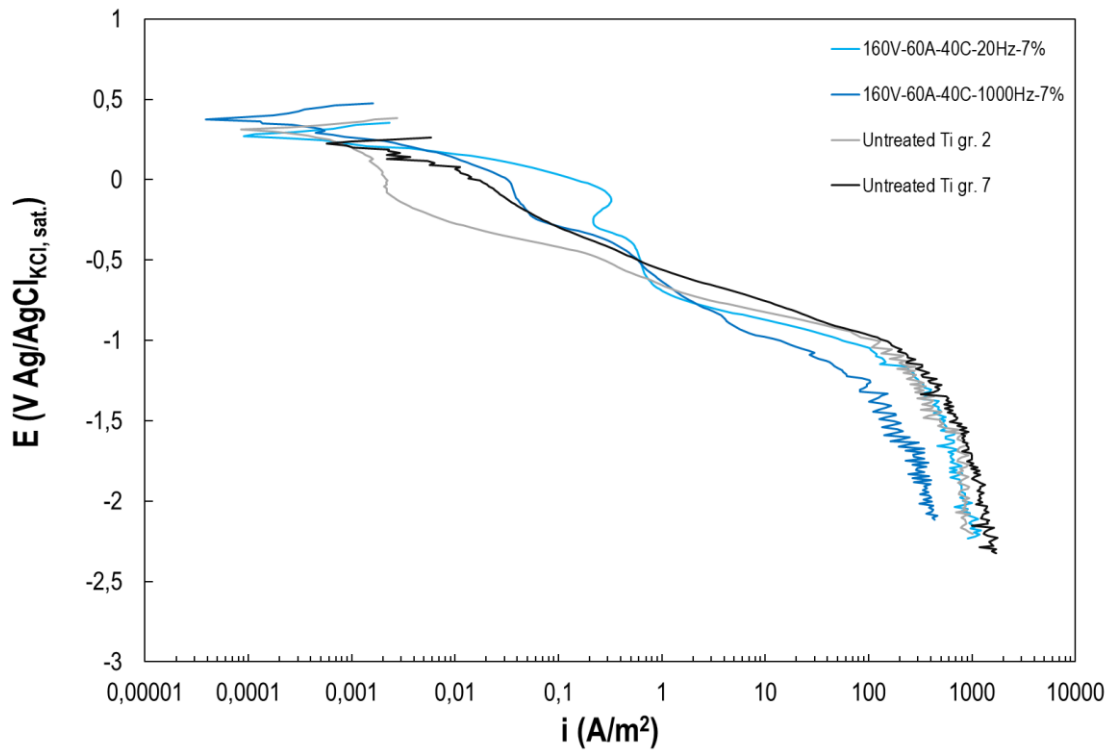
Figure 3.3.38 - Cathodic potentiodynamic results for samples anodized with waveforms 60%A – 40%C at 7% cathodic peak.

Table 3.3.12 - Structure, morphology and uniform corrosion behavior of duty cycles with cathodic peak at 7% (H=high, M=medium, L=low).

Sample n°	C.R. [mm/y]	Thickness [μm]	Anatase	Rutile	Porosity [%]
9	6.7	2.9	L	M	13.92
10	8.0	1.72	M	L	9.71
11	6.0	1.66	L	M	16.1
12	0.04	3.54	M	H	25.55

The cathodic curves for the samples treated at 7% cathode peak are collected in Figures 3.3.37 and 3.3.38. Condition 9 (90%A - 10%C at 20 Hz) shows an important increase in the anodic current at 0 V SCC, of almost three orders of magnitude, then has an indentation at -0.3 V SCC. Sample 11 (60%A - 40%C at 20 Hz) shows a similar pattern, but with a more pending curve. On the contrary, sample 12, the same high-frequency cycle, exhibits lower current density in hydrogen diffusion limit than all the other samples, in spite of its highest porosity.

Figures 3.3.39 and 3.3.40 show the results of cathodic potentiodynamic tests for 10% work cycles. It is interesting to notice a particular formation of two OCP for the duty cycle 90%A - 10%C at 20 Hz. This system has two operating points, this happens because the anodic curve is intersected by the total cathodic curve in two points, in the first with the passive branch of the materials and in the second, lower down, in the active one of the same.

Table 3.3.13 - Structure, morphology and uniform corrosion behavior of duty cycles with cathodic peak at 10% (H=high, M=medium, L=low).

| Sample n°	C.R. [mm/y]	Thickness [μm]	Anatase	Rutile	Porosity [%]
13	7.1	1.48	M	L	16.73
14	7.1	2.05	M	L	13.35
15	6.1	1.36	L	L	19.56
16	0.35	4.2	M	H	18.50
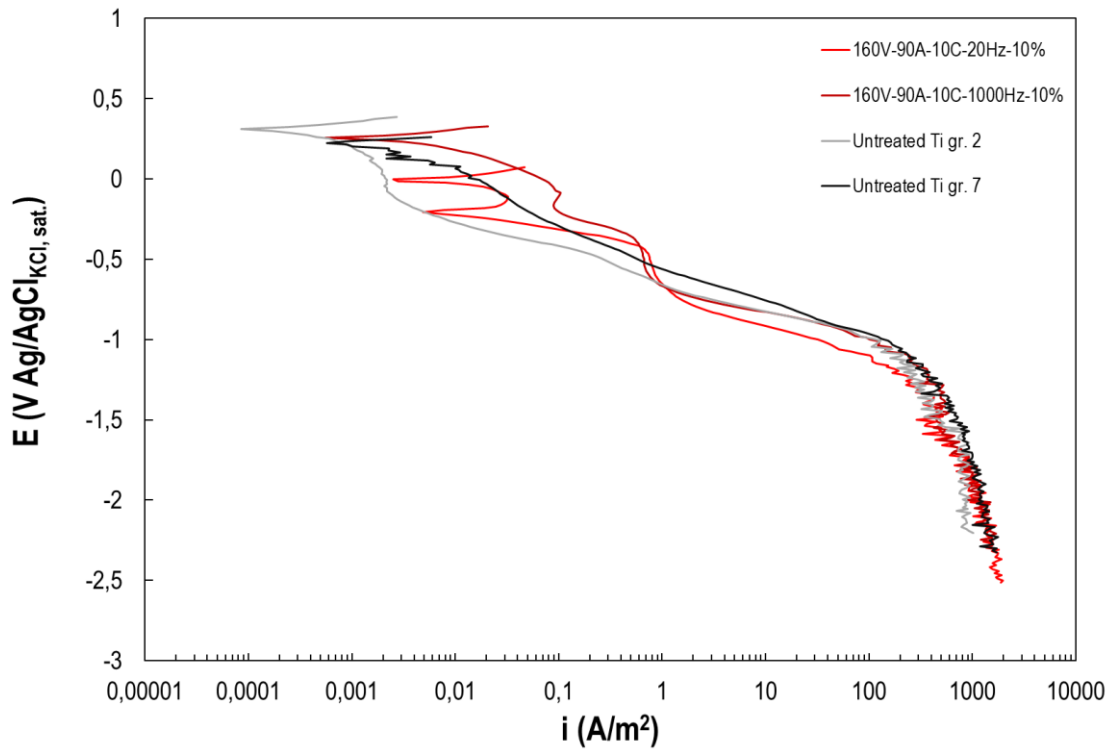
Figure 3.3.39 - Cathodic potentiodynamic results for samples anodized with waveforms 90%A – 10%C at 10% cathodic peak
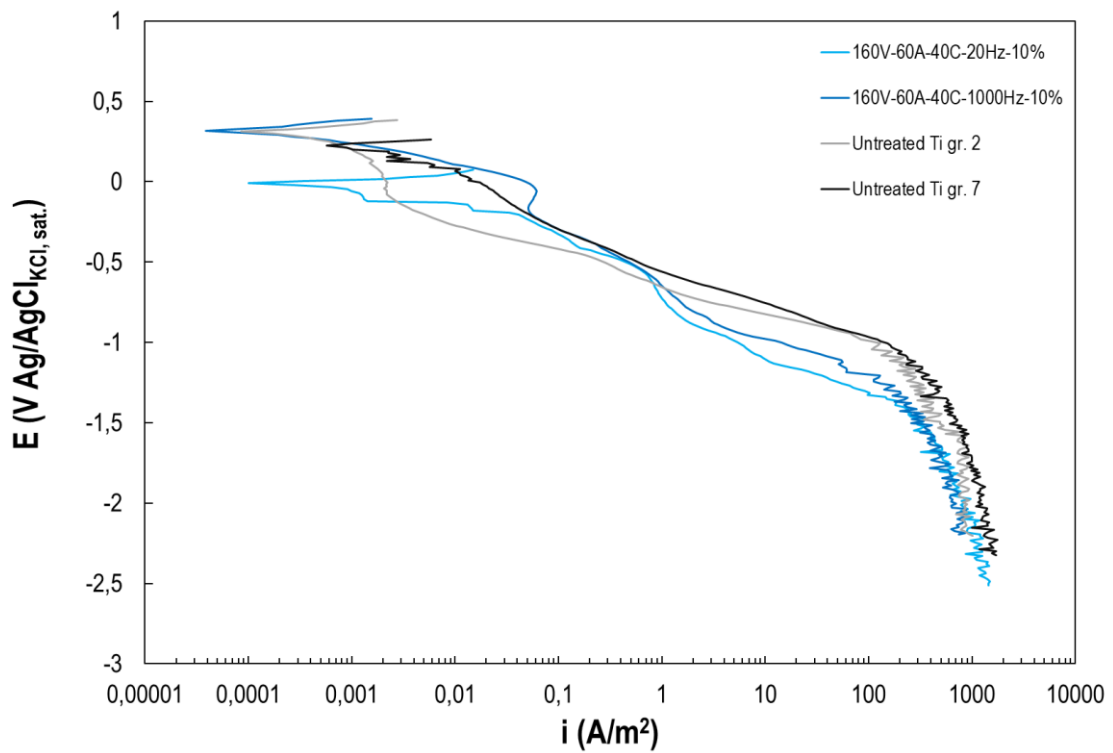
Figure 3.3.40 - Cathodic potentiodynamic results for samples anodized with waveforms 60%A – 40%C at 10% cathodic peak.

All the samples for potentials less than about -0.85 V SCC have lower cathodic currents than the untreated grade 2 titanium, with exclusion of the condition 3 (60% A - 40% C at 20 Hz).
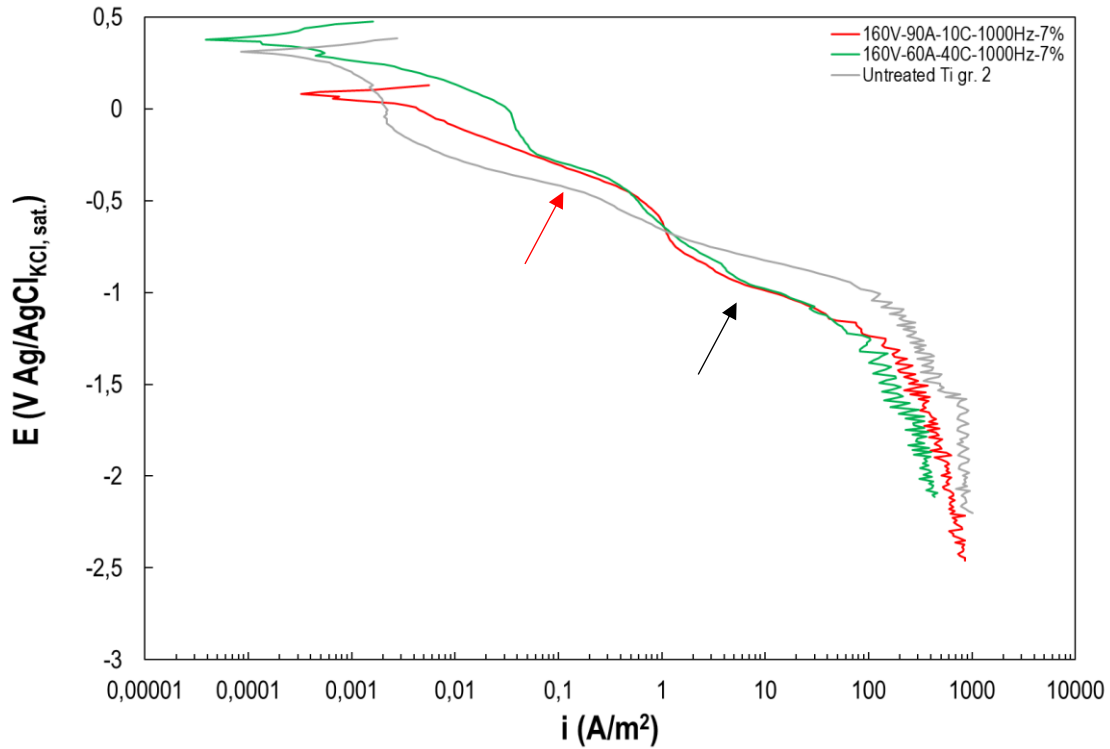
Figure 3.3.41 - Comparison between the cathodic curves of the best (12) and worst (10) sample in immersion tests.

In Figure 3.3.41 the cathodic curves of the samples 12 and 10 are represented, that is the best and worst condition with reference to the uniform corrosion test. Cycle 12 (60%A - 40%C at 7% C peak and 1000 Hz) showed again the best result in terms of limit currents, both as regards the diffusion of oxygen (0.161 A/m^2) and for the diffusion of hydrogen (438 A/m^2). Instead, in cycle 10 (90%A - 10%C at 7% C peak and 1000 Hz), the limit current with reference to the oxygen diffusion is one order of magnitude greater (1.21 A/m^2) while for the one in reference hydrogen diffusion is almost double (857 A/m^2). The Tafel slopes give an indication of the speed of the electrochemical reaction, correlated with the intensity of the current, as the electric potential varies. Table 3.3.14 shows the values of these slopes, with reference to the activation of oxygen and hydrogen, for sample 10 and 12. The Tafel slope for oxygen reduction is generally 60 mV/decade and the values of the two cycles are in line with the theoretical values. While the slope due to the evolution of hydrogen, which in general should be 120 mV/decade, are much greater, specifically 180 mV/decade for the

114

sample 10 and 185 mV/decade for the sample 12. The greater slope is due to the frictions that the oxide opposes towards hydrogen evolution, therefore in reference to the conditions 10 and 12, the latter offers a greater performance and therefore a better behavior.

Table 3.3.14 - Tafel slopes of the samples 10 and 12. (b=Tafel constant)

Sample	b oxigen	b hydrogen	B final
10	61	180	313
12	74	185	378

3.4 – Energy consumption

On the basis of the definition of a current plateau clarified in paragraph 2.2, it is possible to qualitatively deduce the trend of energy consumption of the tested anodizing conditions, also allowing comparison with the DC regime. The following equation was used to calculate the average current. This parameter was applied as a term of comparison between the different samples and consists of the product between the correct anodic/cathodic current plateau with the corresponding percentage of anodic and cathodic part of the duty cycle.

$$I_{average} = I_{anodic} \bullet \text{DUTY\%(A)} + |I_{cathodic}| \bullet \text{DUTY\%(C)}$$

The average current for a direct current anodization, performed at 160 V, was verified at 0.8 A. From Table 3.4.1, it can be deduced that generally an increase in the cathode peak has led to a higher energy consumption, since the amount of cathodic current needed to sustain the prescribed polarization level increases. The anode contribution, on the other hand, does not seem to be so influenced. The waveforms 90%A - 10%C generally show a lowering of the average currents passing from the frequencies 20 Hz to 1000 Hz, with the exception of the cycle with cathodic peak at 2%. The opposite behavior occurs with an increase in the frequency for the work cycle 60%A - 40%C, which produced a higher energy consumption regardless of the cathode peak selected. The most energy-consuming anodization condition was 12, which can be easily deduced from the fact that this treatment led to the highest heating of the electrolyte and to the greater surface porosity, that are correlated to the aggressiveness of the anodic spark deposition.

Table 3.4.1 - Collection of the average current evaluated for all the anodization condition tested.

Sample n°	Waveform	$I_{ANOD.}(A)$	$I_{CATH.}(A)$	$I_{AVE}(A)$
DC	-	-	-	0.800
1	90%A-10%C - 20 Hz - 2%	0.224	-0.267	0.228
2	90%A-10%C - 1000 Hz - 2%	0.487	-2.575	0.695
3	60%A-40%C - 20 Hz - 2%	0.265	-0.155	0.221
4	60%A-40%C - 1000 Hz - 2%	0.516	-0.470	0.497
5	90%A-10%C - 20 Hz - 5%	0.220	-2.080	0.406
6	90%A-10%C - 1000 Hz - 5%	0.150	-0.984	0.233
7	60%A-40%C - 20 Hz - 5%	0.116	-1.679	0.741
8	60%A-40%C - 1000 Hz - 5%	0.844	-3.000	1.706
9	90%A-10%C - 20 Hz - 7%	0.240	-3.210	0.537
10	90%A-10%C - 1000 Hz - 7%	0.173	-2.042	0.360
11	60%A-40%C - 20 Hz - 7%	0.221	-2.600	1.172
12	60%A-40%C - 1000 Hz - 7%	1.088	-3.740	2.148
13	90%A-10%C - 20 Hz - 10%	0.457	-6.565	1.067
14	90%A-10%C - 1000 Hz - 10%	0.163	-2.485	0.395
15	60%A-40%C - 20 Hz - 10%	0.386	-4.000	1.831
16	60%A-40%C - 1000 Hz - 10%	0.349	-3.660	1.673

CHAPTER 4 – Conclusion

The present work focused on the application of a bipolar plasma enhanced oxidation (PEO) process on titanium gr.2, to evaluate the influence of a cathodic current on the morphological and structural characteristics of its oxide. The goal was to achieve an improvement in corrosion resistance combined with energy savings, in spite of titanium grade 7 and a coating obtained with the traditional DC process.

The initial anodizing tests carried out in a solution of 0.5M sulfuric acid at room temperature, had preset parameters: 160V, with a speed of 0.5 V/s, two frequencies (20 Hz and 1000 Hz) and cathode peaks at 2%, 5%, 7% and 10%. The selected cycles were 90%A – 10%C and 60%A - 40%C; the first was chosen because it is close to the DC regime while the second as the maximum cathodic phase condition to obtain an opaque oxide for all cathode peaks.

Surface analysis with SEM showed that the bipolar PEO treatment allows to tune surface porosities, passing from a minimum of 7.3% for condition 90%A - 10%C – 1000 Hz-2% to a maximum of 25.55% for the signal 60%A - 40%C -1000Hz -7%. Surprisingly the thickest oxide coatings, for all the proposed cathode peaks, were the cycles with high cathodic phase (60%A - 40%C) at 1000 Hz, up to 4.2 µm. On the other hand, the same cycle but at low frequencies (20 Hz), for peaks at 7% and 10%, had the lowest values in terms of thickness, respectively 1.2 and 1.36 µm. The crystal structure was analyzed with XRD. For the conditions of minimum thickness (60%A - 40%C – 20 Hz 7% and 10%) the lowest amounts of crystalline phases were found, both in terms of anatase and of rutile. Interesting for those applications where a high amount of amorphous structure is required. The 90%A - 10%C waveform at 1000 Hz with 5% cathode peak, instead, presented the highest rutile and anatase phase formation, of possible interest for applications such as photocatalysis. Finally, the comparison of the conditions 60%A - 40%C - 10% C peak and 60%A - 40%R (monopolar), with GDOES, did not show the presence of hydrogen.

The corrosion behavior of the samples was evaluated in three ways: immersion test; anodic and cathodic potentiodynamic tests.

Initially the uniform corrosion was performed on the Ti gr.2 and gr.7 at different temperatures and concentrations of strong reducing acids: HCl, H_3PO_4, Sulfamic, Oxalic and H_2SO_4. This led to identify the worst corrosion condition which is 0.5M sulfuric acid at 60°C. This condition was tested for all samples treated with bipolar PEO, showing that this treatment, with appropriate selection of the initial parameters, leads to a better resistance to corrosion. In particular, the 60%A - 40%C -1000 Hz- 7% duty cycle has an average corrosion rate for 24 h of 0.04 mm/y, with better performance than Ti gr.7 (0.24 mm/y) and is highly recommended for applications in an acid environment.

Localized corrosion was evaluated by potentiodynamic tests in 0.5M NaBr at 50°C. In general, all the samples did not show any E_{pitt} in the investigated scan range (from -0.1V to 8V), excluding the conditions 60%A - 40%C - 20Hz for peaks 5%, 7% and 10%. It can be concluded in general that coatings with an average thickness of less than 2 μm, with a surface porosity greater than 15% and a low amount of crystalline phase show anodic dissolution.

Cathodic potentiodynamic tests were performed in 0.5M sulfuric acid at 25°C. The treated samples have a lower cathodic current than pure titanium for potentials lower than -0.85V SCC. As for immersion tests, also in this case the 60%A - 40%C - 1000Hz cycle at 7% C peak showed the best result, with the lowest limiting current density for hydrogen diffusion 438 A/m^2.

The introduction of a cathodic phase in the pulsed PEO process leads to control of the morphological and structural characteristics of TiO2 and to obtain better anticorrosive characteristics. On the other hand, in order to increase the thickness of the coating a high amount of cathodic polarization is required, thus determining an increase in energy consumption. For example, the condition 90%A - 10%C - 20 Hz - 2% leads to a 71% energy saving, while the 60%A - 40%C - 1000 Hz - 7% cycle leads to an increase in the 168%.

CHAPTER 5 – BIBLIOGRAPHY

[1]   W. Gregor, *William Gregor, Beobachtungen und Versuche über den Menakanite, einen in Cornwall gefundenen magnetischen Sand., in Lorenz Crell's Chemische Annalen, 1791, p40.* 1791.

[2]   "'Titanium.' Chemicool Periodic Table. Chemicool.com. 18 Oct. 2012. Web. 10/13/2019 <https://www.chemicool.com/elements/titanium.html>." .

[3]   "Titanium processing | Technology, Methods, & Facts | Britannica.com." [Online]. Available: https://www.britannica.com/technology/titanium-processing#ref81522.

[4]   O. Takeda, T. Uda, and T. H. Okabe, *Rare Earth, Titanium Group Metals, and Reactive Metals Production*, vol. 3. Elsevier Ltd., 2014.

[5]   Sebastian, "Timeline of titanium," 2018. [Online]. Available: https://timelines.issarice.com/index.php?title=Timeline_of_titanium&oldid=24632# References.

[6]   Christoph Leyens and Manfre Peters, *Titanium and Titanium Alloys*. Wiley-VCH, 2003.

[7]   E. Sedaghati *et al.*, "Detection of titanium oxide in the atmosphere of a hot Jupiter," *Nature*, vol. 549, no. 7671, pp. 238–241, Sep. 2017.

[8]   MatWeb - Material Property Data, "Aluminum 7075-T6; 7075-T651." [Online]. Available: http://www.matweb.com/search/DataSheet.aspx?MatGUID=4f19a42be94546b686b bf43f79c51b7d.

[9]   MatWeb - Material Property Data, "Titanium Ti-6Al-4V (Grade 5), Annealed." [Online].   Available: http://www.matweb.com/search/DataSheet.aspx?MatGUID=a0655d261898456b958 e5f825ae85390.

[10]   MatWeb - Material Property Data, "AISI 1015 Steel, normalized at 925°C (1700°F)." [Online]. Available: http://www.matweb.com/search/DataSheet.aspx?MatGUID=22786dfe88b74449949 ddd3cc56af203.

[11]   MatWeb - Material Property Data, "AISI 1340 Steel, annealed at 800°C, furnace cooled 11°C/hour to 600°C, air cooled, 25 mm (1 in.) round." [Online]. Available: http://www.matweb.com/search/DataSheet.aspx?MatGUID=176d43ca213b4727b41 edc9bd0cc5664.

[12]   MatWeb - Material Property Data, "314 Stainless Steel, annealed sheet." [Online]. Available: http://www.matweb.com/search/DataSheet.aspx?MatGUID=2b588e3b50c24c3d969 c8f90f8381e98.

[13]   J. Pouilleau, D. Devilliers, F. Garrido, S. Durand-Vidal, and E. Mahé, "Structure and composition of passive titanium oxide films," *Materials Science and Engineering B*, vol. 47, no. 3, pp. 235–243, 1997.

[14]   A. T. Sidambe, "Biocompatibility of advanced manufactured titanium implants-A review," *Materials*, vol. 7, no. 12. MDPI AG, pp. 8168–8188, 2014.

[15]   E. I. Paschalis *et al.*, "In vitro and in vivo assessment of titanium surface modification for coloring the backplate of the Boston keratoprosthesis," *Investigative Ophthalmology and Visual Science*, vol. 54, no. 6, pp. 3863–3873, 2013.

[16]   W. Zhao, Hongbo & Jun, "Review on Mineral Processing Technology of Rutile in China," Sciencepaper Online, 2013.

[17]   K. Deysel, "Leucoxene study: a mineral liberation analysis (MLA) investigation," *Southern African Institute of Mining and Metallurgy*, pp. 167–172, 2007.

[18]   F. H. Froes, "Titanium: Alloying," in *Encyclopedia of Materials: Science and Technology*, Elsevier, 2001, pp. 9361–9364.

[19]   M. ElGuindy, "Platinum Group Metals: Alloying, Properties, and Applications," in *Encyclopedia of Materials: Science and Technology*, Elsevier, 2001, pp. 7117–7121.

[20]   ASTM International, "Designation: B 265-08b Standard Specification for Titanium and Titanium Alloy Strip, Sheet, and Plate 1," pp. 1–10, 2009.

[21]   L. Titanium, "Chemical-Physical and mechanical charateristics of titanium." [Online]. Available: http://www.lls.it/assets/sviluppo/Sviluppo/pdf_mod1.pdf.

[22]   T. H. E. Arts, C. Policy, C. Justice, N. Security, P. Safety, and H. Security, *The RAND Corporation is a nonprofit research Support RAND Purchase this document Make a charitable contribution*. 2010.

[23]   Linda Maphango, *Overview of South Africa's Titanium Industry and Global Market Review*. 2013.

[24]   I. I. T. TAKECHI and Y. S. N. ARIYASU, "Application and Features of Titanium for the Aerospace Industry," *NIPPON STEEL & SUMITOMO METAL TECHNICAL REPORT*, no. 106, 2014.

[25]   J. P. D. C. Veiga A.J.R. Loureiro, "Proprties and applications of titanium alloys," *Reviews on Advanced Materials Science*, vol. 32, p. s. 133-148, 2012.

[26]   C. Cui, B. M. Hu, L. Zhao, and S. Liu, "Titanium alloy production technology, market prospects and industry development," *Materials and Design*, vol. 32, no. 3, pp. 1684–1691, 2011.

[27]   "Titanium Industries Industrial - Chemical Processing - Hydro-Metallurgical." [Online]. Available: https://titanium.com/markets/industrial/.

[28]   Q. Zhang *et al.*, "Long term corrosion estimation of carbon steel, titanium and its alloy in backfill material of compacted bentonite for nuclear waste repository," *Scientific Reports*, vol. 9, no. 1, Dec. 2019.

[29]   and M. A. M. C.N. Elias, J.H.C. Lima, R. Valiev, "Biomedical applications of titanium and its alloys | Marc Meyers - Academia.edu," 2008.

[30] "Consumer Products | Titanium Industries, Inc." [Online]. Available: https://titanium.com/markets/consumer-products/.

[31] M. C. K. T. H. Y. K. Kimura, "Applications of Titanium to Consumers' Products and Their Associated Strategy," 2002.

[32] A. Acharya and V. A. Gokhale, "Titanium: A New Generation Material for Architectural Applications," 2015.

[33] IUPAC, "Compendium of Chemical Terminology, 2nd ed. (the 'Gold Book'). Compiled by A. D. McNaught and A. Wilkinson. Blackwell Scientific Publications, Oxford (1997). Online version (2019-) created by S. J. Chalk. ISBN 0-9678550-9-8. https://doi.org/10.1351/goldbo." p. 1670, 2014.

[34] G. S. WAS and G. S. Was, "Corrosion and Stress Corrosion Cracking Fundamentals," in *Fundamentals of Radiation Materials Science*, Springer New York, 2017, pp. 857–949.

[35] H. Gräfen, E.-M. Horn, H. Schlecker, H. Schindler, and R. Feser, "Corrosion, 3. Corrosion Protection and Testing," in *Ullmann's Encyclopedia of Industrial Chemistry*, Wiley-VCH Verlag GmbH & Co. KGaA, 2015, pp. 1–20.

[36] F. Malik, "A study of passive films on valve metals," *Thin Solid Films*, vol. 206, no. 1–2, pp. 345–348, 1991.

[37] R. W. Schutz, "2003 F.N. Speller Award Lecture: Planning group metal additions to titanium: A highly effective strategy for enhancing corrosion resistance," *Corrosion*, vol. 59, no. 12, pp. 1043–1057, 2003.

[38] R. Krishna Alla, K. Ginjupalli, N. Upadhya, M. Shammas, R. Krishna Ravi, and R. Sekhar, "Surface Roughness of Implants: A Review," 2011.

[39] R. Piontelli and P. Pedeferri, "Electrochemical Painting of Titanium," *Journal of the Electrochemical Society*, vol. 115, no. 10, pp. 1046–1047, 1968.

[40]   di George F. Vander Voort, "Metallography, Principles and Practice," ASM International, 1984, pp. 116–124 pp 752.

[41]   P. Pedeferri, "Corrosione e Protezione dei Materiali," p. 428, 2005.

[42]   V. Vijayaraghavan, A. v. Sabane, and K. Tejas, "Hypersensitivity to titanium: A less explored area of research," *Journal of Indian Prosthodontist Society*, vol. 12, no. 4. pp. 201–207, Dec-2012.

[43]   J. Morales, "Evaluating biocompatible barrier films as encapsulants of medical micro devices," 2015.

[44]   D. Prando *et al.*, "Corrosion of titanium: Part 1: Aggressive environments and main forms of degradation," *Journal of Applied Biomaterials and Functional Materials*, vol. 15, no. 4, pp. e291–e302, 2017.

[45]   "Corrosion resistance TIMET." [Online]. Available: https://www.timet.com/assets/local/documents/technicalmanuals/corrosion.pdf.

[46]   T. Hodgkiess and A. Asimakopoulos, "Studies of the localised-corrosion behaviour of some stainless steels, incology 825 and titanium in seawater," *Desalination*, vol. 38, no. C, pp. 247–256, 1981.

[47]   Kathy Donina, "Density of Bone - The Physics Factbook," 2002. [Online]. Available: https://hypertextbook.com/facts/2002/AnnaYarusskaya.shtml.

[48]   B. Pattanaik, S. Pawar, and S. Pattanaik, "Biocompatible implant surface treatments," *Indian Journal of Dental Research*, vol. 23, no. 3. pp. 398–406, May-2012.

[49]   M. T. Pham, M. F. Maitz, W. Matz, H. Reuther, E. Richter, and G. Steiner, "Promoted hydroxyapatite nucleation on titanium ion-implanted with sodium," *Thin Solid Films*, vol. 379, no. 1–2, pp. 50–56, Dec. 2000.

[50]   M. Kolafová, J. Št ' Ovíček, J. Strnad, J. Zemek, and J. Dybal, "In Vitro Bioactivity Test of Real Dental Implants According to ISO 23317," *The International Journal of Oral & Maxillofacial Implants*, vol. 32, pp. 1221–1230, 1221.

[51]   Y. Oshida, "Chemical and Electrochemical Reactions," in *Bioscience and Bioengineering of Titanium Materials*, Elsevier, 2013, pp. 35–85.

[52]   J. C. M. Souza *et al.*, "Corrosion behaviour of titanium in the presence of Streptococcus mutans," *Journal of Dentistry*, vol. 41, no. 6, pp. 528–534, Jun. 2013.

[53]   M. Nakagawa, S. Matsuya, T. Shiraishi, and M. Ohta, "Effect of fluoride concentration and pH on corrosion behavior of titanium for dental use," *Journal of Dental Research*, vol. 78, no. 9, pp. 1568–1572, 1999.

[54]   B. Lindholm-Sethson and B. I. Ardlin, "Effects of pH and fluoride concentration on the corrosion of titanium," *Journal of Biomedical Materials Research - Part A*, vol. 86, no. 1, pp. 149–159, Jul. 2008.

[55]   Z. B. Wang, H. X. Hu, C. B. Liu, and Y. G. Zheng, "The effect of fluoride ions on the corrosion behavior of pure titanium in 0.05 M sulfuric acid," *Electrochimica Acta*, vol. 135, pp. 526–535, Jul. 2014.

[56]   A. S. Derbyshev, A. N. Suriev, A. N. Efimov, I. A. Beresneva, and F. A. Ladygin, "Corrosion of materials in hydrochloric acid solutions," *Chemical and Petroleum Engineering*, vol. 47, no. 9–10. pp. 632–634, Jan-2012.

[57]   Ronald W. Schutz, "Corrosion of Titanium and Titanium Alloys," in *Corrosion: Materials*, ASM International, 2005, pp. 252–299.

[58]   Imperial Metal Industries. New Metals Division., *Corrosion resistance of titanium. Imperial Metal Industries (Kynoch) Ltd., New Metals Division.* Birmingham, [England] : IMI, [19--], 1960.

[59]   F. Heakal, F. El-Taib Heakal, and K. A. Awad, "Electrochemical Corrosion and Passivation Behavior of Titanium and Its Ti-6Al-4V Alloy in Low and Highly Concentrated HBr Solutions," 2011.

[60]   I. N. Andijani, S. Ahmad, and A. U. Malik, "Corrosion behavior of titanium metal in the presence of inhibited sulfuric acid at 50°C," *Desalination*, vol. 129, no. 1, pp. 45–51, Jun. 2000.

[61]   K. A. de Souza and A. Robin, "Influence of concentration and temperature on the corrosion behavior of titanium, titanium-20 and 40% tantalum alloys and tantalum in sulfuric acid solutions," *Materials Chemistry and Physics*, vol. 103, no. 2–3, pp. 351–360, Jun. 2007.

[62]   J. shu LU, "Corrosion of titanium in phosphoric acid at 250 °C," *Transactions of Nonferrous Metals Society of China (English Edition)*, vol. 19, no. 3, pp. 552–556, Jun. 2009.

[63]   R. Bäßler, C. Schmidt, and H. Alves, "Recent Experiences on Suitability of Titanium and High Alloyed Materials in Acids at 200 0C," May 2015.

[64]   "Corrosion Resistance of Titanium to Nitric Acid." [Online]. Available: http://www.metalspiping.com/corrosion-resistance-of-ti-to-nitric-acid.html.

[65]   G. S. Frankel, "Pitting Corrosion of Metals A Review of the Critical Factors," *Journal of the Electrochemical Society*, vol. 145, no. 6, pp. 2186–2198, 1998.

[66]   Z. Chen, G. Zhang, and F. Bobaru, "The influence of passive film damage on pitting corrosion," *Journal of the Electrochemical Society*, vol. 163, no. 2, pp. C19–C24, 2016.

[67]   S. B. Basame and H. S. White, "Pitting corrosion of titanium the relationship between pitting potential and competitive anion adsorption at the oxide film/electrolyte interface," *Journal of the Electrochemical Society*, vol. 147, no. 4, pp. 1376–1381, 2000.

[68]   N. Casillas, "Pitting Corrosion of Titanium," *Journal of The Electrochemical Society*, vol. 141, no. 3, p. 636, 1994.

[69]   X. He, J. J. Noël, and D. W. Shoesmith, "Crevice corrosion damage function for grade-2 titanium of iron content 0.078wt%at95°C," *Corrosion Science*, vol. 47, no. 5, pp. 1177–1195, May 2005.

[70]   S. Yue, *Stress-Corrosion Cracking, Materials Performance and Evaluation, Second Edition*. 2016.

[71]   F. Hua, K. Mon, P. Pasupathi, G. Gordon, and D. Shoesmith, "Modeling the hydrogen-induced cracking of titanium alloys in nuclear waste repository environments," *JOM*, vol. 57, no. 1, pp. 20–26, 2005.

[72]   D. W. Shoesmith, J. J. Noël, D. Hardie, and B. M. Ikeda, "Hydrogen absorption and the lifetime performance of titanium nuclear waste containers," *Corrosion Reviews*, vol. 18, no. 4–5, pp. 331–359, 2000.

[73]   F. Hua, K. Mon, P. Pasupathi, G. Gordon, and D. Shoesmith, "A review of corrosion of titanium grade 7 and other titanium alloys in nuclear waste repository environments," *Corrosion*, vol. 61, no. 10. National Assoc. of Corrosion Engineers International, pp. 987–1003, 2005.

[74]   C. S. Brossia and G. A. Cragnolino, "Effect of palladium on the corrosion behavior of titanium," *Corrosion Science*, vol. 46, no. 7, pp. 1693–1711, Jul. 2004.

[75]   S. Kim, D. Nguyen-Manh, G. D. W. Smith, and D. G. Pettifor, "Site preference of Ru and Pd additions to γ-based TiAl intermetallics," *Philosophical Magazine A: Physics of Condensed Matter, Structure, Defects and Mechanical Properties*, vol. 80, no. 11, pp. 2489–2508, 2000.

[76]   A. Biesiekierski, D. H. Ping, Y. Yamabe-Mitarai, and C. Wen, "Impact of ruthenium on microstructure and corrosion behavior of β-type Ti-Nb-Ru alloys for biomedical applications," *Materials and Design*, vol. 59, pp. 303–309, 2014.

[77]   R. Z. Valiev, R. K. Islamgaliev, and I. v Alexandrov, "Bulk nanostructured materials from severe plastic deformation," 1999.

[78]   A. Balyanov *et al.*, "Corrosion resistance of ultra fine-grained Ti," *Scripta Materialia*, vol. 51, no. 3, pp. 225–229, Aug. 2004.

[79]   T. D. Burleigh, "Oxides formed on titanium by polishing, etching, anodizing, or thermal oxidizing," *Corrosion*, vol. 56, no. 12, pp. 1233–1241, 2000.

[80]   C. Byrne, R. Fagan, S. Hinder, D. E. McCormack, and S. C. Pillai, "New approach of modifying the anatase to rutile transition temperature in TiO2photocatalysts," *RSC Advances*, vol. 6, no. 97, pp. 95232–95238, 2016.

[81]   S. Kumar, T. S. N. S. Narayanan, S. G. S. Raman, and S. K. Seshadri, "Thermal oxidation of CP Ti - An electrochemical and structural characterization," *Materials Characterization*, vol. 61, no. 6, pp. 589–597, Jun. 2010.

[82]   T. D. Burleigh, "Oxides formed on titanium by polishing, etching, anodizing, or thermal oxidizing," *Corrosion*, vol. 56, no. 12, pp. 1233–1241, 2000.

[83]   R. W. Schutz and L. C. Covington, "Effect of Oxide Films on the Corrosion Resistance of Titanium," *Corrosion*, vol. 37, no. 10, pp. 585–591, 1981.

[84]   X. X. Wang, S. Hayakawa, K. Tsuru, and A. Osaka, "Bioactive titania gel layers formed by chemical treatment of Ti substrate with a H2O2/HCl solution," *Biomaterials*, vol. 23, no. 5, pp. 1353–1357, Mar. 2002.

[85]   M. Wang *et al.*, "Corrosion behavior of hydrophobic titanium oxide film pre-treated in hydrogen peroxide solution," *Materials and Corrosion*, vol. 62, no. 4, pp. 320–325, Apr. 2011.

[86]   D. Krupa *et al.*, "Effect of the heating temperature on the corrosion resistance of alkali-treated titanium," *Journal of Biomedical Materials Research - Part A*, vol. 88, no. 3, pp. 589–598, Mar. 2009.

[87]   Nathan. Qin, Shu;Current,Michael;Felch,Susan; Cheung, "Plasma Immersion Ion Implantation (PIII)," 2014.

[88]   D. Prando *et al.*, "Corrosion of titanium: Part 2: Effects of surface treatments," *Journal of Applied Biomaterials and Functional Materials*, vol. 16, no. 1, pp. 3–13, 2018.

[89]   D. Krupa *et al.*, "Effect of calcium-ion implantation on the corrosion resistance and biocompatibility of titanium," *Biomaterials*, vol. 23, no. 16, pp. 3329–3340, 2002.

[90]   D. Krupa *et al.*, "Effect of phosphorus-ion implantation on the corrosion resistance and biocompatibility of titanium," *Biomaterials*, vol. 23, no. 16, pp. 3329–3340, 2002.

[91]   D. Krupa *et al.*, "Effect of dual ion implantation of calcium and phosphorus on the properties of titanium," *Biomaterials*, vol. 26, no. 16, pp. 2847–2856, Jun. 2005.

[92]   D. Krupa *et al.*, "The influence of calcium and/or phosphorus ion implantation on the structure and corrosion resistance of titanium," in *Vacuum*, 2001, vol. 63, no. 4, pp. 715–719.

[93]   S. Ningshen, U. Kamachi Mudali, P. Mukherjee, P. Barat, and B. Raj, "Oxygen ion irradiation effect on corrosion behavior of titanium in nitric acid medium," *Journal of Nuclear Materials*, vol. 408, no. 1, pp. 1–6, Jan. 2011.

[94]   D. Krupa *et al.*, "Effect of carbon ion implantation on the structure and corrosion resistance of OT-4-0 titanium alloy," *Surface and Coatings Technology*, vol. 114, no. 2–3, pp. 250–259, May 1999.

[95]   F. Malik, "A study of passive films on valve metals," *Thin Solid Films*, vol. 206, no. 1–2, pp. 345–348, Dec. 1991.

[96]   M. V. Diamanti, P. Garbagnoli, B. Curto, and M. P. Pedeferri, "On the Growth of Thin Anodic Oxides Showing Interference Colors on Valve Metals," *Current Nanoscience*, vol. 11, no. 3, pp. 307–316, Apr. 2015.

[97]   L. Casanova Matr and A. Marcolin Matr, "Photocatalytic Reactor for Dye Degradation with TiO2 Nanotubes," 2016.

[98]   T. Shibata and Y. C. Zhu, "The effect of temperature on the growth of anodic oxide film on titanium," *Corrosion Science*, vol. 37, no. 1, pp. 133–144, 1995.

[99]   M. E. Sibert, "Electrochemical Oxidation of Titanium Surfaces," *Journal of The Electrochemical Society*, vol. 110, no. 1, p. 65, 1963.

[100]   M. V. Diamanti, M. Ormellese, and M. P. Pedeferri, "Alternating current anodizing of titanium in halogen acids combined with Anodic Spark Deposition: Morphological and structural variations," *Corrosion Science*, vol. 52, no. 5, pp. 1824–1829, May 2010.

[101]   Y. T. Sul, C. B. Johansson, Y. Jeong, and T. Albrektsson, "The electrochemical oxide growth behaviour on titanium in acid and alkaline electrolytes," *Medical Engineering and Physics*, vol. 23, no. 5, pp. 329–346, 2001.

[102]   M. V. Diamanti, B. del Curto, and M. Pedeferri, "Anodic oxidation of titanium: From technical aspects to biomedical applications," *Journal of Applied Biomaterials and Biomechanics*, vol. 9, no. 1, pp. 55–69, Jan. 2011.

[103]   M. v. Diamanti and M. P. Pedeferri, "Effect of anodic oxidation parameters on the titanium oxides formation," *Corrosion Science*, vol. 49, no. 2, pp. 939–948, Feb. 2007.

[104]   J. Liu, J. Yi, S. Li, M. Yu, G. Wu, and L. Wu, "Effect of electrolyte concentration on morphology, microstructure and electrochemical impedance of anodic oxide film on titanium alloy Ti-10V-2Fe-3Al," *Journal of Applied Electrochemistry*, vol. 40, no. 8, pp. 1545–1553, Aug. 2010.

[105]   Y. Mizukoshi, N. Ohtsu, and N. Masahashi, "Structural and characteristic variation of anodic oxide on pure Ti with anodization duration," *Applied Surface Science*, vol. 283, pp. 1018–1023, Oct. 2013.

[106]   D. Prando *et al.*, "Corrosion of titanium: Part 2: Effects of surface treatments," *Journal of Applied Biomaterials & Functional Materials*, vol. 16, no. 1, pp. 3–13, Jan. 2018.

[107] M. P. Diamanti, M.V.; Pedeferri, "Production and characterization of thick titanium oxide films by anodic oxidation," Milano, 2012.

[108] H. Hu, X. Liu, and C. Ding, "Preparation and cytocompatibility of Si-incorporated nanostructured TiO2 coating," *Surface and Coatings Technology*, vol. 204, no. 20, pp. 3265–3271, Jul. 2010.

[109] M. Babaei, C. Dehghanian, and M. Vanaki, "Effect of additive on electrochemical corrosion properties of plasma electrolytic oxidation coatings formed on CP Ti under different processing frequency," *Applied Surface Science*, vol. 357, pp. 712–720, Dec. 2015.

[110] S. Aliasghari, T. Hashimoto, P. Skeldon, and G. E. Thompson, "Effect of chloride ions in plasma electrolytic oxidation of titanium," *ECS Electrochemistry Letters*, vol. 3, no. 5, 2014.

[111] M. R. Kaluđerović, J. P. Schreckenbach, and H. L. Graf, "Titanium dental implant surfaces obtained by anodic spark deposition – From the past to the future," *Materials Science and Engineering C*, vol. 69. Elsevier Ltd, pp. 1429–1441, 01-Dec-2016.

[112] J. M. Macak *et al.*, "TiO2 nanotubes: Self-organized electrochemical formation, properties and applications," *Current Opinion in Solid State and Materials Science*, vol. 11, no. 1–2. pp. 3–18, Feb-2007.

[113] D. Regonini, C. R. Bowen, A. Jaroenworaluck, and R. Stevens, "A review of growth mechanism, structure and crystallinity of anodized TiO2 nanotubes," *Materials Science and Engineering R: Reports*, vol. 74, no. 12. Elsevier Ltd, pp. 377–406, 2013.

[114] Q. Cai, L. Yang, and Y. Yu, "Investigations on the self-organized growth of TiO2 nanotube arrays by anodic oxidization," *Thin Solid Films*, vol. 515, no. 4, pp. 1802–1806, Dec. 2006.

[115] S. Huang, B. Jiang, C. Liu, Q. Shao, and H. Li, "Effect of Negative Current on the Microstructure of Oxide Coatings Prepared by Hybrid Pulse Anodization," *Metals*, vol. 9, no. 1, p. 22, Dec. 2018.

[116] R. S. Williamson, J. Disegi, A. v. Janorkar, J. A. Griggs, and M. D. Roach, "Effect of duty cycle on the crystallinity, pore size, surface roughness and corrosion resistance of the anodized surface on titanium," *Surface and Coatings Technology*, vol. 277, pp. 278–288, Sep. 2015.

[117] L. Wu, J. H. Liu, G. L. Wu, S. M. Li, and M. Yu, "Growth behaviour of anodic oxide film on titanium alloy," *Surface Engineering*, vol. 31, no. 12, pp. 904–911, Dec. 2015.

[118] D. A. Torres-Cerón, F. Gordillo-Delgado, and S. N. Moya-Betancourt, "Effect of the voltage pulse frequency on the structure of TiO2 coatings grown by plasma electrolytic oxidation," in *Journal of Physics: Conference Series*, 2017, vol. 935, no. 1.

[119] M. Babaei, C. Dehghanian, and M. Vanaki, "Effect of additive on electrochemical corrosion properties of plasma electrolytic oxidation coatings formed on CP Ti under different processing frequency," *Applied Surface Science*, vol. 357, pp. 712–720, Dec. 2015.

[120] Y. Wang *et al.*, "Effect of frequency on the structure and cell response of Ca- and P-containing MAO films," *Applied Surface Science*, vol. 256, no. 7, pp. 2018–2024, Jan. 2010.

[121] S. Gowtham, T. Arunnellaiappan, and N. Rameshbabu, "An investigation on pulsed DC plasma electrolytic oxidation of cp-Ti and its corrosion behaviour in simulated body fluid," *Surface and Coatings Technology*, vol. 301, pp. 63–73, Sep. 2016.

[122] Z. Yao, Y. Xu, Z. Jiang, and F. Wang, "Effects of cathode pulse at low frequency on the structure and composition of plasma electrolytic oxidation ceramic coatings," *Journal of Alloys and Compounds*, vol. 488, no. 1, pp. 273–278, Nov. 2009.

[123] W. T. Kim and W. Y. Choi, "Fabrication of TiO2 photonic crystal by anodic oxidation and their optical sensing properties," *Sensors and Actuators, A: Physical*, vol. 260, pp. 178–184, Jun. 2017.

[124]   ASTM International, "Standard Practice for Preparing , Cleaning , and Evaluating Corrosion Test (G1)," *Significance*, vol. 90, no. Reapproved 2011, pp. 1–9, 1999.

[125]   ASTM International, "ASTM Standards: G31-72," *Annual Book of ASTM Standards*, vol. 72, no. Reapproved 2004, pp. 1–8, 2012.

[126]   D. Prando, D. Nicolis, M. Pedeferri, and M. Ormellese, "Pitting corrosion on anodized titanium: Effect of halides," *Materials and Corrosion*, vol. 69, no. 10, pp. 1441–1446, Oct. 2018.

[127]   ASTM Standards, "ASTM G5-14 Standard Reference Test Method for Making Potentiodynamic Anodic Polarization," *ASTM International*, pp. 1–9, 2014.

[128]   D. A. Torres-Cerón, F. Gordillo-Delgado, and S. N. Moya-Betancourt, "Effect of the voltage pulse frequency on the structure of TiO2 coatings grown by plasma electrolytic oxidation," in *Journal of Physics: Conference Series*, 2017, vol. 935, no. 1.

[129]   C. Jaeggi, P. Kern, J. Michler, J. Patscheider, J. Tharian, and F. Munnik, "Film formation and characterization of anodic oxides on titanium for biomedical applications," *Surface and Interface Analysis*, vol. 38, no. 4, pp. 182–185, Apr. 2006.

[130]   Z. Qin, Y. Zeng, and D. W. Shoesmith, "Modeling hydrogen permeation through a thin titanium oxide film and palladium," *Thin Solid Films*, vol. 534, pp. 673–679, May 2013.

[131]   Z. Yao, Y. Jiang, F. Jia, Z. Jiang, and F. Wang, "Growth characteristics of plasma electrolytic oxidation ceramic coatings on Ti-6Al-4V alloy," *Applied Surface Science*, vol. 254, no. 13, pp. 4084–4091, Apr. 2008.

[132]   F. Contu, "The cathodic behavior of titanium: Serum effect," *Journal of Biomedical Materials Research Part B: Applied Biomaterials*, vol. 100B, no. 2, pp. 544–552, Feb. 2012.

[133]   Y. Liu, Z. H. Ren, J. Liu, R. F. Schaller, and E. Asselin, "Electrochemical investigation and identification of titanium hydrides formed in mixed chloride sulfuric

acid solution," *Journal of the Electrochemical Society*, vol. 166, no. 11, pp. C3096–C3105, 2019.

[134]   J. M. Casas, V. G. Papangelakis, and H. Liu, "Performance of Three Chemical Models on the High-Temperature Aqueous Al2(SO4)3 −MgSO4 −H2SO4 −H2O System," *Industrial & Engineering Chemistry Research*, vol. 44, no. 9, pp. 2931–2941, Apr. 2005.